A Reconstituted System for Studying Kinetochore-Microtubule Attachments

Andrew D Franck

A dissertation

submitted in partial fulfillment of the

requirements for the degree of

Doctor of Philosophy

University of Washington

2012

Reading Committee:

Charles Asbury, Chair

Linda Wordeman

Trisha Davis

Program Authorized to Offer Degree:

Physiology and Biophysics

University of Washington

Abstract

A Reconstituted System for Studying Kinetochore-Microtubule Attachments

Andrew D Franck

Chair of the Supervisory Committee:
Associate Professor Charles Asbury
Physiology and Biophysics

Before physically dividing into two nascent daughter cells, a cell must first duplicate, organize and segregate its entire genome. During mitosis, chromosomes are aligned along an axis of symmetry and then pulled apart by force-generating elements in the cell. Advances in genetic, biochemical and biophysical tools have enabled us to identify and study key components of this force-generating apparatus. Here, I will focus on interactions between chromosome-bound organelles called kinetochores and microtubules, dynamic protein filaments. My goal was to better understand how kinetochores harness the work generated by dynamic microtubules to drive chromosome movement. To do so, I used purified kinetochore components and employed biophysical techniques adapted from the study of single molecules. With this system I was able to reconstitute fundamental biological phenomena: persistent kinetochore-like attachments to growing and shortening microtubules, cooperative interactions between components that enhance attachment strength and force-dependent regulation of microtubule dynamics. Using a combination of single molecule techniques and modeling, I have also initiated study into the biophysical mechanisms underlying kinetochore-microtubule attachment. This work has given us valuable insights as to how these essential mitotic machines function within living, dividing cells.

TABLE OF CONTENTS

LIST OF FIGURES

LIST OF TABLES

ACKNOWLEDGEMENTS

The author thanks the Department of Physiology and Biophysics for its support and the laboratories of Chip Asbury, Linda Wordeman, Trisha Davis, and Sue Biggins for their contributions as mentors, peers, collaborators and co-authors. He extends special thanks to the horses of Save a Forgotten Equine of Monroe, Washington.

DEDICATION

This work is dedicated to my family and friends, without whom none of this would be possible.

Chapter 1
Introduction

MITOSIS AND THE MITOTIC SPINDLE

During the cell cycle, a cell replicates and segregates it genome before dividing. The complete, duplicated genome is packaged into a discrete set of linked sister chromatids called chromosomes. A typical cell builds a machine called a mitotic spindle to efficiently and reliably transfer chromosomes to its daughters. The spindle is an array of dynamic microtubule filaments organized between two poles with each pole serving to nucleate and bundle microtubules. Here we will focus exclusively on microtubules linked to chromosome-bound kinetochores. Kinetochores form stable attachments to microtubule tips, even as the filaments assemble and disassemble under their grip, coupling chromosome movement to microtubule growth and shortening (Koshland, Mitchison et al. 1988; Inoue and Salmon 1995; Maddox, Straight et al. 2003). Sister kinetochores must only capture microtubules radiating from their proximal pole. This condition is known as biorientation and ensures that, upon separating, all sister chromatids are drawn to opposite poles. During congression, coordinated microtubule growth and shortening moves chromosomes to spindle midzone. When the appropriate signal is given, links between sisters are severed and chromatids are pulled to opposite poles of the spindle. Soon afterwards, fission separates the two sets of chromatids, poles and surrounding cellular components into two new daughter cells. This highly orchestrated process is carefully monitored and controlled, as the gain or loss of genetic material frequently results in serious types of cancer and birth defects (Gordon, Resio et al. 2012).

MICROTUBULE STRUCTURE AND DYNAMICS

Microtubules are composed of αβ-tubulin heterodimers approximately 8 nm in length. Dimers bind head to tail to form protofilaments. The typical microtubule contains 13 protofilaments, although microtubules seen in vitro and in vivo may have anywhere from 8 to 19 protofilaments (Chretien and Wade 1991). Lateral associations between neighboring protofilaments form microtubules, hollow, cylindrical tubes approximately 25 nm in diameter. Microtubules are inherently polarized, with β subunits found at the fast-growing plus end and α subunits at the slow-growing minus end.

At sufficient concentrations of free tubulin and GTP, microtubules exhibit a characteristic behavior called dynamic instability (Mitchison and Kirschner 1984; Desai and Mitchison 1997). Individual filaments undergo phases of extended growth and shortening by the addition and loss of tubulin dimers from their tips. Transitions between growth and shortening occur at random but with frequencies dependent on free tubulin concentration, buffer conditions and the presence of microtubule-modifying proteins (Walker, O'Brien et al. 1988; Drummond 2011). This distinctly non-equilibrium behavior is powered by GTP hydrolysis. Although both α and β tubulin bind GTP, hydrolysis and exchange occurs only within the β tubulin binding pocket (Desai and Mitchison 1997). Microtubule growth is driven by favorable association of GTP-containing tubulin dimers. Hydrolysis occurs soon after dimers are incorporated into the lattice. Conformational changes accompanying hydrolysis create mechanical strain within the filament, converting chemical energy into potential mechanical energy (Howard 2001). It is thought that a stabilizing structure at a growing tip, such as a cap of GTP-containing subunits, prevents

accumulated strain from pulling the filament apart (Desai and Mitchison 1997). In the absence of a stabilizing structure, mechanical strain overwhelms the lateral bonds between neighboring protofilaments, causing them to curl. As protofilaments peel away from each other, subunits dissociate, causing the microtubule to shorten. Exchange of GDP for GTP within dimers occurs in solution, priming them for another cycle of microtubule and shortening. Dynamic instability can be described by four parameters: speeds of growth and shortening and transition frequencies between growth and shortening (Walker, O'Brien et al. 1988; Inoue and Salmon 1995).

As a consequence of biorientation, microtubules attached to opposite poles must coordinate their dynamics to produce productive chromosome movement. In addition, congression requires that kinetochore-microtubule dynamics must also be regulated in a length dependent manner (Nicklas 1983; Nicklas 1988; Skibbens, Skeen et al. 1993; Inoue and Salmon 1995; Gardner, Pearson et al. 2005; Goshima, Wollman et al. 2005; Civelekoglu-Scholey, Sharp et al. 2006). Since microtubules display inherent dynamic instability, how can filament growth and shortening be coordinated and controlled? Classic micromanipulation experiments show that kinetochore-microtubules elongate when a pulling force is applied (Nicklas 1988; Skibbens, Rieder et al. 1995; Khodjakov and Rieder 1996; Skibbens and Salmon 1997). As a consequence, tension-dependent effects on microtubule dynamics are thought to control filament lengths and coordinate chromosome alignment, most likely by altering parameters of dynamic instability. Tension-promoted microtubule elongation may be directly or indirectly mediated by kinetochores. Load-bearing components at kinetochores may indirectly regulate separate microtubule modifying proteins or act directly on the filament itself to confer stability.

KINETOCHORES AND KINETOCHORE-MICROTUBULE ATTACHMENT

Kinetochores act as a mechanical linkage between chromosomes and microtubules and also as a signaling module that regulates progression through mitosis. At present kinetochores are thought to contain >65 distinct proteins, a number likely to increase as studies of kinetochore genetics and proteomic progress (McAinsh, Tytell et al. 2003; Westermann, Drubin et al. 2007; Tanaka and Desai 2008). The number of microtubules per kinetochore varies from species to species, ranging from just one at budding yeast to greater than 20 in humans (Winey, Mamay et al. 1995; McEwen, Ding et al. 1998). However, it is thought that kinetochores which bind multiple microtubules are tiled, modular assemblies each of which is capable of binding an individual filament (Joglekar, Bouck et al. 2006; Joglekar, Bouck et al. 2008; Joglekar, Bloom et al. 2009). Kinetochores are bound primarily to microtubule plus ends while minus ends are typically anchored at the spindle poles (McIntosh and Euteneuer 1984). Electron micrographs of kinetochores show three distinct morphological regions, which serve as useful, if rough delineations between relationships of structure to function (Brinkley and Stubblefield 1966). Kinetochores assemble in a hierarchical fashion, based on studies showing that deletions of outer components usually does not disrupt the localization of inner ones, but that deletions of inner components often results in a complete inhibition of kinetochore assembly (Westermann, Drubin et al. 2007). The inner plate contains proteins that stably bind the organelle to the condensed DNA of the chromosome. All kinetochore-DNA linkages are mediated by one or more specialized nucleosomes containing a specific histone H3 variant called CENP-A, around which are wrapped lengths of centromeric DNA (Westermann, Drubin et al. 2007). The middle layer of the kinetochore contains the Ctf19 and Mtw1 complexes. At the very least, these complexes serve to link microtubule-binding components to the DNA-binding structure of the inner

kinetochore (Grishchuk, Efremov et al. 2008). It is highly likely that these complexes serve other, as yet undiscovered, roles as well. The outer kinetochore plate contains components required for microtubule binding. These may include plus- and minus-end directed microtubule motors, but also passive binding elements such as the Dam1 and Ndc80 kinetochore complexes.

What is the molecular mechanism underlying kinetochore-microtubule attachment? One conventional view holds that kinetochore-associated motor proteins mediate tip attachment. Motors such as kinesin and dynein bind and walk along the side of microtubule filaments, using ATP hydrolysis as a source of power (Howard 1996; Vale 2003). Since chromosome motion is tightly coupled to microtubule growth and shortening, additional microtubule modifying factors may be required to coordinate filament dynamics with motor-directed motion. However, deletion of kinetochore-associated motors in both yeasts and higher eukaryotes produces relatively mild phenotypes (Cottingham, Gheber et al. 1999; West, Malmstrom et al. 2001; Garcia, Koonrugsa et al. 2002; McIntosh, Grishchuk et al. 2002; Weaver, Bonday et al. 2003; Kapoor, Lampson et al. 2006; Yang, Tulu et al. 2007). Even with depleted or inactivated motors, kinetochores in vitro harness the energy of shortening microtubules to produce force and motion(Inoue and Salmon 1995). Clearly kinetochore motility is primarily microtubule-based, relying somehow on filament growth and shortening.

Protofilament peeling at disassembling microtubule tips may contribute to kinetochore attachment and motility. Curling and peeling releases mechanical strain stored in the lattice, created by conformational changes accompanying GTP-hydrolysis (Desai and Mitchison 1997). In theory, a conformational wave of strain release could generate mechanical pushing or pulling forces against kinetochore components(Koshland, Mitchison et al. 1988). An *in vitro* optical trapping assay lends some support to this model (Grishchuk, Molodtsov et al. 2005). In the assay, a bead coated with strepavidin is tightly bound to biotinylated microtubule and held within a stationary optical trap. When the shortening filament disassembled back to the bead, peeling protofilaments attached to the bead exerted a brief force against the trap before breaking away from the lattice. Further enthusiasm for this model was generated by the discovery that the Dam1 complex forms rings and spirals around microtubules in vitro, since a sliding ring represents an ideal structure for capturing forces generated by protofilament pushing (Miranda, De Wulf et al. 2005; Westermann, Avila-Sakar et al. 2005; Efremov, Grishchuk et al. 2007). At present, ring-like structures have not been observed at kinetochores in vivo, but fibril-like structures are often found in proximity to peeling protofilaments, raising the possibility that microtubule could exert either pulling or pushing forces via a conformational wave mechanism (McIntosh, L. et al. 2008).

Kinetochore coupling may also be based on biased diffusion (Hill 1985). Here, an array of binding elements undergoes a random walk along a microtubule filament. So long as diffusive motion is sufficiently fast and the binding energy large enough, the tendency for the array to minimize its free energy biases its motion toward the microtubule filament. This creates a thermodynamic driving force that could produce work against an external load. In vitro observations show that individual kinetochore components bind and diffuse along stabilized microtubule filaments (Westermann, Wang et al. 2006; Gestaut, Graczyk et al. 2008; Powers, Franck et al. 2009). On shortening filaments, complexes appear to diffusively bounce off disassembling tips, suggesting that diffusion but not unbinding is energetically favorable (Powers, Franck et al. 2009).

RATIONALE

"Scientists in other fields are wont to express astonishment that the experimental method has been used with so little success in analyzing mitosis. To one who has tried it, the explanation is obvious. It lies in the fact that it is almost impossible to affect a given structure or process of the mitotic mechanism, be it by operation or physiochemical means, without simultaneously affecting several others. Usually it is difficult to determine the nature and precise influence of the disturbing factors thus introduced, and the intrusion of subsidiary effects may not actually become recognizable until a later period, if at all." – Franz Schrader 1953 (Schrader 1953)

My thesis work begins to address how kinetochores maintain attachments to highly dynamic microtubules. Although the complexity of mitosis continues to fascinate and frustrate scientists, advances in biochemistry, molecular biology and microscopy allow us to experiment with cellular components in ways unimaginable sixty years ago. In chapter 2, I introduce an experimental approach that relies on biochemically purified components and biophysical techniques to reconstitute mechanical coupling between chromosomes and force-generating microtubule filaments. With this reduced system, we avoid many of the difficulties that arise when working with living cells, and can begin to answer fundamental questions about chromosome movement during mitosis.

The Dam1 protein complex is an essential outer kinetochore component found in yeast (Cheeseman, Brew et al. 2001; Jones, He et al. 2001; Li, Bachant et al. 2002). In vivo, deletions of its constituent components are lethal and in vitro the complex binds to static microtubules, leading to the hypothesis that the Dam1 complex is a load-bearing component linking chromosomes to microtubules (He, Rines et al. 2001; Janke, Ortiz et al. 2002; Miranda, De Wulf et al. 2005; Westermann, Avila-Sakar et al. 2005; Westermann, Wang et al. 2006). It is unclear, however, whether the Dam1 complex alone can reconstitute two key features of kinetochores: supporting load while attached to growing and shortening microtubule tips and harnessing the energy generated by disassembling microtubules to drive chromosome movement. In chapter 3, I show that Dam1-based microtubule attachments can support continuous loads of up to several picoNewtons (pN), applied by a feedback-controlled optical trap. Under tension, Dam1 remains persistently attached to assembling microtubules and also can harness the force produced by shortening microtubules to do work, strong evidence that the Dam1 complex is a key element that directly links kinetochores to microtubules.

The Ndc80 complex is another essential outer kinetochore component. Genetic and biochemical assays have confirmed that it is required for proper kinetochore-microtubule attachment and that it binds directly to microtubules (Kline-Smith, Sandall et al. 2005; Tanaka and Desai 2008). Unlike Dam1, Ndc80 complex is conserved from yeast to humans, suggesting that in higher metazoans, the complex is the primary constituent of kinetochore-microtubule attachments. Again, it is unclear whether Ndc80 alone can form persistent load-bearing attachments to dynamic microtubules and capture the energy released by disassembling microtubules. In chapter 4, I show by optical trapping-based assays that Ndc80 does possess these abilities. In addition, single-molecule assays using total internal reflection florescent (TIRF) microscopy show that Ndc80 diffuses on stable microtubules and tracks with shortening microtubule filaments. These behaviors are characteristic of attachments based on biased diffusion, suggesting that biased diffusion is one mechanism by which kinetochore components form lasting attachments to dynamic microtubules.

In yeast the presence of both Dam1 and Ndc80 at kinetochores are required for stable microtubule attachment (Kline-Smith, Sandall et al. 2005; Tanaka and Desai 2008). How do the Dam1 and Ndc80 complexes work together to form robust kinetochore-microtubule attachments in yeast? *In vivo* studies have shown that Ndc80 must be present at kinetochores to allow Dam1 to bind, suggesting that Ndc80 not only may contribute to kinetochore microtubule attachment but also serve as a mechanical link between Dam1 and inner kinetochore components (Janke, Ortiz et al. 2002). In chapter 5, I show that the presence of Dam1 increases both the persistence and robustness of Ndc80-mediated attachments under trap-applied loads. In these assays force is transmitted exclusively through the Ndc80 complex, suggesting that that Ndc80 is a key load-bearing structure within kinetochores.

A number of models for kinetochore-microtubule attachment have been proposed, but none have been tested directly. Existing in vitro data is consistent with two models (Grishchuk, Molodtsov et al. 2005; Gestaut, Graczyk et al. 2008; Powers, Franck et al. 2009). The first is based on biased diffusion, where binding interactions between kinetochore complexes and a microtubule create a thermodynamic driving force that can perform work against an external load (Hill 1985). The second is based on a conformational wave generated by a shortening microtubule, capable of exerting mechanical force against kinetochore components (Koshland, Mitchison et al. 1988). In chapter 6, I test quantitative predictions for a hybrid model incorporating aspects of both biased diffusion and the conformation wave using a motility assay based on optical trapping. Biased diffusion alone can account for attachments to growing microtubules but a conformational wave, which acts to slow detachment due to loss of subunits at a disassembling tip, is required for coupling to shortening microtubules. Our model fully accounts for attachments to both growing and shortening microtubules and makes quantitative predictions which we verify with independent experimentation.

During mitosis, kinetochore microtubule must undergo coordinated phases of growth at one sister and shortening at the other to drive productive chromosome movements. Coordination of microtubule assembly and disassembly are strongly correlated with changes in tension at the kinetochore-microtubule interface (Nicklas 1983; Nicklas 1988; Skibbens, Skeen et al. 1993; Inoue and Salmon 1995; Gardner, Pearson et al. 2005). In vivo experiments show that tension at kinetochores promotes growth, probably by affecting parameters of dynamic instability (Nicklas 1988; Skibbens, Rieder et al. 1995; Khodjakov and Rieder 1996; Skibbens and Salmon 1997) . This effect may be indirect, where force at kinetochores modulates the activity of microtubule-modifying proteins, or direct, where load-bearing components act on microtubule in a stabilizing manner. In chapter 7, using an optical trapping based assay, I show that Dam1-mediated attachments alter microtubule dynamics in a tension-dependent manner, promoting growth and inhibiting shortening. This demonstrates that Dam1 is involved in tension-dependent control of microtubule dynamics, and that force acting directly on the microtubule tip is sufficient to modulate filament growth and shortening.

Chapter 2
Direct Physical Study of Kinetochore–Microtubule Interactions by Reconstitution and Interrogation with an Optical Force Clamp

Originally published in Methods 51 (2010) 242–250.

ABSTRACT

We detail our use of computer-controlled optical traps to study interactions between kinetochore components and dynamic microtubules. Over the last two decades optical traps have helped uncover the working principles of conventional molecular motors, such as kinesin and dynein, but only recently have they been applied to study kinetochore function. The most useful traps combine sensitive position detectors and servo-control, allowing them to be operated as force clamps that maintain constant loads on objects as they move. Our instrument, which is among the simplest designs that permits force clamping, relies on a computer-controlled piezoelectric stage and a single laser for trapping and position detection. We apply it in motility assays where beads coated with pure microtubule-binding kinetochore components are attached to the tips of individual dynamic microtubules. Like kinetochores in vivo, the beads remain tip-attached, undergoing movements coupled to filament assembly and disassembly. The force clamp provides many benefits over instruments that lack feedback control. It allows tension to be applied continuously during both assembly- and disassembly-driven movement, providing a close match to the physiological situation. It also enables tracking with high resolution, and simplifies data interpretation by eliminating artifacts due to molecular compliance. The formation of persistent, load-bearing attachments to dynamic microtubule tips is fundamental to all kinetochore activities. Our direct, physical study of kinetochore–microtubule coupling may therefore furnish insights into many vital kinetochore functions, including correction of aberrant attachments and generation of the 'wait-anaphase' signals that delay mitosis until all kinetochores are properly attached.

INTRODUCTION

Biologists and engineers alike know that one of the best ways to learn how something works is to build a functioning model. An electrical engineer who wants to understand a complex circuit begins by constructing a prototype that allows her to probe voltages at various locations and to swap resistors, capacitors, and other elements in and out. Likewise, aeronautic and naval engineers build scale models for wind tunnel and wave tank testing, where flow patterns and forces can be measured. There are two key reasons why these approaches are so successful. First, they distill the system down to a minimum of essential, modifiable components—a reductionist strategy that facilitates testing of well-defined hypotheses. Second, they enable direct observation of system dynamics. These same strategies are useful to biologists when the processes they are studying can be reconstituted *in vitro* using pure components.

A great example is the study of motor proteins over the last two decades. *In vitro* motility assays developed in the 1980s first showed that myosin and kinesin alone are sufficient to generate ATP-powered movement along F-actin and microtubule filaments, respectively

Sheetz and Spudich (1983); (Vale, Reese et al. 1985). These assays then led to an explosion of new biophysical techniques for manipulating and tracking individual molecules that now provide a clear picture of how these motors work (Spudich 2001; Vale 2003; Asbury 2005; Block 2007). Using laser trapping, for example, we can observe the stepwise, 8-nanometer movements of single kinesin molecules as they literally walk along the sides of microtubules (Svoboda, Schmidt et al. 1993; Asbury, Fehr et al. 2003). With ultrasensitive fluorescence microscopy, it is even possible to watch as one ATP molecule binds a motor and causes it to undergo one stepwise movement (Sakamoto, Webb et al. 2008).

Simultaneous with progress in single molecule techniques, efforts began in the mid-1980s to reconstitute kinetochore-microtubule interactions. Kinetochores are large, multi-protein complexes that are central to mitosis. They couple chromosomes to the microtubules of the mitotic spindle, serving as primary sites where force is produced to move the chromosomes (Inoue and Salmon 1995). They also provide critical regulatory functions that ensure the accuracy of chromosome segregation (Nicklas 1997). The first *in vitro* studies of kinetochore activity used whole chromosomes isolated from tissue culture cells (Mitchison and Kirschner 1985; Koshland, Mitchison et al. 1988; Coue, Lombillo et al. 1991). These pioneering experiments established that kinetochores can remain attached to the assembling and disassembling tips of microtubules, allowing them to generate movement by harnessing filament growth and shortening (an idea suggested earlier by observations of mitotic cells; e.g., see Inoue and Salmon 1995). Other early efforts identified microtubule binding factors from budding yeast cell extracts that assemble onto centromeric DNA (Sorger, Severin et al. 1994) and probably participate in the sensing and correcting of aberrant kinetochore-microtubule attachments (Biggins, Severin et al. 1999; Sassoon, Severin et al. 1999). The full benefit of reconstitution could not yet be achieved, however, because so little was known about the molecular components of kinetochores.

Now, armed with a wealth of new information about kinetochore biochemistry, reconstitution is more promising than ever. Nearly-complete lists of kinetochore components are available, particularly in budding yeast, whose kinetochores are among the simplest (McAinsh, Tytell et al. 2003; Westermann, Drubin et al. 2007; Cheeseman and Desai 2008). We also know that kinetochores are organized into distinct subcomplexes, many of which can be expressed recombinantly and purified in active form from *E. coli* (De Wulf, McAinsh et al. 2003; Westermann, Cheeseman et al. 2003; Ciferri, De Luca et al. 2005; Miranda, De Wulf et al. 2005; Wei, Sorger et al. 2005; Westermann, Avila-Sakar et al. 2005; Cheeseman, Chappie et al. 2006). The stoichiometry and rough spatial arrangement of subcomplexes within the kinetochore is known (Emanuele, McCleland et al. 2005; Joglekar, Bouck et al. 2006; Joglekar, Bloom et al. 2009; Wan, O'Quinn et al. 2009), and some of the subcomplexes most likely to form the 'core' attachment to microtubules have been identified (DeLuca, Dong et al. 2005; Miranda, De Wulf et al. 2005; Westermann, Avila-Sakar et al. 2005; Cheeseman, Chappie et al. 2006; DeLuca, Gall et al. 2006; Wei, Al-Bassam et al. 2007; Ciferri, Pasqualato et al. 2008).

With these considerations in mind, our lab is developing new *in vitro* assays that allow kinetochore functions to be interrogated with advanced single molecule techniques. We focus here on optical trapping-based methods for studying how subcomplexes from the outer kinetochore, such as the Dam1 and Ndc80 complexes, can form persistent, load-bearing attachments to the tips of assembling and disassembling microtubules (Asbury, Gestaut et al. 2006; Powers, Franck et al. 2009). The coupling between kinetochores and dynamic microtubule

tips is fundamental to all kinetochore activities. Therefore our methods for studying coupling will likely enable investigations of other functions, such as regulation of the growth of kinetochore-attached microtubules (Franck, Powers et al. 2007), correction of aberrant attachments, and checkpoint signaling. Brief methods have been published elsewhere (Asbury, Gestaut et al. 2006; Franck, Powers et al. 2007; Powers, Franck et al. 2009). Our aim here is to provide a more thorough treatment, discussing some of the challenges we have encountered and offering practical solutions to these challenges.

OPTICAL TRAPPING FOR KINETOCHORE STUDIES

Instrument Design and Construction

An optical trap is essentially an infrared laser beam focused through a high-power objective lens to create a very small (diffraction-limited), very bright spot (Neuman and Block 2004). The spot traps micron-sized transparent objects, such as polystyrene beads, allowing them to be manipulated relative to their surroundings by steering the laser beam or, equivalently, by moving the specimen stage while keeping the beam fixed. The earliest traps were simple, manipulation-only devices (Ashkin and Dziedzic 1987; Ashkin, Dziedzic et al. 1987). However, the utility of trapping comes from the incorporation of additional features, such as photodetectors for measuring the position of the trapped object, and computerized feedback for controlling the applied force. A dizzying variety of trap configurations have been developed over the last decade (e.g., see Lang and Block 2003; Neuman and Block 2004). The instrument we built for studying kinetochore-microtubule interactions is among the simplest possible designs that allows for nanometer-scale tracking and computerized control of the applied force.

Our instrument is based around a Nikon inverted microscope (TE2000), outfitted for video-enhanced differential interference contrast (DIC) imaging. For trapping it is essential to choose a high numerical aperture objective lens with good transmission at the wavelength of the trap laser (Neuman and Block 2004), which in our case is 1064 nm. We currently use a Nikon 100x 1.4 NA oil Plan Apo IR CFI objective, which transmits ~60% at 1064 nm and has been a standard trapping lens for many years. Nikon now offers a newer alternative, the 100x 1.49 Plan Apo TIRF CFI, with similar infrared transmission and higher numerical aperture. To view unlabeled microtubule filaments via DIC, we also use an oil condenser lens with high numerical aperture (1.4), two standard Wollaston prisms and polarizers, and a mercury arc lamp (X-Cite 120) for transmitted-light illumination (see Fig. 1). We couple the mercury lamp to the microscope through a 10-meter optical fiber and place it in a separate room, so the heat and noise it produces cannot interfere with trap stability. Recent reports show that microtubules can also be viewed using diode-based illuminators (e.g., see Bormuth, Howard et al. 2007), which produce far less heat and are probably more cost effective. We capture images with a standard black and white video camera (JAI, CV-M50). The very high contrast needed to resolve individual microtubules exaggerates even slight imaging flaws, usually created by dust on the optics or minor variations in illumination intensity. These variations must be removed by background subtraction to produce acceptable image quality. Stand-alone video image processors, such as the Hamamatsu Argus, have traditionally been used for this purpose. Unfortunately, the Argus is no longer commercially available but computer-based image acquisition and processing is a relatively straightforward alternative (e.g., using LabView). During experiments, we record video onto standard VHS cassette tapes. Digital recording would

likely provide higher image quality, but we use the recordings only for archiving or low-resolution position tracking in experiments without the optical trap.

The trap itself is formed by a diode-pumped continuous wave 1064 nm Nd:YVO_4 laser from Spectra Physics (J20-BL10-106Q). Though relatively costly, these lasers have become a mainstay for optical trapping because they provide excellent power and pointing stability, plus 4 W of output power—enough to form a trap capable of applying 50 pN or more. Thus far, our experiments with individual kinetochore components have not required forces above a few piconewtons, so a less expensive laser such as the 400 mW Chromalase (CLAS-106-STF02-01, from Blue Sky Research), may have been adequate. However, the additional power could become important as we begin to study more complete kinetochore assemblies, which are predicted to sustain higher loads. As a safety precaution, we add a green band pass filter (CVI Melles Griot, VG 14) in-between the eyepieces and the main body of the microscope to prevent eye exposure to the infrared trapping light (which is powerful but invisible).

To direct the trap laser into the objective lens, an infrared-reflecting dichroic mirror is custom-mounted just below the objective but above the traditional fluorescence filter cube turret. This arrangement preserves the fluorescence capabilities of the microscope for future use. As the laser beam passes through the trapped object, its light is partially scattered. Much of the scattered light is collected by the condenser lens and then another (identical) custom-mounted dichroic reflects it towards a position-sensitive photodetector (located in an optical plane conjugate to the back focal plane of the condenser lens), which allows the position of the trapped object to be monitored with high precision for use in feedback control. More elaborate instruments with a computer-steerable trapping laser usually incorporate an additional, low-power, fixed laser for position detection (Lang, Asbury et al. 2002). These extra complexities are justified when fast feedback control is required (i.e., > 50 Hz updates), or when non-uniformity of the trapped objects requires re-calibration of the position sensor for each object. However, our simple system using a single fixed laser for both trapping and position detection is easier to build and maintain. The piezo stage-based steering allows feedback updates at 50 Hz, adequate for clamping the force on beads coupled to dynamic microtubule tips, which move relatively slowly (usually < 12 nm s^{-1} during filament growth and < 200 nm s^{-1} during disassembly). We avoid the need to re-calibrate the position sensor for each bead by using polystyrene beads of uniform size (CV 2.5%, Spherotech).

Steering in our fixed-trap system is accomplished by moving the specimen stage. For long-range movements, we use a two-axis stage with manual, fine-threaded actuator screws. This stage allows much finer control than the stock Nikon stage, but we find it is still inadequate for carefully positioning beads relative to microtubule tips in our assays. For finer movements, we mounted a precision three-axis piezo stage with internal capacitive position sensors (Physik Instrumente, P-517.3CL) atop the manual stage. The piezo controller (E-710) accepts digital commands from a personal computer, generated either in response to a hand-held joystick or during automated calibration and feedback control routines. Adding the stages and the photodetector requires some custom modifications to the microscope body (see Fig. 2). Next to cost, these are the most significant hurdles to trap construction.

To control entry of the trap laser into the microscope, we use a shutter (Vincent Associates, VS25S2ZMO) operated by an inexpensive, foot pedal switch. The foot switch facilitates trapping of objects with very high indices of refraction, such as polystyrene beads, which tend to be pushed away from the trap if they are not precisely in focus (owing to the 'fire

hose' effect of scattering forces; see Neuman and Block 2004). To trap such objects, we temporarily block the laser with the foot switch-controlled shutter, leaving our hands free to maneuver the bead into the trapping site (using either the manual stage or the joystick-controlled piezo stage). Once the bead is properly located and in focus, we capture it by turning the trap back on with the foot switch.

The environment around a trapping instrument can have a significant impact on its performance. We house our instruments in a temperature controlled, quiet, dust-free room. Temperature control is crucial for avoiding instrument drift, since temperature gradients cause differential expansion and contraction of the instrument, producing artifactual changes in the position signals. In a typical biology laboratory, temperature fluctuations can exceed several degrees per hour-easily enough to produce drift comparable to the rate of microtubule growth. Our microscopy room includes a custom recirculating air system to maintain a constant temperature, to within ±0.5° C. Given sufficient warm-up time, the drift in our instruments is negligible, at ~2 Å s^{-1}. The position sensing system also responds to acoustic noise and floor vibrations, so it is essential to minimize these disturbances as well. Our laboratory is in the basement of a sturdy (pre-world war II) concrete building, and the microscopy room has acoustic insulation in the walls. Even with these precautions, our experiments can be fouled when heavy carts are pushed through the adjacent hallway.

Calibrating the optical trap

Quantitative trap assays demand accurate calibration of both the position sensor response and the trapping force. To calibrate the response of the position sensor to our beads, we first attach the beads firmly to a coverslip surface. Then we use an automated routine to raster scan individual coverslip-bound beads through the beam while recording the voltage signals from the photodetector. Signals generated from 15 to 20 different beads are averaged, and then a two-dimensional, fifth-order polynomial fit is generated to provide a voltage-to-position map that is used later to determine the position of trapped beads in real time (Lang, Asbury et al. 2002). This method of sensor calibration requires spherical beads with uniform diameter, identical to those used for trapping assays. Since the method assumes bead movement matches precisely that of the piezo stage, firm attachment to the coverslip is also important. Coverslip attachment can usually be achieved by simply introducing the beads into a clean flow cell in a buffer of moderate ionic strength, without blocking proteins. If necessary, the rigidity of attachment can be improved by evaporating and then replacing the buffer (e.g., by placing the flow cell a dry incubator). The calibration is checked by raster scanning additional coverslip-attached beads and measuring the RMS deviation between the computed and actual positions. A good calibration typically produces RMS errors less than a few nanometers across many beads.

We employ three different methods to calibrate the trap stiffness: power spectrum, equipartition, and drag force. These methods and the physics on which they are based have been discussed at length in previous reviews (Svoboda and Block 1994; Visscher and Block 1998; Lang, Asbury et al. 2002; Neuman and Block 2004). For the sake of brevity, we discuss here only a few details that relate specifically to our use of optical traps for studying kinetochore-microtubule attachments. First, we note that the coverslip-anchored microtubules in our experiments orient randomly on the coverslip surface. Depending on their density, it can be impractical to select for study only those filaments with a particular orientation. Thus, calibration of the trap stiffness in two lateral dimensions (i.e., in the plane parallel to the

coverslip surface) is useful because it enables accurate forces to be applied to microtubules of any orientation (Lang, Asbury et al. 2002). Since polarization effects usually conspire to generate an elliptically-shaped trapping potential in the lateral plane, care must be taken to map the stiffness along the principle elliptical axes (i.e., the two orthogonal directions along which the trap stiffness is most, and least, stiff). Given these principle stiffnesses, the vector force in the lateral plane can be computed for any position within the harmonic region of the trap, which usually extends out to ~100 nm from the trap center.

We use custom software written in LabView for instrument control and data acquisition during the calibration routines outlined above and during force clamp experiments (described below). Analog signals from the position sensor are sampled at 40 kHz using an analog-to-digital conversion board (National Instruments, PCI-6251). Commands are sent to the piezo stage controller through a GPIB digital interface (National Instruments, GPIB-USB-B). Both the bead and stage positions are down-sampled to 200 Hz for file storage.

RECONSTITUTING MICROTUBULE-DRIVEN MOVEMENT AND FORCE PRODUCTION

Obtaining pure, active kinetochore components

The first step in any effort toward biological reconstitution is to obtain pure, active components. For kinetochores, this step would be impossible without the great progress made over the last decade in our understanding of kinetochore biochemistry. Kinetochores are large multiprotein complexes, composed of ~80 distinct proteins grouped loosely into three functional segments: the inner kinetochore that binds DNA, the outer kinetochore that binds microtubules, and the middle kinetochore that forms a structural bridge. Detailed analyses, beginning with budding yeast and now extending to metazoans, have revealed a 'core' of essential proteins organized hierarchically into distinct subcomplexes (McAinsh, Tytell et al. 2003; Westermann, Drubin et al. 2007; Cheeseman and Desai 2008). This discovery, in turn, has facilitated the purification of many core kinetochore proteins in active form, by using polycistronic vectors (Tan 2001) to simultaneously express all the components of a particular subcomplex in *E. coli* (Miranda, De Wulf et al. 2005; Wei, Sorger et al. 2005; Westermann, Avila-Sakar et al. 2005; Cheeseman, Chappie et al. 2006). (In contrast, expressing individual proteins alone generally yields poor expression or inactive, insoluble protein.)

The presence of distinct, stable subcomplexes within the kinetochore also suggests a functional modularity, which is good news for would-be reconstitutors since it implies that building a fully-functional coupler may not require all ~80 proteins. Modularity is further supported by experiments showing that pure, recombinant subcomplexes from the outer kinetochore, such as the Ndc80 and Dam1 complexes, bind directly to taxol-stabilized microtubules (Miranda, De Wulf et al. 2005; Westermann, Avila-Sakar et al. 2005; Cheeseman, Chappie et al. 2006; Wei, Al-Bassam et al. 2007; Ciferri, Pasqualato et al. 2008). These considerations motivated us to attempt reconstitution of kinetochore-microtubule coupling using a 'bottom up' strategy—i.e., beginning with individual microtubule-binding subcomplexes.

Detailed methods for polycistronic expression of kinetochore subcomplexes are given in several previously published papers (Miranda, De Wulf et al. 2005; Wei, Sorger et al. 2005; Westermann, Avila-Sakar et al. 2005; Asbury, Gestaut et al. 2006; Gestaut, Graczyk et al. 2008; Powers, Franck et al. 2009). For general methods of construction of polycistronic expression vectors, we refer the reader to (Tan 2001). For purification, we use metal affinity based on a

His_6 tag fused to one protein within each subcomplex, followed by size-exclusion chromatography. The His_6 tag also facilitates linking the subcomplexes to polystyrene beads (see below).

Functionalizing beads with antibody

Kinetochore subcomplexes are too small to be directly observed in a light microscope or directly manipulated with an optical trap. Therefore we couple them via antibodies to polystyrene microbeads, which serve as position markers, as 'handles' for optical manipulation, and as artificial cargoes (i.e., substituting for the chromosomes). We typically use streptavidin-coated polystyrene beads, 0.44 μm in diameter (Spherotech, SVP-05-10), which are further functionalized by coating with biotinylated anti-His_5 antibodies (Qiagen #34440), as follows. Bead stock (1% w/v) is diluted 8-fold in BRB80 (80 mM PIPES, 1mM $MgCl_2$, 1mM EGTA at pH 6.9) in a 0.6 mL tube. To disperse any aggregated beads, the tube is submerged in ice water (to prevent heating) beneath a tip sonicator (Branson Sonifier 450) and sonicated at medium-power for 5 minutes. After a brief spin in a benchtop centrifuge to remove liquid from the sides of the tube, antibody is then added to a final concentration of 40 μg mL^{-1} and the resulting mixture is incubated on a rotator for 45 minutes at 4 ºC. The density of antibody on the bead surface may also be adjusted (e.g., for titration experiments) by diluting the antibody into free biotin or biotinylated-BSA before mixing with beads. Following incubation, free antibody is removed by six rounds of centrifugal pelleting (15,000 rpm for 8 minutes at 4 ºC), supernatant removal, and resuspension in assay buffer (BRB80 supplemented with 8 mg mL^{-1} BSA). The resulting bead concentration can be estimated from measurements of light scatter (using a spectrophotometer) or from direct counts of the number of beads within a given volume. We typically get a final concentration of ~60 pM (± 11%). Anti-His_5-coated beads can be stored on a rotator at 4 ºC for several weeks without noticeable loss of binding activity.

Growing short, stabilized microtubule seeds

A stable, anchored nucleating structure is required to manipulate individual dynamic microtubules with an optical trap. Microtubules are sometimes nucleated *in vitro* from coverslip-bound flagellar axonemes or demembranated Tetrahymena pellicles (Walker, O'Brien et al. 1988; Coue, Lombillo et al. 1991; Lombillo, Coue et al. 1993; Grishchuk, Molodtsov et al. 2005). Because these are complex organelles, they could introduce protein contaminants. We therefore prefer to use short microtubule 'seeds' comprised of a mixture of regular and functionalized tubulin grown in the slowly hydrolyzable GTP analogue guanosine-5'-[(α,β)-methyleno]triphosphate (GMPCPP). Our seeds are grown from a mixture of unlabeled and biotinylated tubulin (typically 70:1) for adhesion to avidin-functionalized coverslips (detailed below). Specifically, we incubate ~70 μM bovine brain tubulin (purified as described in Castoldi and Popov 2003), 1 μM biotinylated tubulin (Cytoskeleton, Denver), and 1 mM GMPCPP (Jena Bioscience, Jena, Germany) in BRB80 plus 10% glycerol at 37 °C for 45 minutes. This mixture is then aliquotted, snap-frozen in liquid nitrogen and stored at -80 °C.

Creating kinetochore complex-coated beads

Kinetochore complexes are bound to beads and used in motility assays on the same day. We dilute our antibody-coated beads an additional five-fold (to ~12 pM) in assay buffer (BRB80

supplemented with 8 mg mL^{-1} BSA) and sonicate in an ice-water bath for 2 minutes to disperse aggregates. Kinetochore components are diluted to working concentrations of 1 to 25 nM in assay buffer. Beads and kinetochore components are then mixed 1:1 and allowed to incubate 60 to 90 minutes at 4 ºC on a rotator. Unbound complex can be removed from the bead mixture at this stage by multiple rounds of centrifugal pelleting and resuspension in assay buffer. In our experience, the presence or absence of excess free complex has not had any clear, statistically significant effects on bead behavior (Asbury, Gestaut et al. 2006). However, a recent study suggested that the interaction of Dam1-coated beads with microtubules may be stronger in the presence of excess free Dam1, which could oligomerize with the bead-bound Dam1 complexes (Grishchuk, Spiridonov et al. 2008).

Flow cell preparation

We construct disposable flow chambers using conventional microscope slides (Gold Seal #3011), cleaned coverslips (Corning #2940-224) and double-stick office tape (Scotch #665). As purchased from the manufacturer, coverslips are typically coated with a proprietary anti-sticking compound, which inhibits their functionalization with avidin, and gives them a rough-textured appearance in video-enhanced DIC imaging that can obscure single microtubules. To remove this coating, we clean the coverslips in a saturated solution of KOH (~5.9 M) in ethanol. Three separate beakers of de-ionized water are used for rinsing off residual KOH-ethanol. Prior to initial use, beakers of cleaning solution and water are degassed by placing in an ultrasonic bath for 15 minutes. Coverslips are placed in a custom Teflon rack and submerged in the beaker containing KOH-ethanol. The beaker is placed in an ultrasonic bath for 10 minutes. After a quick rinse in the first water-containing beaker, the rack is immersed in the second water-containing beaker and the beaker is placed in the ultrasonic bath for 10 minutes. After a rinse in the third water-containing beaker, the racked coverslips are sprayed with ~0.5 L of de-ionized water, followed by ~0.5 L of ethanol and placed in clean incubator (37-40 °C) for 45 minutes or until completely dry. After drying, the racks and coverslips are placed in clean plastic containers to prevent dust contamination.

Flow chambers consist of two lengths of double-stick tape placed across the width of a microscope slide to form an inverted channel. A cleaned coverslip is pressed onto the tape such that it forms the bottom of the channel and overhangs the slide on both sides, creating ledges that allow solutions to be pipetted and aspirated from the channel. To prevent leaking, gentle pressure must be applied to seal the coverslip to the tape. A good seal will appear relatively transparent and is free of bubbles and voids near edges.

Nucleating dynamic microtubules

Biotinylated microtubule seeds are anchored to coverslips using a simple, two-layer surface preparation based on the method of Janson et al (Janson, de Dood et al. 2003). The flow chamber is first incubated with 5 mg mL^{-1} biotinylated-BSA (Vector Labs, Burlingame, CA) for 10 minutes, and then washed with BRB80, followed by incubation with 0.3 mg mL^{-1} avidin DN (Vector Labs). A second BRB80 wash is used to remove free avidin, and then seeds are introduced. For good surface coverage, we typically dilute 4 µL seed aliquots 50-fold in warm BRB80 prior to introduction to the sample chamber. Unbound seeds are washed out with growth buffer (BRB80 plus 8 mg mL^{-1} BSA with 1 mM GTP). Finally, we introduce beads in growth buffer supplemented with bovine brain tubulin, 1 mM DTT, and an oxygen scavenging system

consisting of 250 μg ml^{-1} glucose oxidase, 30 μg ml^{-1} catalase and 4.5 mg ml^{-1} glucose. Oxygen scavenging is absolutely required to maintain protein function during trap-based assays, since trap lasers damage proteins when free oxygen is present (Neuman, Chadd et al. 1999; Neuman and Block 2004).

Our experiments are performed at the temperature of the microscopy room (usually set at 22° C), rather than at 37° C where microtubule stability would be higher. Working at room temperature avoids the need to warm the specimen stage with a localized heat source, which can interfere with the stability of the position detection system. Typically, we include 9 to 12 μM tubulin, which is enough to grow dynamic extensions of several micrometers (despite the relatively cool temperature) while maintaining a relatively high rate of catastrophe. Higher tubulin concentrations can be used to grow longer extensions, with a concomitant decrease in the rate of spontaneous catastrophes.

The motility assay

The assay begins with a search for free beads. Singlet beads appear as symmetrical rings when out of focus and they exhibit more rapid Brownian motion than doublets and other bead clumps. Once a singlet bead is trapped, the tip of an anchored, growing microtubule filament is brought near the bead by controlling the piezo stage manually using joystick input. A good microtubule has a discernible plus-end extension (typically longer and faster-growing than the minus end) bent slightly upward from the coverslip surface by thermal motion, minimizing any potential undesirable coverslip interactions. The microtubule tip is repeatedly brought into proximity of the bead, and the signal from the position sensor is displayed in real time on an x-y plot (e.g., on an oscilloscope) to monitor bead motion in the lateral plane. A dramatic reduction in bead deflection along the microtubule axis characterizes a binding event and is usually accompanied by decreased Brownian motion of the free microtubule extension.

For initial testing and troubleshooting, it can be informative to observe bead-microtubule interactions under gentle conditions, without any trap-applied force. This is easily accomplished by shuttering the trap off once the bead binds a microtubule filament. Without tensile force, we find that Ndc80-coated beads usually diffuse randomly along the microtubule lattice, showing no particular preference for growing tips (Powers, Franck et al. 2009). In contrast, tip-attached Dam1-coated beads often undergo persistent movement coupled to microtubule growth (Asbury, Gestaut et al. 2006), indicating that the Dam1 complex has a higher affinity for growing tips than for the microtubule lattice. Shortening microtubule tips drive Ndc80- and Dam1-coated beads alike in the direction of disassembly (Asbury, Gestaut et al. 2006; Westermann, Wang et al. 2006; Powers, Franck et al. 2009). Because thermal bead fluctuations are large during experiments without tensile load, high-resolution laser-based position tracking is unwarranted. Instead, we measure the durations of these events and the distances travelled using standard video tracking methods. Both Dam1- and Ndc80-based linkages support microtubule-driven movement across distances comparable to or exceeding the displacements of chromosomes during mitosis (Asbury, Gestaut et al. 2006; Powers, Franck et al. 2009).

Applying the feedback-controlled force clamp

In vivo, the linkage between a kinetochore and a microtubule tip sustains tensile load continuously, even as thousands of tubulin subunits are added and removed from the tip. To test our reconstituted couplers under continuous load, we use a computer-controlled feedback system

to implement a force clamp. The clamp automatically moves the piezo stage to accommodate changes in filament length while keeping the bead-trap separation, Δx, fixed (Fig. 3). Since the optical restoring force is proportional to Δx, this automatically keeps the force constant (i.e., with RMS deviations less than 0.2 pN). Changes in filament length are then recorded by monitoring the movement of the stage.

Using stage-based feedback to clamp the force provides numerous benefits. Most importantly, it allows continuous loading during long-distance movements, up to the maximum travel of the piezo stage (100 μm), which is essential for tracking the micrometer-scale movements produced in our assays. Simpler fixed trap systems, such as those used previously to study force production via biotin-avidin linkages to disassembling microtubules (Grishchuk, Molodtsov et al. 2005), can only measure displacements < 200 nm, because of the small size of the trap. A second benefit is that keeping the force constant simplifies data interpretation, since bead movement in this case is a direct reflection of the movement of the molecular coupler. In contrast, bead displacements measured without a force clamp are attenuated—by an unknown fraction that can vary with force—relative to that of the coupler, owing to its series elastic compliance (Svoboda, Schmidt et al. 1993; Visscher and Block 1998). A third benefit is that continuous tensile force facilitates collection of records with higher spatiotemporal resolution, since tension suppresses Brownian fluctuations. With a few pN of tension, our assay typically yields recordings with ~5 nm RMS noise, a vast improvement over the ~300 nm RMS noise typical of our records from experiments without load. Further improvement may be possible if higher forces can be sustained.

When positioned at the tip of a growing microtubule and placed under 0.5 to 3 pN of continuous tension, a bead coated with either the Dam1 or Ndc80 kinetochore complex often remains tip-bound, moving slowly away from the anchored seed as the filament lengthens by several micrometers or more (Asbury, Gestaut et al. 2006; Franck, Powers et al. 2007; Powers, Franck et al. 2009). Depending on the catastrophe frequency, the bead sometimes remains attached long enough for the microtubule to undergo a spontaneous catastrophe and begin shortening, driving the bead back toward the seed and performing mechanical work against the load of the optical trap (Fig. 3). These observations show that Dam1- and Ndc80-based linkages can make a direct and significant contribution to kinetochore-microtubule coupling and microtubule-driven force production.

A word of caution is in order regarding comparative single molecule measurements. Although rarely mentioned, it is common to observe considerable variability in behavior from molecule to molecule, filament to filament, slide to slide, day to day, and protein preparation to preparation, even in the simplest of single molecule assays (e.g., even in studies of individual kinesin motors). Consequently, small datasets are untrustworthy, since they can misleadingly show apparent differences between conditions that represent random variability rather than true, statistically significant differences. To guard against this, we pool many measurements made across multiple days and multiple protein preparations whenever possible. An advantage of the *in vitro* methods described here is that very little protein is required per experiment, so small preparations are usually adequate for many repetitions.

New and improved: ramping instead of clamping, and laser scissors

Recently we added two new features to our trapping instruments to improve versatility and productivity. The first improvement was to create a force ramp that gradually increases the

applied force. Ramping the force is useful for determining rupture force distributions, as a measure of attachment robustness. To implement a simple force ramp, we modified our previously-developed force clamp software so that the bead-trap separation, rather than being held constant, is increased gradually at a user-specified constant rate (and the trap power remains fixed). This scheme allows ramping from roughly 10% to 100% of the maximum (escape) force that the trap is capable of exerting. An alternative scheme, where the trap power is increased while the bead-trap separation is held fixed, would provide greater dynamic range but it requires additional optical elements (e.g., an acousto-optic modulator) (Visscher and Block 1998). Using our force ramp, we are beginning to test whether Dam1 and Ndc80 complexes working in tandem form load-bearing attachments that are more processive and support greater loads than either complex alone.

In previous work we measured disassembly-driven movement under force by waiting for catastrophes, spontaneous switches from growth to shortening [51]. Since the beads often detached prior to catastrophe, collecting a large, statistically significant data set was difficult. The task would be easier if one could induce microtubule disassembly at will. Several novel methods for this have been described, including photodamage of stabilizing fluorescent GMPCPP caps [62], mechanical severing of filaments by a microneedle [71], and filament severing by a UV laser [72]. We sought a method that could be easily incorporated into our existing system without requiring fluorescent GMPCPP caps. The transmissivity of our objective precluded addition of a UV laser, and our need for oil-immersion on both sides of the sample (for imaging microtubules by DIC) made addition of a microneedle difficult. Instead, we found that an inexpensive, 100 mW, 473 nm blue laser (LaserPath Technologies, DPSS-473–100) focused to a narrow ellipse cuts microtubules within seconds of initial exposure, even in the presence of oxygen scavenger, inducing disassembly of any remaining lattice (Fig. 4). This ‘laser scissor’ is introduced via an auxiliary port on the microscope body and reflected into the objective by a dichroic mounted in the standard Nikon fluorescence filter cube turret. The blue laser is aligned so that its focus is offset several microns from the trapping laser,
ensuring that it does not interfere with trap operation. Individual microtubules are cut by moving the stage so that the blue laser impinges on the filament when a manual shutter is opened.

RELEVANCE TO KINETOCHORE BIOLOGY

A fundamental unanswered question about kinetochore function is which components participate in formation of load-bearing attachments to dynamic microtubule tips. Feedback-controlled optical trapping is already helping to answer this question by enabling quantitative assessment of coupling performance in reconstituted systems. For example, the performance of Ndc80- and Dam1-based couplers is comparable in many ways to the behavior of kinetochore-microtubule linkages during mitosis, indicating that these subcomplexes probably make a direct and significant contribution *in vivo*. Other components are also likely to participate. For example, a network of three subcomplexes, the Ndc80 complex, the Mtw1 complex (also called MIND or the Mis12 complex), and Spc105 (also called Blinkin or Knl-1), may act cooperatively to form the core, conserved microtubule-binding interface of the outer kinetochore (Cheeseman, Chappie et al. 2006). Comparative measurements of the coupling performance of these subcomplexes, both individually and in various combinations, will allow their contributions to kinetochore-microtubule attachment to be mapped.

Our optical force clamp has also enabled us to study how tensile forces, transmitted through specific tip-attached proteins, affect the dynamics of microtubules. Force-dependent microtubule regulation is often invoked to explain how the intrinsically random growth and shortening of spindle microtubules is controlled to achieve much more orderly behaviors that are hallmarks of mitosis, such as the congression and coordinated oscillations of sister kinetochores (Skibbens, Skeen et al. 1993), the formation of spindles of stereotypical size (Goshima, Wollman et al. 2005), and the positioning of spindles (or nuclei) centrally within dividing cells (Daga, Yonetani et al. 2006). By using our feedback-controlled optical trap, we demonstrated for the first time that tension transmitted through a kinetochore component (the Dam1 complex) affects microtubule shortening speed, catastrophe frequency (the rate of switching from growth to shortening) and rescue frequency (the rate of switching from shortening to growth) (Franck, Powers et al. 2007). These effects may explain how sister kinetochores oscillate in a coordinated fashion by tugging on one another to induce nearly-synchronous reversals in direction (Skibbens, Skeen et al. 1993), and how kinetochore movements may be influenced by gradients in 'polar ejection forces' to bring chromosomes to the equator during metaphase (Rieder and Salmon 1994). In principle, tension-dependent regulatory effects might also occur at spindle poles and the cell cortex, where they could help control spindle size and position.

CONCLUSION

The utility of optical trapping for biophysics comes from its ability to measure forces and movements generated by molecular systems, with high spatiotemporal resolution. Given the importance of force production at kinetochores and the regulatory effects of force on kinetochore-microtubule attachments, quantitative studies using optical traps should continue to provide key insights into kinetochore function.

FIGURES

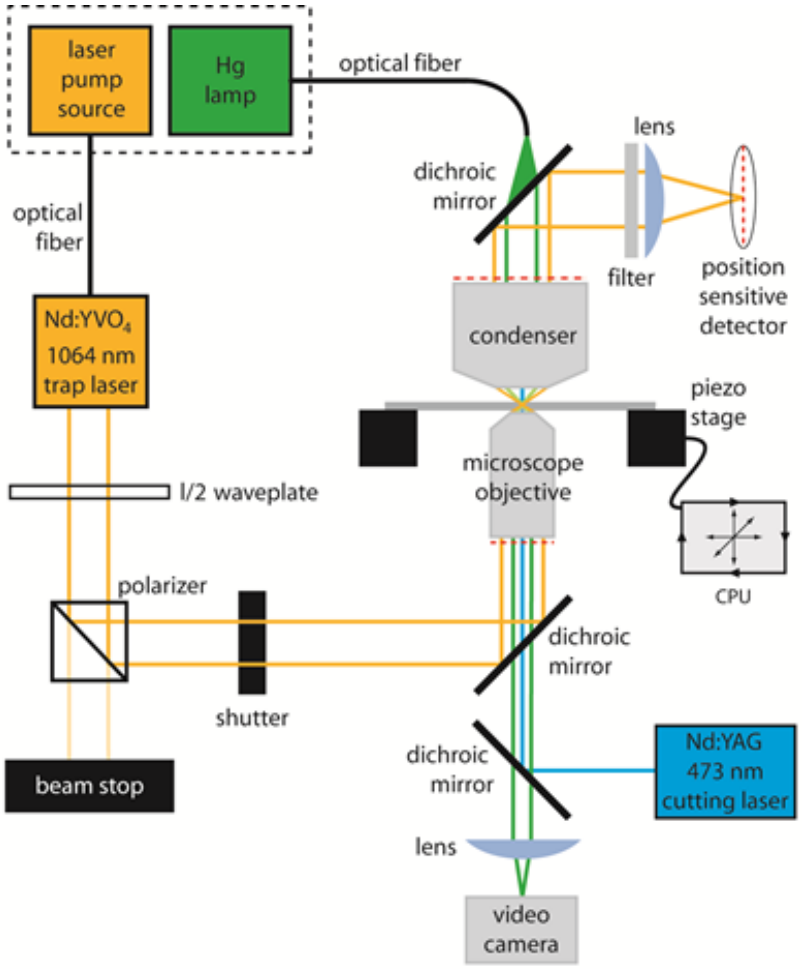

Figure 1: Layout of a simple feedback controlled optical trap

The diode pump source for the 1064 nm laser and the mercury arc lamp are located outside the microscope room (dashed box) to minimize heat and noise and are coupled via optical fibers to the laser head and microscope. The waveplate and polarizer select a fraction of the total power from the trapping laser as a stiffness adjustment. An operator-controlled shutter is used to turn the trap on and off during experiments. The trapping beam enters and exits the microscope via dichroic mirrors which pass light in the visible range for specimen illumination and laser scission. A filter and lens isolates the trapping beam and images it on a position sensitive detector. Beam position data from the detector is used to move the piezo specimen stage by computer controlled feedback. A video camera is used for contrast-enhanced DIC imaging of individual microtubules. A second dichroic introduces the 473 nm microtubule cutting laser into the microscope objective.

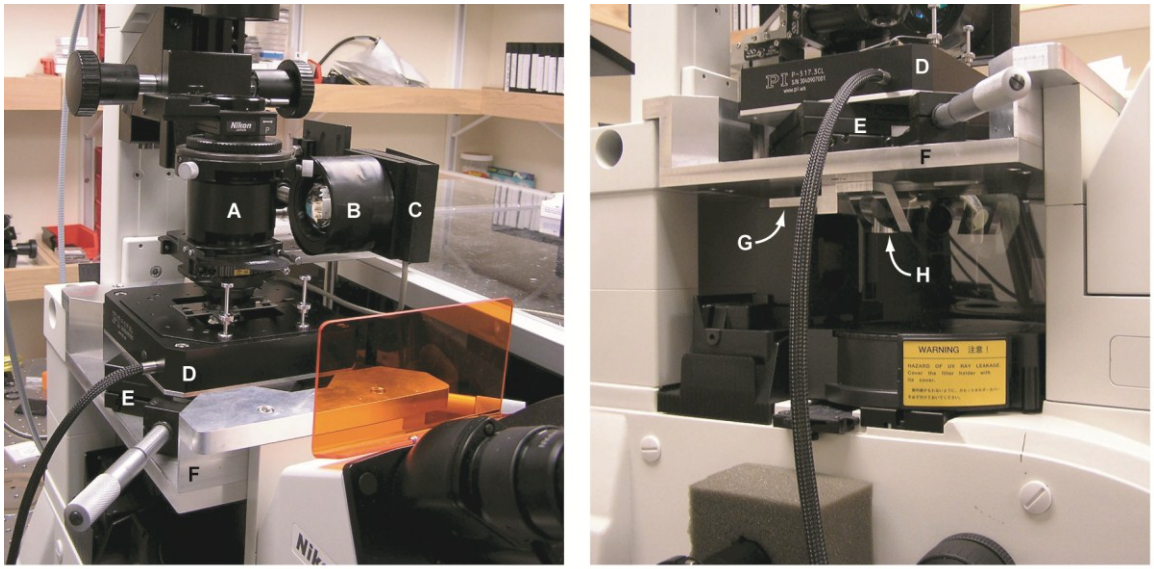

Figure 2: Microscope customizations for adding photodetector, stages, and trap laser

(Left) View of condenser assembly and stages. We modified a hollow extension tube (**A**) to hold the dichroic mirror that deflects light scattered upward from the trap through a hole (out of view) cut through the right side of the tube. A separate lens and filter assembly (**B**) focuses the scattered light onto the photodetector (**C**). The piezo stage (**D**) sits atop a manual stage (**E**). A custom platform (**F**) is required to accommodate the height of the stages. (Right) Side view showing stages (**D**, **E**) and additional modifications underneath the custom platform (**F**). We replaced the stock objective turret with a custom piece (**G**) that holds a single objective lens (plus a Wollaston prism) and dove-tails into the Nikon focusing mechanism. Another custom piece (**H**), fixed to the underside of the platform (**F**), holds the dichroic that deflects the trap laser into the objective.

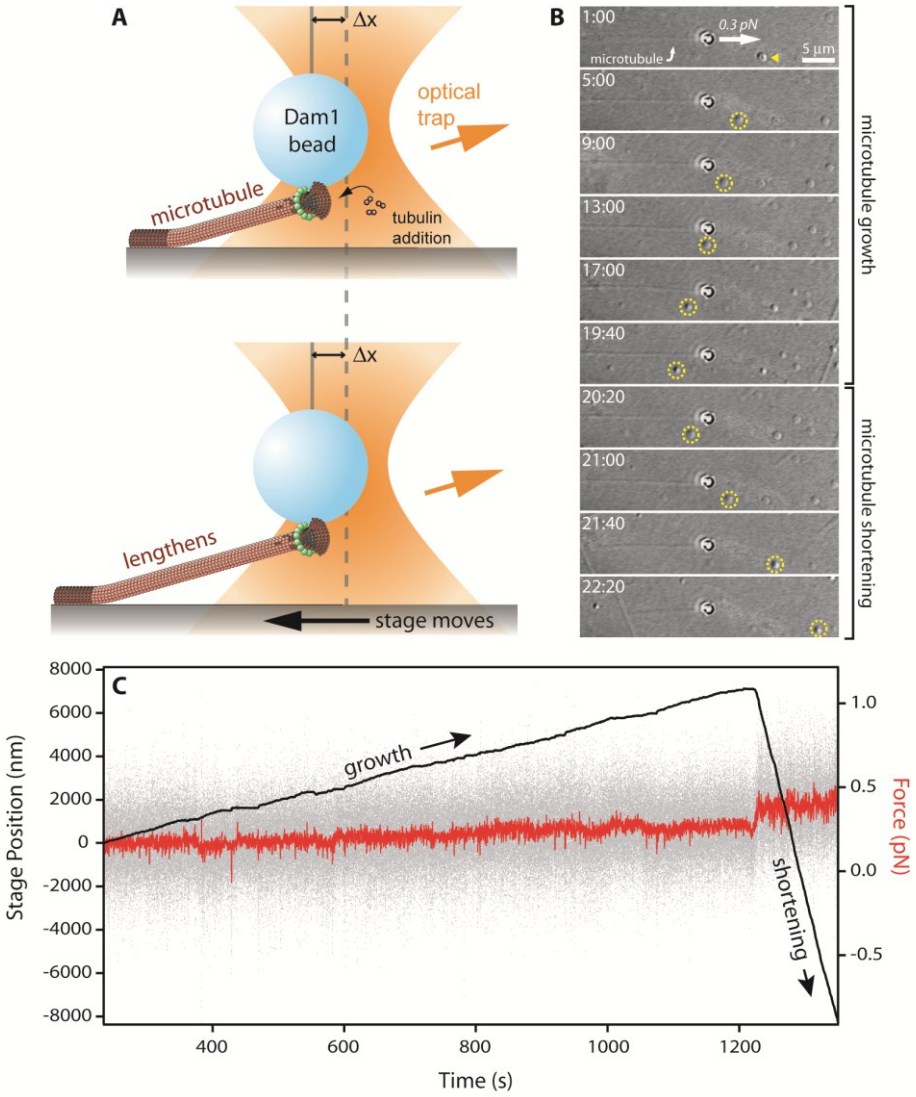

Figure 3: Applying continuous tension with a stage-based force clamp

(**A**) Dynamic microtubules are grown from stable, coverslip-anchored seeds. Polystyrene beads coated with purified recombinant kinetochore protein (here, the Dam1 complex) are bound to the microtubule tip using a stationary optical trap, and tension is applied to the bead-microtubule interface by positioning the stage to create an offset, Δx, between the trapping laser and the bead. As the microtubule grows and shortens, the stage is moved under feedback control to keep Δx constant. (**B**) DIC filmstrip of a Dam1 complex-coated bead tracking with microtubule growth (1 min: 00 sec to 19:40) and shortening (20:20 to 22:20) under constant force (0.25 and 0.4 pN, during growth and shortening, respectively). The stage is moved leftward during growth, as evident by a coverslip-adsorbed fiducial (yellow arrowhead, circles), and rightward during shortening. (**C**) Record of stage position (black trace) and force (instantaneous, gray trace; average, red trace) over time for the event depicted in (B).

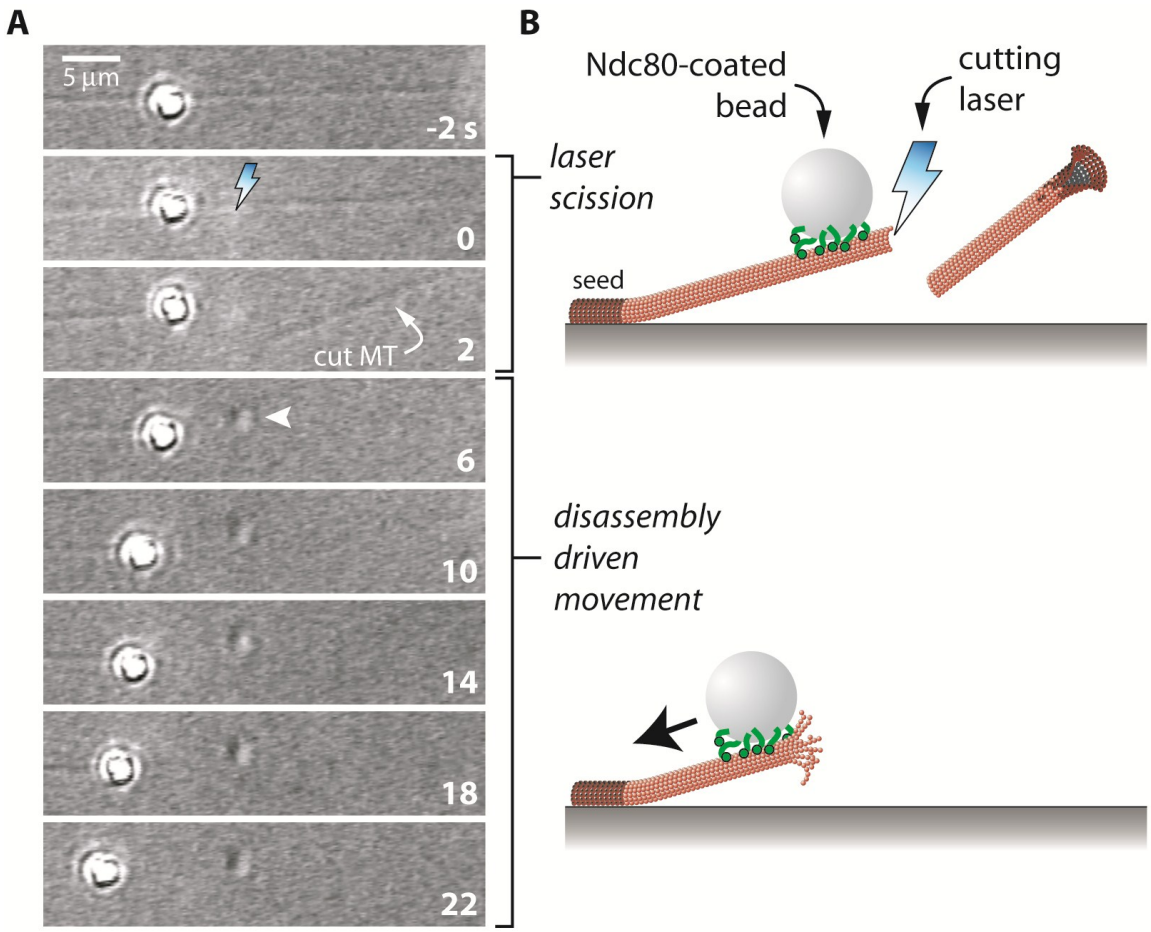

Figure 4: Inducing microtubule disassembly with laser scission

(**A**) DIC filmstrip and (**B**) cartoon depiction of laser scission-induced disassembly of a dynamic, coverslip-anchored microtubule. At t = -2s, a Dam1 complex-coated bead is bound to the lattice of a dynamic microtubule. The microtubule is then cut following a 2 second exposure to a 473 nm cutting laser (lightning bolt), causing the microtubule tip to diffuse away and inducing disassembly of the newly created tip (t = 2 s). Exposure to the cutting laser leaves an impression on the coverslip surface (arrowhead). When the shortening microtubule tip reaches the lattice-bound bead, the bead undergoes disassembly-driven movement toward the microtubule seed.

Chapter 3

The Dam1 Kinetochore Complex Harnesses Microtubule Dynamics to Produce Force and Movement

Originally published in the Proceedings of the National Academy of Sciences of the United States of America 103 (2006) 9873–9878

ABSTRACT

Kinetochores remain attached to microtubule (MT) tips during mitosis even as the tips assemble and disassemble under their grip, allowing filament dynamics to produce force and move chromosomes. The specific proteins that mediate tip attachment are uncertain, and the mechanism of MT-dependent force production is unknown. Recent work suggests that the Dam1 complex, an essential component of kinetochores in yeast, may contribute directly to kinetochore–MT attachment and force production, perhaps by forming a sliding ring encircling the MT. To test these hypotheses, we developed an *in vitro* motility assay where beads coated with pure recombinant Dam1 complex were bound to the tips of individual dynamic MTs. The Dam1-coated beads remained tip-bound and underwent assembly- and disassembly-driven movement over ~3μm, comparable to chromosome displacements *in vivo*. Dam1-based attachments to assembling tips were robust, supporting 0.5–3 pN of tension applied with a feedback-controlled optical trap as the MTs lengthened ~1μm. The attachments also harnessed energy from MT disassembly to generate movement against tension. Reversing the direction of force (i.e., switching to compressive force) caused the attachments to disengage the tip and slide over the filament, but sliding was blocked by areas where the MT was anchored to a coverslip, consistent with a coupling structure encircling the filament. Our findings demonstrate how the Dam1 complex may contribute directly to MT-driven chromosome movement.

INTRODUCTION

A long-standing mystery of mitosis is how kinetochores interact with the tips of microtubules (MTs) to organize and move chromosomes (Inoue and Salmon 1995; McIntosh, Grishchuk et al. 2002; Gadde and Heald 2004). A common view is that motor proteins of the kinesin and dynein families mediate tip attachment, but conventional motors cannot completely account for the interactions between kinetochores and MTs. Conventional motors bind and walk along the sides of the filaments (Howard 1996; Vale 2003). In contrast, kinetochores remain attached to the filament tips even as the tips assemble and disassemble under their grip, undergoing back-and-forth movements that are tightly coupled to tip growth and shortening (Skibbens, Skeen et al. 1993; Inoue and Salmon 1995). Even when conventional motors are removed or disrupted, kinetochores harness energy from MT disassembly to produce force and movement (Inoue and Salmon 1995). Thus kinetochores possess a non-conventional MT-based motility mechanism that relies on filament growth and shortening to drive movement.

While a number of candidate MT-binding proteins are found at kinetochores, the relative contributions these molecules make to MT-driven motility are unknown. In principle, 'plus-end-tracking' proteins (+TIPs), which co-localize with growing MT tips in cells (Schuyler and Pellman 2001) might be involved. However, +TIPs are static with respect to the MT lattice

(Perez, Diamantopoulos et al. 1999; Tirnauer, Grego et al. 2002) and they have never been shown to mediate MT-driven cargo transport *in vitro*. Beads coated with inactivated kinesin and dynein motors can remain attached to disassembling MT tips *in vitro* (Lombillo, Stewart et al. 1995), probably because the motors provide a large number of weak, transient binding interactions with the filaments (Lombillo, Stewart et al. 1995; Peskin and Oster 1995). But these motor-based tip attachments are sensitive to buffer conditions (Inoue and Salmon 1995; Lombillo, Stewart et al. 1995) and it is unclear whether they are robust enough to support the tensile loads supported by kinetochore-MT junctions *in vivo*. Furthermore, deletion of kinetochore motors in budding (Cottingham, Gheber et al. 1999) and fission yeast (West, Malmstrom et al. 2001; Garcia, Koonrugsa et al. 2002) causes relatively mild phenotypes, suggesting that kinetochore-MT attachment in these organisms may not require motors (McIntosh, Grishchuk et al. 2002). Thus, considerable uncertainty remains about the molecular mechanism by which kinetochores maintain load-bearing attachments to MT tips.

Recent work suggests the Dam1 complex (also called DASH or DDD), an essential component of kinetochores in yeast (Cheeseman, Enquist-Newman et al. 2001; Jones, He et al. 2001; Li, Bachant et al. 2002), makes a direct contribution to tip attachment and MT-driven movement. The Dam1 complex consists of ten subunits that co-purify as a stable heterodecamer (Cheeseman, Brew et al. 2001; Miranda, De Wulf et al. 2005) with biochemical affinity for MTs (Hofmann, Cheeseman et al. 1998; Cheeseman, Brew et al. 2001). The complex is required for sister kinetochores to make bipolar, load-bearing attachments to MTs from opposite spindle poles (He, Rines et al. 2001; Janke, Ortiz et al. 2002). Electron microscopy reveals that when pure recombinant Dam1 is mixed with stabilized MTs it oligomerizes into rings (each containing many individual complexes) that surround the filaments (Miranda, De Wulf et al. 2005; Westermann, Avila-Sakar et al. 2005). Theoretical considerations suggest such rings may represent optimal structures for harnessing energy from MT disassembly to produce motion and force (Hill 1985; Koshland, Mitchison et al. 1988; Molodtsov, Grishchuk et al. 2005). Additional support for a direct role in MT attachment is provided by time-lapse fluorescence microscopy showing that Dam1 co-localizes with the tips of disassembling MTs *in vitro* (Westermann, Wang et al. 2006). However, while these observations are provocative, they do not establish whether the complex can link cargo to both assembling and disassembling tips, or whether Dam1-based tip attachments support tension—two key properties necessary for persistent kinetochore-to-MT attachment *in vivo*. Moreover, evidence that the rings seen by electron microscopy are important for tip tracking or other Dam1 functions is lacking.

Using a newly-developed *in vitro* motility assay, we show here that the Dam1 complex can couple cargo to the tips of individual dynamic MTs. Dam1-based tip attachments remain bound during both filament assembly and disassembly, moving several micrometers and supporting tension applied continuously with a feedback-controlled optical trap. These results demonstrate that the complex can contribute significantly to force production and MT-driven chromosome movement during yeast mitosis. We also find that Dam1-based linkages exhibit unique mechanical behaviors, such as sliding movements that are blocked by areas where the MT is anchored to a coverslip, which suggest a coupling structure encircling the MT.

RESULTS

The Dam1 complex couples cargo to dynamic MT tips

In our experiments, beads coated with the Dam1 complex were bound to the tips of individual dynamic MTs polymerized from stable, coverslip-anchored seeds (Dogterom and Yurke 1997; Janson, de Dood et al. 2003). The filaments exhibited dynamic instability typical for MTs *in vitro* (Walker, O'Brien et al. 1988), with periods of slow growth interrupted occasionally by rapid shortening that usually continued until the filament disassembled completely and just the seed remained. Dam1-coated beads were introduced into the slide and then tested for MT binding using an optical trap (Lang, Asbury et al. 2002; Asbury, Fehr et al. 2003; Block, Asbury et al. 2003). Each candidate bead was held near the tip of an assembling MT until it bound, or until 1 – 2 min had passed without binding. Beads coated with the Dam1 complex frequently bound the MT tip (15%, 88 of 574 beads tested). Control beads without complex did not bind (89 beads tested). Dam1 beads active in MT binding could usually be reattached repeatedly to different MTs and the fraction of active beads was not reduced when free complex was removed from the buffer by centrifugation (21%, 27 of 128 washed beads tested). These observations show that MT attachment depends on Dam1 complexes stably bound to the bead, and suggest that free Dam1 in solution is not required.

The Dam1 complex mediated persistent attachment to the tip of a dynamic MT, allowing filament assembly and disassembly to drive bead movement (Fig. 1 and Movies 1 – 3, which are included as supplemental online material). Initially, we recorded movement in the absence of external load by shutting off the optical trap after MT binding. During assembly without load, tip-attached beads moved away from the anchored MT seed, as the length of intervening filament increased (Fig. 1a, 0 – 835 s, and Movie 1). Assembly-driven movement usually continued for several minutes, terminating in one of three ways: (1) the bead detached from the growing MT (~41%); (2) the bead remained attached but disengaged from the tip as the filament continued to lengthen (~24%); (3) the filament spontaneously underwent catastrophe, switching abruptly to rapid shortening (~35%). After catastrophe, tip-attached beads were carried toward the seed, in the direction of filament shortening (Fig. 1a, 835 – 850 s, and Movies 2 and 3). Disassembly-driven beads usually (~96%) detached before the filament had shortened completely back to the seed (Movie 3 is an exception).

We quantified Dam1-based movement in the absence of load by tracking beads in video recordings (Fig. 2). On average, assembly-driven beads moved 2400 ± 220 nm (avg. ± s.e.m., N = 54) before detaching, disengaging from the tip, or switching to disassembly-driven movement (Fig. 2b). Disassembly-driven beads moved 3400 ± 420 nm (N = 26) before detaching (Fig. 2c). Periods of bead movement lasted 200 ± 24 s (N = 67; Fig. 2d), and the velocities of assembly- and disassembly-driven movement, 11 ± 1.0 nm s^{-1} and 490 ± 46 nm s^{-1}, were similar to growth and shortening rates for microtubules alone (Walker, O'Brien et al. 1988). At the spatial resolution of these records (~290 nm RMS, limited by thermal motion of the bead), the movement usually appeared smooth (Fig. 2a).

The Dam1 complex supports tension and harnesses energy from MTs to produce force

To apply tensile force in the bead assay, a tip-attached bead was held continuously in the optical trap, and its position monitored by back focal plane interferometry (Lang, Asbury et al. 2002) (Fig. 3). The force was kept constant using a feedback-controlled piezoelectric stage to maintain a fixed offset between the bead and the trap center (Lang, Asbury et al. 2002; Asbury,

Fehr et al. 2003; Block, Asbury et al. 2003) (see Movies 4 and 5). Even with 0.5 to 3 pN of continuous tension, the complex maintained a robust link to an assembling tip that persisted, on average, for 250 ± 70 s and moved 700 ± 170 nm in the direction of filament growth before detachment or catastrophe (N = 40; Fig. 3c and d). Distributions of attached times and distances moved were broad and included very long events where attachment lasted > 300 s and the bead moved > 1000 nm (Fig. 3c and d). The applied tension reduced thermal fluctuations, allowing movement to be recorded with comparatively high spatial resolution (~5 nm RMS, depending on the series elastic compliance of the filament, the complex, etc.). Viewed in finer detail, the movement appeared irregular, including pauses, rapid jumps, and periods of relatively smooth motion (Fig. 3a and b).

The Dam1 complex harnessed energy released during MT disassembly to produce mechanical work. Linkages supporting tension during assembly-coupled movement sometimes remained attached long enough for the filament to undergo catastrophe. When this occurred, the bead usually reversed direction (~80%), moving against the applied force toward the MT seed (Fig. 3a inset, 3b, and Movie 5). Moving against 0.5 to 3 pN of tension, beads traveled between 40 and 480 nm, with an average displacement of 170 ± 60 nm (N = 9; Fig. 3e). These observations show that Dam1-based tip attachments allow disassembling MTs to generate forces comparable to those produced by conventional motor proteins such as dynein and kinesin (Block, Asbury et al. 2003). We note that the 0.5 to 3 pN of tension we applied did not stall disassembly-driven movement, so higher forces can theoretically be produced. However, applied tension caused more frequent detachment of the bead from the MT, so episodes of disassembly-driven movement were observed less frequently and they produced shorter displacements than in the absence of external load.

The Dam1 complex forms a coupler that slides along the MT

We began each experiment by attaching a Dam1 bead to the tip of a filament. However, tip-attached beads undergoing assembly-driven movement without load sometimes disengaged from the tip but remained attached to the lattice (i.e. they stopped moving and the tip grew beyond the point at which they were attached). When this occurred, a brief pull toward the tip could reposition the bead onto the tip and restart assembly-driven movement. Conversely, pushing tip-attached beads toward the coverslip-anchored seed invariably caused them to disengage the tip and slide along the filament. By using feedback control to apply a pushing force of 0.2 – 1.3 pN, beads could be displaced by many micrometers along the MT without detachment (N = 74 sliding events, averaging 5100 ± 300 nm; Fig. 4a, Movies 6 and 7). Several lines of evidence demonstrate the beads remained attached during sliding. First, when the trap was shut off during sliding the beads remained associated with the MT and underwent thermal motion synchronous with that of the filament (N = 11; Movies 8 and 9). If detachment had occurred, the beads would simply have diffused away. Second, recorded position signals showed that frictional forces (0.2 – 1.3 pN) were transmitted to the beads during sliding. This friction was much greater than the viscous drag caused by movement through the surrounding fluid. Third, when beads reached the filament tips, sliding stopped (N = 32; Movies 6 – 9). If the beads had been free or bumping along the coverslip surface, the force clamp would have continued to push them past the tip of the filament.

Both the MT seed and the assembling tip presented barriers to sliding. When a sliding bead reached the anchored MT seed, movement halted (N = 23; Movies 6 and 7). If the direction

of force was then reversed, the bead could be pulled back to the tip where sliding stopped and the bead resumed assembly-coupled movement, which was slower and easily distinguished from sliding. The response to force at either barrier was asymmetric. The same magnitude of force that was insufficient to slide a bead past the anchored seed or the assembling tip, when reversed, could readily move it back from these barriers onto the intervening portion of the filament (N = 34 total observations, including 17 each at the tip and the seed; Fig. 4b). Importantly, there was no discernible delay between force reversal and the onset of sliding. This observation shows that the barrier-like behavior does not arise from a higher affinity of Dam1 for the seed or tip relative to the MT lattice.

In most of our experiments, the anchored MT seeds differed from the free extensions in their composition. The seeds contained GMPCPP for stabilization, rather than GDP, and were biotinylated to facilitate anchoring to the coverslip (ratio of biotinylated to native tubulin, 1:75). To test whether these differences were responsible for the barrier-like behavior at the seed, we grew uniform MTs with GMPCPP and biotin incorporated along their entire length. Dam1-coated beads bound readily and slid along these MTs. The barrier-like behavior was qualitatively unchanged (N = 26 total observations, including 13 each at the seed and the tip; Fig. 5, included as supplementary online material). This observation shows that blockage at the seed is not due to differences in MT composition.

DISCUSSION

Our experiments demonstrate several remarkable and previously unobserved properties of the Dam1 complex, which indicate it can contribute directly to MT attachment and MT-driven movement of kinetochores in yeast. We find the complex can link cargo to both growing and shortening MT tips, allowing filament assembly and disassembly to drive movement over several micrometers (Figs. 1 and 2). Dam1-based linkages remain tip-bound for long times, even with applied tension (Fig. 3). The attached times, often > 3 min, are similar to the time over which kinetochore-MT junctions support tension during mitosis in yeast, 2 – 10 min (He, Rines et al. 2001; Sanchez-Perez, Renwick et al. 2005). Yeast kinetochores in metaphase make MT-driven oscillatory movements 200 – 600 nm in amplitude (He, Rines et al. 2001; Pearson, Maddox et al. 2001) and they are pulled ~500 nm toward spindle poles in anaphase (Pearson, Maddox et al. 2001). We show here that Dam1 linkages allow MTs to drive movement *in vitro* over similar distances and to generate significant pulling forces, in the 0.5 to 3 pN range. This level of force is similar to what is generated by ATP-powered motors that move various organelles inside living cells (e.g., neuronal vesicles, mitochondria, pigment granules in melanophores, etc. (Vale 2003)). Thus the Dam1 complex forms load-bearing tip attachments that are stable over the relevant time scale, that generate movement over relevant distances, and that produce forces sufficient to drive organelle movement. These observations, together with the established requirement for the Dam1 complex at kinetochores (Cheeseman, Enquist-Newman et al. 2001; Jones, He et al. 2001; Li, Bachant et al. 2002), strongly suggest it makes a direct contribution to MT-driven kinetochore movement *in vivo*.

Thousands of tubulin subunits were added to or removed from the filament tip during a typical MT-driven movement in our assays, yet Dam1-based linkages remained tip-bound. This ability may depend on interactions with the GTP-containing subunits that cap growing tips, or with unique structural features at the tips of growing and shortening MTs. During shortening, a disassembling tip becomes frayed as individual rows of subunits (protofilaments) curl and peel

away from the main filament before breaking off (Mandelkow, Mandelkow et al. 1991; Tran, Joshi et al. 1997). During growth, newly added subunits are thought to form a flared sheet that closes into a tube (Chretien, Fuller et al. 1995; Wang and Nogales 2005).

An attractive model for Dam1-based MT attachment postulates that it depends on ring-like structures encircling the filament (Koshland, Mitchison et al. 1988; Miranda, De Wulf et al. 2005; Westermann, Avila-Sakar et al. 2005). In this view, an appropriately-sized ring slides over the MT lattice but is unable to slide past areas where the filament is wider, such as a frayed tip. During disassembly, ring movement could be driven by biased diffusion (Hill 1985; Koshland, Mitchison et al. 1988), or by a conformational wave where the frayed tip pushes continuously against the ring while propagating in the direction of shortening (Koshland, Mitchison et al. 1988). Consistent with this picture, the Dam1 rings seen by electron microscopy appear large enough to slide over the filaments (32 – 35 nm ring inner diameter (Miranda, De Wulf et al. 2005; Westermann, Avila-Sakar et al. 2005) compared to ~25 nm MT outer diameter (Mandelkow, Mandelkow et al. 1991)) but too small to slide past disassembling tips (typically ~50 nm in width (Mandelkow, Mandelkow et al. 1991)). However, electron microscopy studies of yeast kinetochores have so far failed to find evidence for rings *in vivo* (McIntosh 2005). Observations of fluorescent-tagged Dam1 diffusing along stabilized MTs and accumulating at disassembling MT tips during filament shortening (Westermann, Avila-Sakar et al. 2005; Westermann, Wang et al. 2006) are also consistent with the ring model, but these activities can be explained by alternative mechanisms that do not depend on rings. One such mechanism, for example, has been proposed where coupling is provided by a disordered collection of proteins with weak MT-affinity, to explain the disassembly-driven movement of motor-coated beads (Lombillo, Stewart et al. 1995). Thus, an important open question is whether the rings that Dam1 forms around MTs are functionally significant.

We found by direct manipulation that Dam1-based attachments slide along the MT when they are pushed with an optical trap, and that both growing tips and coverslip-anchored seeds present barriers to sliding (Fig. 4a). Once a Dam1 coupler comes in contact with either barrier it responds asymmetrically to force: if the direction of force is maintained (i.e. the force is directed toward the barrier) no further movement occurs, but if the direction of force is reversed the coupler slides immediately back away from the barrier (Fig. 4b). These are predicted behaviors for a ring or collar that closely surrounds the filament. Such a collar would be topologically prevented from sliding past the coverslip-anchored seed, but would slide back immediately upon force reversal because the blockage occurs for purely structural reasons. A similar structural picture can explain the barrier-like behavior at assembling tips. Flared protofilament sheets are thought to occur at growing MT tips (Chretien, Fuller et al. 1995; Wang and Nogales 2005). If the flares are wide enough they will also block ring sliding (Fig. 4c). An alternative interpretation is also possible, where coupling is based on biochemical or electrostatic affinity for the MT. Weak affinity for the MT lattice could produce a coupler that slides along the filament without detaching (Hill 1985; Lombillo, Stewart et al. 1995; Peskin and Oster 1995), and an abrupt loss of affinity at the seed or the tip might present an energetic barrier that prevents sliding past these locations (Hill 1985). However, blockage at the seed does not arise from differences in biotin labeling or GMPCPP incorporation (Fig. 5), arguably the two features most likely to alter affinity of Dam1 for the seed. Based on these considerations, we think coupling in our assays is more likely to depend on Dam1-based structures that encircle the filaments. We note that our beads are coated with many Dam1 complexes (presumably thousands), so their

attachment to MTs probably involves many individual complexes. Further experiments will be necessary to determine the minimum number of complexes and the structural requirements for attachment.

In summary, we have demonstrated how the Dam1 complex can contribute directly to kinetochore-MT attachment and chromosome movement in yeast by forming load-bearing attachments to both growing and shortening MT tips. By direct manipulation, we show that Dam1-based MT attachments exhibit unique mechanical properties that are consistent with a coupling structure encircling the filament. In the future, we anticipate our biophysical approach will be useful for further testing this hypothesis, and for studying various functional aspects of Dam1 and other MT-binding kinetochore components.

MATERIALS AND METHODS

Protein purification

All 10 subunits of the Dam1 complex were expressed in *E. coli* (BL21 Rosetta, Novagen) from a single plasmid (gift of J.J. Miranda, Harvard) and purified essentially as described (Miranda, De Wulf et al. 2005; Westermann, Avila-Sakar et al. 2005). The gene for one subunit (Spc34p) included a His_6-tag to facilitate purification and bead binding. Cells harboring the plasmid were induced to express the complex in mid-log phase by addition of 0.2 mM IPTG, grown for 5 hrs at 37 °C, pelleted, and snap frozen. Pellets were re-suspended in PB (20 mM phosphate, pH 7.0, 500 mM NaCl, 1 mM PMSF and Complete protease inhibitors without EDTA, (Roche)), lysed in a French press, and clarified by centrifugation. The supernatant was mixed with metal-affinity resin (Talon, BD Biosciences), washed in PB, and eluted with 200 mM imidazole. The eluate was purified on a size-exclusion column (Superdex 200 10/300GL, Amersham Biosciences), equilibrated with PB, and snap frozen in 5 µl aliquots.

Motility assays

To bind the His_6-tagged complex, 0.44-µm-diameter streptavidin-coated polystyrene beads (Spherotech) were further functionalized by incubation with biotinylated penta-His antibody (Qiagen) and washed in BRB80 (80 mM Pipes, 1 mM $MgCl_2$, 1 mM EGTA, pH 6.9) plus 8 mg ml^{-1} bovine serum albumin (BSA), included as a blocking protein. Beads functionalized with anti-His antibody were used for the negative binding control experiments. Dilute suspensions of anti-His beads (0.01 – 0.05% solids) were coated with Dam1 by mixing with 0.2 – 6.5 µM of the complex in BRB80 plus BSA and incubating > 30 min. In many experiments, free Dam1 was removed from the beads by centrifugation before introducing them into the flow chamber. Washing away free complex did not significantly change the behavior of MT-attached beads, so data from washed and unwashed beads are combined in Fig. 2. The experiments with applied force (i.e., Figs. 3 – 5) were performed with washed beads. Stable MT seeds were grown by incubating 68 µM bovine brain tubulin, 1 µM biotinylated tubulin (Cytoskeleton), and 1 mM GMPCPP (Jena Bioscience) in BRB80 plus 10% glycerol at 37 °C for > 30 min. KOH-cleaned coverslips were fixed with double-stick tape to glass slides to create flow chambers, which were functionalized by incubation with 5 mg ml^{-1} biotinylated BSA (Vector Labs) followed by 1 mg ml^{-1} avidin DN (Vector Labs). Seeds were bound and then washed with GB (BRB80 plus BSA with 1 mM GTP) prior to introduction of Dam1 beads and tubulin (at indicated concentrations) in GB supplemented with 1 mM DTT and an oxygen

scavenging system consisting of 250 μg ml^{-1} glucose oxidase, 30 μg ml^{-1} catalase, and 4.5 mg ml^{-1} glucose. After MT growth, thermal fluctuations tended to bend the extensions slightly away from the coverslip, making them easily distinguishable from coverslip-bound seeds and their tips accessible for bead binding. All values reported in the text are mean ± s.e.m. unless otherwise noted. Assays were performed at 22 °C.

Instrumentation and data collection

The optical trap was essentially as described elsewhere (Lang, Asbury et al. 2002; Asbury, Fehr et al. 2003; Block, Asbury et al. 2003), except a single laser was used for trapping and position detection, and it was not steered by acousto-optic deflectors. For assays without applied load, bead positions were tracked in recorded videos at 30 Hz using custom software written in LabView (National Instruments). For the force-clamp assays, position sensor response was mapped using the piezo stage to raster-scan a stuck bead through the beam, and trap stiffness was calibrated along the two principle axes using the drag force, equipartition, and power spectrum methods (Lang, Asbury et al. 2002). Feedback was implemented with custom LabView software. During clamping, bead-trap separation was sampled at 40 kHz while stage position was updated at 50 Hz to maintain the desired load. Bead and stage position data were decimated to 200 Hz before storing to disk. To minimize force errors, trap stiffness was chosen so that bead-trap separations > 50 nm achieved the desired load (Lang, Asbury et al. 2002). To slide Dam1 beads along MTs over distances > 500 nm, it was helpful to apply load gently by using feedback control to keep the force below 1 or 2 pN. Manually applying load with hand micrometers or a joystick-operated piezo usually caused detachment.

FIGURES

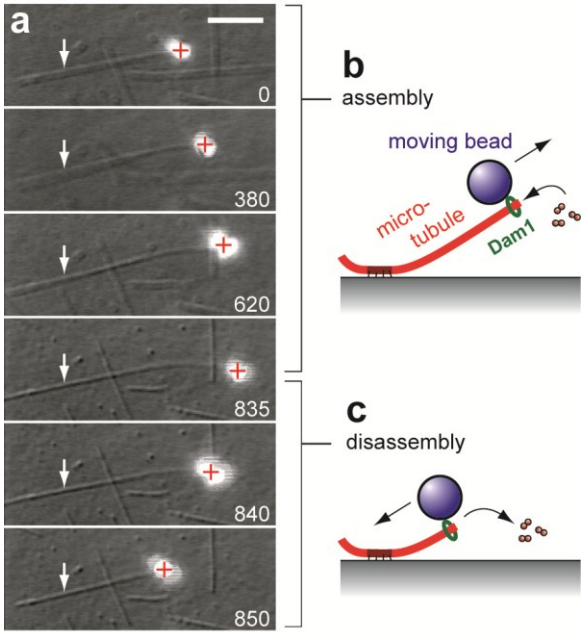

Figure 1: Dam1 couples cargo to the tips of assembling and disassembling MTs.

(**a**) Selected frames from a movie (Movie 1, included as supplemental online material) in which movement of a Dam1-coated bead is driven by MT assembly (0 – 835 s) and disassembly (835 – 850 s). Approximate locations for the coverslip-anchored portion of the MT seed (arrows) and the bead center (crosses) are indicated. Elapsed times are in seconds. Scale bar, 5 μm. (**b** and **c**) Schematic diagrams of the Dam1 bead motility assay. During assembly (b), the MT grows slowly by addition of tubulin subunits to the tip. During shortening (c), tubulin subunits are rapidly lost from the tip. During both phases, Dam1-based linkages remain tip-bound.

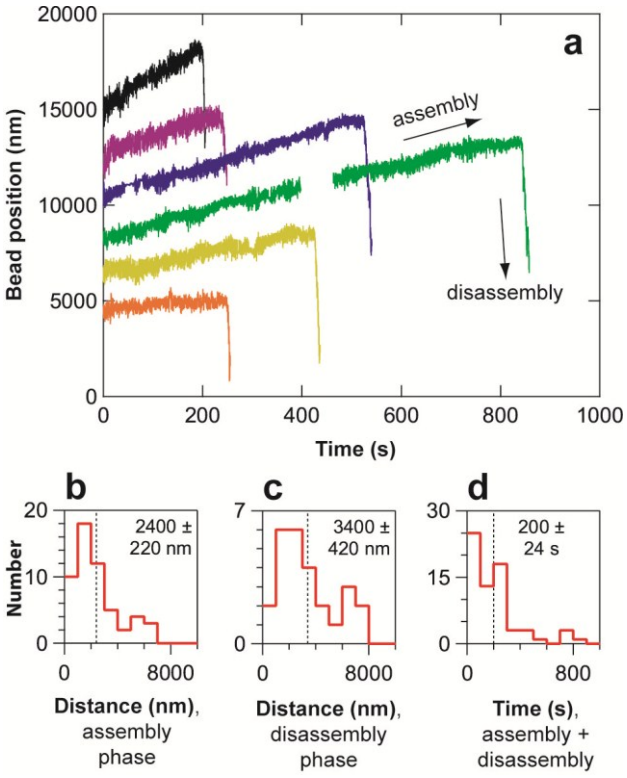

Figure 2: MTs drive movement of Dam1-based linkages over several micrometers.

(**a**) Records of bead position versus time measured without applied force showing slow assembly-driven movement followed by rapid disassembly-driven movement. Increasing position represents movement away from the anchored portion of the MT. For clarity, each record is offset vertically by an arbitrary amount. (**b** – **d**) Histograms of bead displacement during MT assembly (b), bead displacement during disassembly (c), and total duration (including both assembly and disassembly phases) of MT-driven movement (d) for a population of beads. Dotted vertical lines indicate the mean value for each histogram. These data were recorded at a tubulin concentration of 17 μM.

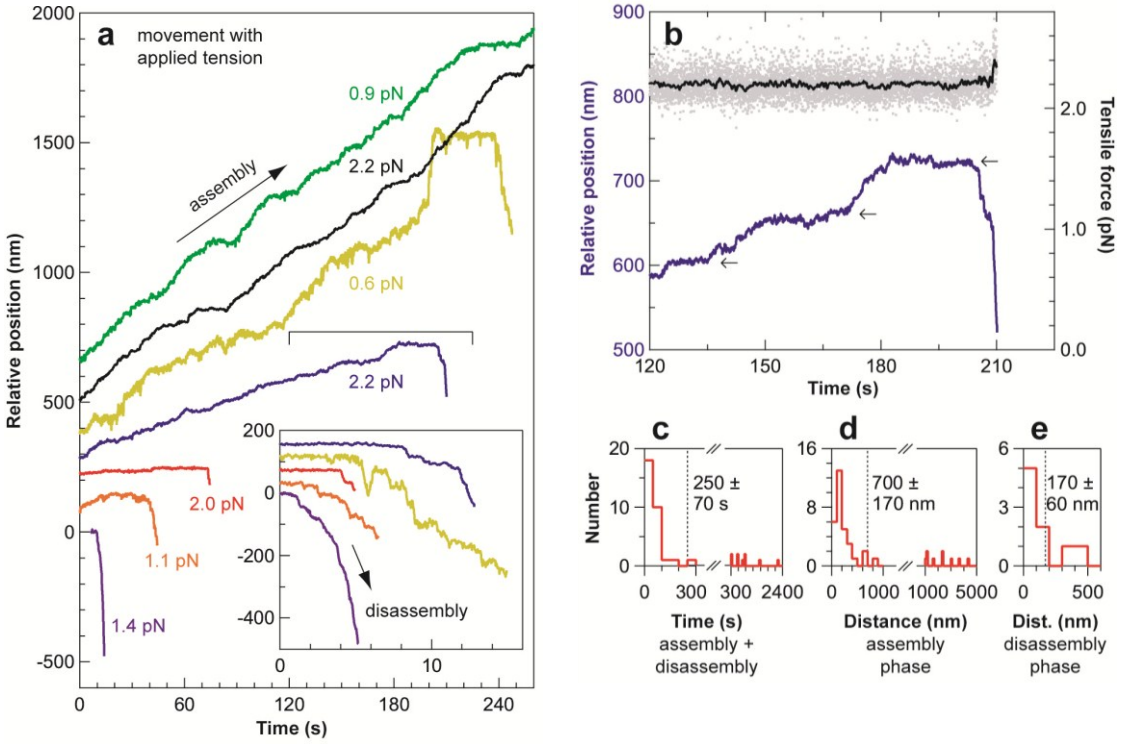

Figure 3: Dam1-based linkages remain tip-attached even when tension is applied.

(**a**) Records of bead position versus time during continuous application of tensile load using a feedback-controlled optical trap. Increasing position represents assembly-coupled movement in the direction of applied force, away from the anchored portion of the MT (e.g., green and black traces, blue trace < 200 s). Some records terminate with episodes of disassembly-driven movement against the load (e.g. blue trace, 200 – 210 s), expanded views of which are shown in the inset. Records are offset vertically (and horizontally in the inset) for clarity. (**b**) Expanded view of the bracketed portion of the record in (a), showing transition from assembly- to disassembly-driven movement (blue trace). Arrows highlight positions where the bead paused during movement. The measured bead-trap separation is shown above (black trace, scale at right), after converting to force by multiplying by the trap stiffness. The gray dots show raw data, and the black trace shows the same data after smoothing with a 500 ms sliding boxcar average. (**c** – **e**) Histograms of total attached time (including both assembly and disassembly phases) (c), distance moved during assembly (d), and distance moved during disassembly (e) for tip-attached beads moving under 0.5 to 3 pN of tension. Dotted vertical lines indicate the means for each histogram. Tubulin concentration, 10 μM. (Figure layout is modified from original.)

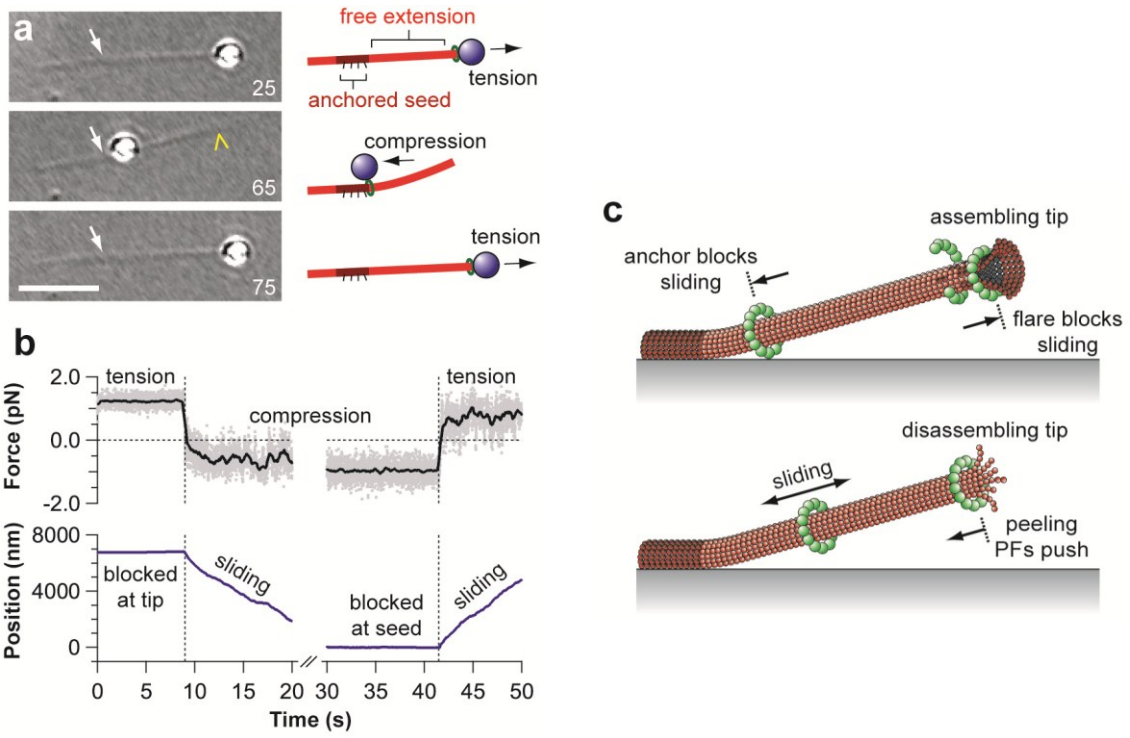

Figure 4: Dam1-based couplers slide over the MT lattice without detaching, and both the growing tip and the coverslip-anchored portion of the MT present barriers to sliding.

(**a**) Selected frames from a movie are shown (Movie 6), beginning with a tip-attached bead under tension (25 s). Reversing the direction of load (i.e. switching to compression) causes the bead to disengage the tip (denoted by the yellow chevron) and slide until it reaches the seed (white arrow), where sliding halts (65 s). Reversing the load again (i.e. reapplying tension) causes the bead to slide back and reengage the tip (75 s). Scale bar, 5 mm. (**b**) Beads located at the growing tip or the anchored seed respond asymmetrically to force: the same magnitude of force that is insufficient to slide them past the barrier, when reversed, immediately causes the bead to slide back away from the barrier. The lower plot shows bead position versus time, and the upper plot shows bead-trap separation after conversion to force by multiplying by the trap stiffness. Gray dots show raw data, black trace shows same data after smoothing with a 500 ms window. Dashed vertical lines mark the time when force was reversed. (**c**) Ring model for Dam1-based attachment and movement. In this view, between 10 and 16 Dam1 complexes (Miranda, De Wulf et al. 2005; Westermann, Wang et al. 2006) oligomerize into a ring encircling the filament that is large enough to slide over the lattice (arrows), but too small to slide past areas where the filament is widened. Such a ring would be topologically prevented from sliding past the anchored segment of the MT (dotted line at left), as we observed. Growing tips also blocked sliding, perhaps due to the flared protofilament sheets that are thought to occur at assembling tips (Chretien, Fuller et al. 1995; Wang and Nogales 2005). Protofilaments (PFs) curl and peel away from the main filament during disassembly (Mandelkow, Mandelkow et al. 1991; Tran, Joshi et al. 1997), and could push continuously against a Dam1 ring to drive movement in the direction of shortening. An alternative model, where coupling is provided by a disordered collection of MT-binding proteins, is also consistent with our observations (see Discussion).

SUPPLEMENTAL FIGURE

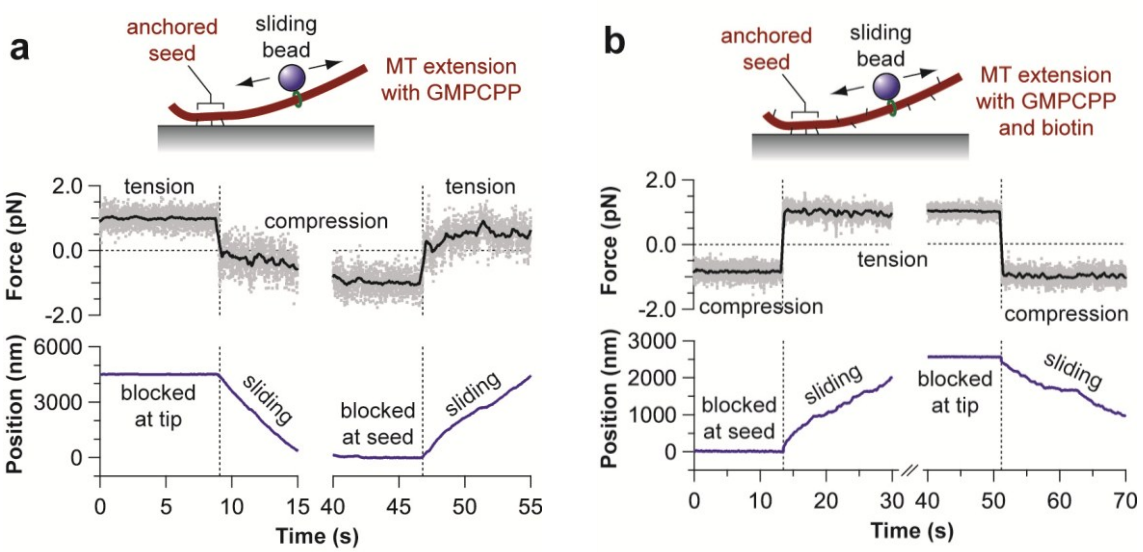

Figure 5: The barrier-like behavior at the seed does not arise from differences in the composition of the seed relative to the extension.
(**a**) Blockage at the seed (and the tip) occurs on MTs containing GMPCPP along their entire length.
(**b**) Blockage also occurs on filaments containing both GMPCPP and biotin along their entire length. The same ratio of biotinylated to native tubulin (1:75) was used to grow the seeds and the extensions. Pre-blocking the avidin-coated surface with free biotin prior to growing the extensions prevented them from binding the surface. The lower plot in each panel shows bead position versus time, and the upper plot shows bead-trap separation after conversion to force by multiplying by the trap stiffness. Gray dots show raw data, black trace shows same data after smoothing with a 500 ms window. Dashed vertical lines mark the time when force was reversed. (Supplemental online figure; layout is modified from original.)

Chapter 4

The Ndc80 Kinetochore Complex Forms Load-Bearing Attachments to Dynamic Microtubule Tips via Biased Diffusion

Originally published in Cell 136 (2009), 865–875.

SUMMARY

Kinetochores couple chromosomes to the assembling and disassembling tips of microtubules, a dynamic behavior that is fundamental to mitosis in all eukaryotes but poorly understood. Genetic, biochemical and structural studies implicate the Ndc80 complex as a direct point of contact between kinetochores and microtubules, but these approaches provide only a static view. Here, using techniques for manipulating and tracking individual molecules *in vitro*, we demonstrate that the Ndc80 complex is capable of forming the dynamic, load-bearing attachments to assembling and disassembling tips required for coupling *in vivo*. We also establish that Ndc80-based coupling likely occurs through a biased diffusion mechanism, and that this activity is conserved from yeast to humans. Our findings demonstrate how an ensemble of Ndc80 complexes may provide the combination of plasticity and strength that allows kinetochores to maintain load-bearing tip attachments during both microtubule assembly and disassembly.

INTRODUCTION

Chromosomes are organized and separated during cell division by a molecular machine, the mitotic spindle. A central component of this machine is the kinetochore, a specialized site on each chromosome that forms attachments to spindle microtubules. Besides mechanically coupling the chromosomes to microtubules, kinetochores are also regulatory hubs. They control chromosome movement by altering the growth and shortening of attached microtubules, they sense and correct errors in attachment, and they emit diffusible 'wait' signals until they are properly attached. These regulatory functions are all vital for accurate mitosis, and they are all related to microtubule attachment. To understand kinetochore function, the basis for its most fundamental behavior—microtubule attachment—must be uncovered.

As the spindle forms, kinetochores make initial attachments to the sides of spindle microtubules. These lateral ('side-on') attachments convert quickly into ('end-on') tip attachments and thereafter, chromosome movement is coupled to filament assembly and disassembly (Rieder and Salmon 1998). Kinetochore-microtubule coupling requires a puzzling combination of strength and dynamicity. Molecules at each kinetochore-microtubule interface must maintain a persistent, load-bearing attachment to the filament tip even while thousands of tubulin subunits are added and removed. This strong yet dynamic coupling allows kinetochores to harness microtubule shortening to drive poleward chromosome movement and also to track with growing tips during anti-poleward movement (or during microtubule 'flux'). While the behavior is conserved from yeast to humans (Rieder and Salmon 1998; McAinsh, Tytell et al. 2003), its molecular basis remains uncertain.

Models for kinetochore-microtubule coupling fall into several classes. In one class, coupling is based on ATP-powered motor enzymes. Motors likely contribute to coupling in many organisms (Sharp, Rogers et al. 2000; Yang, Tulu et al. 2007), and some motors can

mediate attachment to disassembling tips *in vitro* (Lombillo, Stewart et al. 1995). However, kinetochore-bound motors are largely dispensable in yeast (McAinsh, Tytell et al. 2003; Grishchuk and McIntosh 2006) and their depletion in higher eukaryotes does not completely disrupt tip attachment (Weaver, Bonday et al. 2003; Kapoor, Lampson et al. 2006; Yang, Tulu et al. 2007). In a second class of models, peeling protofilaments at disassembling tips drive kinetochore movement either by pushing against a sliding ring (Koshland, Mitchison et al. 1988) or by tugging on tightly-bound kinetochore fibrils (McIntosh, L. et al. 2008). Enthusiasm for the ring model was generated recently by the discovery that the Dam1 kinetochore complex forms rings around microtubules *in vitro* (Miranda, De Wulf et al. 2005). However, while the Dam1 complex is very likely to contribute to tip coupling, microtubule-based force production, and regulation of kinetochore-attached microtubules in yeast (Asbury, Gestaut et al. 2006; Westermann, Wang et al. 2006; Franck, Powers et al. 2007; Tanaka, Kitamura et al. 2007), no clear homologues have been identified outside fungi. Moreover, ring formation is not required for microtubule-driven movement of the Dam1 complex *in vitro* (Gestaut, Graczyk et al. 2008). The fibrils model offers an attractive, ring-independent way for peeling protofilaments to exert force on the kinetochore (McIntosh, L. et al. 2008). However, processive disassembly-driven movement by this mechanism requires tight binding of the fibrils to the microtubule, which would prevent assembly-coupled movement. Thus neither motor-, ring-, nor tight fibril-based mechanisms appear to fully account for tip coupling in all eukaryotes.

In a third class of models, kinetochore-microtubule coupling depends on biased thermal diffusion. This idea was first proposed by Hill (1985), who demonstrated theoretically that an array of individually weak microtubule binders will track with disassembling microtubule tips provided that its diffusion along the filament is sufficiently fast and that its total binding energy is large enough. Because this mechanism provides molecular friction that resists translocation of the microtubule through the attachment, it is sometimes called a 'slip clutch' (Maddox, Straight et al. 2003). Importantly, a biased diffusion-based coupler supports tension continuously while remaining tip-attached during both assembly and disassembly. This behavior distinguishes it from models based on ATP-powered motor proteins or peeling protofilaments, which are fundamentally unidirectional. Although Hill imagined a sleeve-like arrangement of binding elements completely encircling the filament, the physical underpinnings of his model can apply generally to any array of microtubule binders that are linked together, even a disordered array.

Extensive genetic, biochemical and structural studies have established that the Ndc80 complex is crucial for maintaining a robust attachment between kinetochores and microtubule tips across eukaryotes (reviewed in Tanaka and Desai 2008). However, the ability of the complex to support the strong yet dynamic attachment required for kinetochore-microtubule coupling has never been demonstrated. Here we show that ensembles of Ndc80 complexes can form load-bearing attachments to assembling and disassembling tips. The properties of this attachment can be fully described by a biased diffusion mechanism. Based on these findings, we propose that the Ndc80 complex forms a slip clutch at the eukaryotic kinetochore.

RESULTS

The Ndc80 complex couples cargo to dynamic microtubules

To study Ndc80-based coupling we adapted a recently developed bead motility assay (Asbury, Gestaut et al. 2006; Franck, Powers et al. 2007). All four subunits of the *S. cerevisiae* Ndc80 complex, Ndc80, Nuf2, Spc24, and Spc25, were co-expressed in *E. coli* and purified by

affinity chromatography followed by gel filtration (Wei, Sorger et al. 2005; Gestaut, Graczyk et al. 2008) (Figure S1). Purification and binding of the complex to beads were facilitated by a His_6-tag on the C-terminus of Spc24, a location near the kinetochore-facing end of the complex (~20 nm away) and farther (~40 nm) from the N-terminal regions of Ndc80 and Nuf2 shown previously to mediate binding to taxol-stabilized microtubules (Wei, Sorger et al. 2005; Cheeseman, Chappie et al. 2006; Wei, Schnell et al. 2006; Ciferri, Pasqualato et al. 2008). Beads decorated with the complex were introduced into a chamber containing dynamic microtubules growing from stable, coverslip-anchored seeds. The filaments exhibited dynamic instability typical for microtubules *in vitro*, switching stochastically between periods of slow growth (at ~10 nm s^{-1}) and rapid shortening (~100 nm s^{-1}). To test for binding, candidate beads diffusing freely in solution were captured with a laser trap and held near the tip of a growing filament. Binding was evident from a sharp reduction in the Brownian motion of the bead, which was monitored with high spatiotemporal resolution using back focal plane interferometry (Asbury, Gestaut et al. 2006; Franck, Powers et al. 2007). Beads coated with full-length Ndc80 complex almost always bound microtubules (82%, 42 of 51 beads tested). Control beads coated with a 'headless' version of the complex, 2NCC:2S, lacking the N-terminal regions of Ndc80 and Nuf2 (Wei, Sorger et al. 2005), failed to bind (116 tested). Thus binding of Ndc80-coated beads to assembling microtubule tips in our assay requires the same molecular domains that mediate binding of the free complex to taxol-stabilized microtubules.

In our initial experiments we shut off the laser trap when the bead bound the microtubule tip to record movement in the absence of external load. Without load, the beads exhibited longitudinal diffusion along the filament as the tip continued to grow (65%, 26 of 40 beads tested; see Figure 1) or remained stationary on the microtubule lattice (35%, 14 of 40). Most attachments persisted until the filament tip underwent a spontaneous 'catastrophe', disassembling rapidly back to the bead and then carrying it in the direction of shortening (73%, 29 of 40), usually all the way to the coverslip-anchored seed (52%, 21 of 40). Most of the remaining events were terminated artificially (40%, 16 of 40), often because the bead stuck irreversibly to the coverslip. Spontaneous detachment from the microtubules was rare (8%, 3 of 40). We used automated centroid tracking from video recordings to quantify bead position over time (Figure 1C). The Ndc80-based attachments remained bound to the filaments for a mean duration of 180 ± 30 s (Figure 1F) and underwent disassembly- driven movement over 4,800 ± 400 nm on average (Figure 1E). These values underestimate the capacity of the linkages to remain bound and track with disassembly, because most events were terminated by the microtubule shortening completely back to the seed, not by detachment. For the subset of beads that diffused along the filaments, mean squared displacement increased linearly with time and indicated a diffusion constant of 2,300 ± 400 nm^2 s^{-1} (Figure 1D). The diffusion was unbiased. Diffusing and non-diffusing beads alike were able to track with disassembly (Figure 1C). These observations demonstrate that the Ndc80 complex forms persistent dynamic attachments to microtubules, allowing filament disassembly to drive movement.

Coupling and force production are conserved properties of the Ndc80 complex

To determine whether the ability to form dynamic, load-bearing tip attachments is conserved in the human Ndc80/Hec1 complex, all four subunits were co-expressed in *E. coli* and purified by affinity chromatography followed by gel filtration (Figure S1). As above, a His_6-tag on the C-terminus of Spc24 was used both for purification and bead binding. Beads coated with

the full-length Ndc80/Hec1 complex behaved similarly in force clamp experiments to those coated with the yeast complex. After attachment to a growing tip and placement under 0.5 to 2.5 pN of tension, the beads often remained tip-bound for many minutes through phases of filament growth and shortening (Table S1; Figure S2A). The mean displacements during filament assembly, 1,900 ± 300 nm (N = 46), and disassembly, 970 ± 270 nm (N = 25), and the average duration of attachment, 280 ± 50 s (N = 50), were comparable to those measured for the yeast complex (see Figure S2B – D). These results show that the capacity of the Ndc80 complex to couple force to dynamic microtubule tips is conserved from yeast to humans.

Coupling and force production persist at low surface densities

Kinetochores *in vivo* contain 6 to 30 copies of the Ndc80 complex per attached microtubule (Emanuele, McCleland et al. 2005; Joglekar, Bouck et al. 2008). To estimate the number of complexes required *in vitro* for a load-bearing coupler we measured coupling performance as a function of the surface density of Ndc80 on the beads. Anti-His beads (at 5.6 pM) were incubated with the His_6-tagged yeast Ndc80 complex at molar ratios ranging from 110 to 2,700 complexes per bead. At each molar ratio, we measured displacements for a population of tip-attached beads subject to 1 pN of continuous tension during microtubule growth and, if possible, during shortening. We also calculated detachment rates for each condition by counting the number of detachment events and dividing by the total observation time. At molar ratios of ~360 complexes per bead and higher (i.e., ≥ 2 nM Ndc80 complex), we routinely observed tip attachments that persisted for minutes and moved 400 to 1,000 nm during growth and shortening (Figure 3A). Below ~360 complexes per bead, the detachment rate from growing tips increased (Figure 3B), an effect that reduced the distance moved during growth and made measurements during shortening more difficult (because fewer beads remained bound long enough for the filament to undergo catastrophe). Below ~110 complexes per bead (< 0.6 nM Ndc80 complex), microtubule binding still occurred but the beads detached within a few seconds when placed under tension. These observations suggest a lower bound for the formation of a load-bearing coupler of ~360 complexes per bead.

Simple geometric considerations indicate that Ndc80 complexes on only a small fraction of the bead surface, ≤ 4%, can simultaneously interact with the microtubule (Figure 3C). Assuming a random distribution of complexes on the bead surface, 360 complexes per bead corresponds to 14 ± 5 interacting with the filament. This calculation may overestimate the number of interactions, since it assumes (1) that all Ndc80 complexes are functional, (2) that they bind very efficiently to the bead surface, (3) that every bead-bound Ndc80 complex within 40 nm can attach to the filament, and (4) that the bead rests directly against the side of a filament whose tip extends > 120 nm past the point of contact. Relaxing any of these assumptions would lead to a lower estimate. We also note that our estimate includes a relatively large uncertainty (± 33%) arising from the inherent uncertainty in our measurements of bead and protein concentration, and from counting statistics (see Materials and methods). Nevertheless, we can conclude that the number of microtubule-interacting Ndc80 complexes required to form a load-bearing coupler in our bead assay is close to the 6 to 30 found at kinetochores *in vivo*.

Individual Ndc80 complexes exhibit diffusion along microtubules

To study interactions between Ndc80 complexes and microtubules at the level of single molecules, we applied total internal reflection fluorescence (TIRF) microscopy (Figure 4). A

fluorescent-tagged version of the yeast complex was created by fusing green fluorescent protein (GFP) to the C-terminus of Nuf2, a modification which causes no detectable phenotype *in vivo* (Shimogawa, Graczyk et al. 2006). At the low concentrations of free Ndc80 necessary for recording single molecules (i.e., < 10 nM), we observed very little binding in a standard microtubule growth buffer. However, in buffers with reduced ionic strength and at a concentration of 20 pM, individual fluorescent particles of Ndc80 complex bound transiently to taxol-stabilized microtubules and underwent one-dimensional diffusion along the filaments (Figure 4B). The brightness of the particles suggested they were composed of one or two complexes. Most disappeared in a single step, which probably represents detachment from the microtubule (Figure 4C). However, a small fraction showed a stepwise loss of half their intensity while they remained attached to the filament, consistent with photobleaching of one GFP molecule within a particle containing two. We fit the initial brightness distribution for all the particles by the sum of two Gaussian functions (Figure 4D), corresponding to a large population (89%) with a unitary brightness of 16,200 ± 5,500 arbitrary units and a small population (11%) with twice the brightness (32,400 ± 5,500 a.u.). The unitary brightness was similar to that of individual GFP molecules, 17,000 ± 11,000 a.u., measured in control experiments where GFP-MCAK was bound tightly to microtubules under otherwise identical conditions (data not shown).

Sensitivity to ionic strength is a hallmark of protein-protein interactions that rely on electrostatic attraction. To quantify the sensitivity of Ndc80-microtubule interactions to ionic strength, we recorded particle binding and diffusion on taxol-stabilized microtubules across a range of total potassium ion concentrations from 30 to 90 mM (Figure 5). At each potassium ion concentration, we measured association and dissociation rates, k_{on} and k_{off}, and used these values to estimate an equilibrium dissociation constant, $K_d = k_{off} \cdot k_{on}^{-1}$. Diffusion coefficients were estimated for each condition from linear fits to plots of mean squared displacement versus time. Raising the ionic strength lowered the association rate (i.e., fewer particles bound) and also increased the dissociation rate (residence times became shorter). As a result the apparent K_d increased 4-fold, from 0.23 ± 0.02 μM at 30 mM potassium to 0.84 ± 0.12 μM at 90 mM potassium (Figure 5D). These K_d values fall within the range of previous estimates, which vary from 0.04 μM to 3 μM depending on the Ndc80 construct and the buffer composition (Cheeseman, Chappie et al. 2006; Wei, Al-Bassam et al. 2007; Ciferri, Pasqualato et al. 2008). Raising the ionic strength also caused a modest (50%) increase in the apparent diffusion coefficient, which went from 0.117 ± 0.004 $\mu m^2 s^{-1}$ at 30 mM potassium to 0.17 ± 0.01 $\mu m^2 s^{-1}$ at 90 mM potassium (Figure 5E). We note that these changes are unlikely to reflect differences in the oligomeric state of the complex, because particle brightness values were indistinguishable at the three ionic strengths (Figure S3). Collectively, these results show that particles consisting of one or two Ndc80 complexes form transient, electrostatically based interactions with the microtubule that allow rapid diffusion along the filament lattice. Lattice diffusion implies that the energetic barrier for complete detachment of the particles from the microtubule is higher than for movement between neighboring sites on the filament lattice. This confirms a key property required for effective tip coupling via Hill's biased diffusion mechanism.

Ensembles are required for tracking with disassembling tips

Another critical assumption of Hill's model is that when the coupler encounters a disassembling tip its otherwise random diffusion must become biased in favor of movement back

toward the filament lattice. To test this we modified the TIRF assay to study interactions with dynamic rather than stabilized microtubules. Short, GMPCPP-stabilized microtubule seeds were anchored to the coverslip and dynamic extensions of several micrometers were grown from them by the addition of free tubulin and GTP. Fluorescent Ndc80 complex was then introduced by buffer exchange, which also lowered the level of free tubulin to trigger filament disassembly. We used 1 nM Ndc80 complex, a concentration at which the microtubules were crowded with diffusing particles, so that each tip would encounter many particles as it disassembled. No clear tip tracking was evident. However, the density of particles sometimes (15%, 20 of 132 tips recorded) became noticeably higher at a disassembling tip as compared to the lattice. When individual particles could be discerned as they encountered a disassembling tip, they sometimes appeared to 'bounce' repeatedly off the tip, diffusing back onto the lattice rather than dissociating (Figure 6A, top). These observations confirm that the diffusion of Ndc80 particles becomes biased at disassembling tips, as required for the biased diffusion mechanism.

Given the results from our bead assays, we reasoned that tip tracking might occur in our TIRF assay if larger particles containing more complexes could be generated. To test this we recorded the behavior of Ndc80 complexes that had been pre-incubated with antibodies directed against the His_6-tag on Spc24, to drive oligomerization. After antibody treatment, the fraction of disassembling tips that accumulated fluorescent particles was higher (46%, 17 of 35 tips) and they were 3-fold brighter than those in control experiments without antibody treatment (Figure 6B). In addition, some brighter particles in the antibody-treated samples exhibited clear episodes of processive tip tracking (Figure 6A, bottom). Together these observations indicate that tip tracking is not a property exhibited by individual Ndc80 complexes. Assembly of an array of complexes is required.

Biased diffusion fully describes the behavior of Ndc80-based couplers

To test whether the biased diffusion mechanism can account for the performance of Ndc80-based couplers, we used computational (Monte Carlo) methods to simulate Hill's model (1985) with parameters chosen to match the properties of individual Ndc80 complexes. The simulations recapitulate our experimental observations very closely (Figure 7). When bound to growing microtubules in the absence of external load, the simulated couplers have no tendency to follow the tip. Instead, they remain on the microtubule lattice where they exhibit unbiased diffusion at a rate that slows as the number of binders in the ensemble increases (Figure 7B). At disassembling tips their random movement becomes biased: Small, highly diffusive couplers (e.g., with $M = 2$ binding elements) tend to stay ahead of the disassembling tip and only occasionally 'bounce' off the tip (Figure 7A). In contrast, couplers with more elements track unidirectionally with disassembly (Figure 7B). Interestingly, couplers with very high numbers of binders (e.g., $M = 100$) diffuse at undetectably slow rates, yet they still track with disassembling tips (see Supplemental Discussion). When tensile loads are applied, couplers with very few binding elements detach quickly but larger couplers can sustain substantial forces indefinitely. Couplers with $M = 14$ elements, for example, support 2.5 pN while remaining persistently attached to the filament tip over many micrometers of growth and shortening (Figure 7C). These observations show that the behavior of Ndc80-based couplers is well described by a biased diffusion mechanism.

DISCUSSION

The Ndc80 complex can make a direct and significant contribution to kinetochore-microtubule coupling

We measured the mechanical performance of Ndc80-based tip attachments in experiments that recapitulate the *in vivo* situation far more closely than previous assays. Even in the absence of other kinetochore components, we find that the Ndc80 complex can form dynamic tip attachments that permit assembly- and disassembly-coupled movement over distances comparable to the excursions of tip-attached kinetochores *in vivo*, which range from 0.5 to 5 μm depending on the cell type (Pearson, Maddox et al. 2001; Stumpff, von Dassow et al. 2008). Under continuous tensile load the linkages often persist for many minutes, similar to the 2 to 10 minutes during which kinetochores support tension in yeast (Pearson, Maddox et al. 2001). Also, the number of Ndc80 complexes required to form a load-bearing coupler in our assay is close to the 6 to 30 complexes found per microtubule at kinetochores *in vivo* (Emanuele, McCleland et al. 2005; Joglekar, Bouck et al. 2008). The loads we applied here are comparable to the forces supported by kinetochore-microtubule junctions *in vivo*. Thermodynamic considerations suggest that a disassembling microtubule tip might be capable of producing as much as 20 to 60 pN of tensile force (Desai and Mitchison 1997). However, based on the amount of stretching between sister kinetochores and the elasticity of the chromatin that links them, the tension transmitted to bi-oriented sister kinetochores during normal chromosome movement is probably closer to 0.4 to 8 pN per attached microtubule (Nicklas 1988; Pearson, Maddox et al. 2001; see Supplemental discussion; Brower-Toland, Smith et al. 2002). Ndc80-based linkages in our assay support similar forces of 0.5 to 2.5 pN, so the experiments provide a close approximation to the physiological situation.

Ndc80-based coupling likely depends on biased diffusion

At the level of individual complexes, Ndc80 binds microtubules transiently, exhibiting moderate (micromolar) affinity and rapid lattice diffusion. These properties make it ideally suited for efficient tip coupling through a biased diffusion mechanism (Hill 1985). An alternative view proposed recently, that the complex mediates processive attachment to depolymerizing tips by binding tightly to peeling protofilaments (McIntosh, L. et al. 2008), seems less likely given the mobility and transiency of the Ndc80-microtubule interaction (but the mechanism could apply to other kinetochore components). Instead, a mechanism based purely on biased diffusion is sufficient to describe the ability of Ndc80-based couplers to mediate attachments to both polymerizing and depolymerizing tips. Coupling by this mechanism relies on a gradient in binding energy, which exists at any tip, independent of whether it is assembling or disassembling. Importantly, the mechanism accounts for the ability of Ndc80-based couplers to sustain tensile forces comparable to those found *in vivo*. It will also provide molecular friction that resists movement of the microtubule through the attachment (Hill 1985). Together these observations suggest that the Ndc80 complex forms a slip clutch at the kinetochore.

General implications for kinetochore-microtubule coupling

The idea that the Ndc80 complex forms a slip clutch at the kinetochore can explain aspects of spindle physiology. For example, when 9G3 antibodies against Ndc80/Hec1 are injected into dividing cells, kinetochore-microtubule attachments are stabilized, the chromosomes stop oscillating, sister kinetochores become hyperstretched, and kinetochore fiber flux slows (DeLuca, Gall et al. 2006). These changes are all consistent with an increase in molecular friction at the kinetochore. If an ensemble of Ndc80 complexes provides a kinetochore slip clutch, then antibody treatment could dramatically increase its friction by rafting the complexes together or by otherwise tightening their interaction with the filament (e.g., by blocking phosphorylation). The slip clutch idea can also explain the seemingly incongruous observations that the Ndc80 complex possesses only moderate microtubule affinity, yet its depletion results in severe detachment defects without major loss of other microtubule-binding kinetochore components (DeLuca, Moree et al. 2002). Notably, the affinity of the complex for microtubules depends on flexibly tethered positive charges that interact with negative charges on the E-hook of tubulin (Wei, Al-Bassam et al. 2007; Ciferri, Pasqualato et al. 2008). This pliant, electrostatic binding is reminiscent of the charge-charge interactions that allow DNA-scanning enzymes to slide freely over the DNA phosphate backbone (Blainey, van Oijen et al. 2006). If flexibly tethered charges on the Ndc80 complex are the basis for a slip clutch activity at the kinetochore, this would explain why their removal severely compromises kinetochore-microtubule coupling (Guimaraes, Dong et al. 2008; Miller, Johnson et al. 2008).

The fact that kinetochores in all eukaryotes maintain load-bearing attachments to growing and shortening microtubule tips suggests that a common molecular mechanism underlies this behavior. We propose that ensembles of Ndc80 complexes acting through a biased diffusion mechanism supply the combination of plasticity and strength that allows kinetochores to hold on loosely to microtubule tips without letting go.

MATERIALS AND METHODS

Protein expression and purification

The *S. cerevisiae* Ndc80 complex was expressed from two vectors encoding the Ndc80/Nuf2 and Spc24/Spc25 sub-complexes (Wei, Sorger et al. 2005). For fluorescent studies, the Nuf2 gene was substituted with Nuf2-GFP from yeast strain MSY107-5d (Shimogawa, Graczyk et al. 2006). For the human Ndc80/Hec1 complex, a polycistronic vector encoding all four subunits was cloned (see Supplemental materials and methods). All complexes included a C-terminal His_6-tag on Spc24 for affinity purification and bead binding. Purification was carried out as described previously except buffers more amenable to the Ndc80 complex were used (Asbury, Gestaut et al. 2006; Franck, Powers et al. 2007; Gestaut, Graczyk et al. 2008). The buffer for purification over talon resin was 50 mM HEPES (pH 7.6) with 300 mM NaCl, 2.5 U mL^{-1} benzonase, and protease inhibitors (0.01 mg mL^{-1} chymostatin, 0.01 mg mL^{-1} aprotinin, 0.01 mg mL^{-1} leupeptin, 0.01 mg mL^{-1} pepstatin, 0.002 mg mL^{-1} benzamadine and 1 mM phenylmethylsulfonyl fluoride). For gel filtration, 50 mM HEPES (pH 7.6) with 200 mM NaCl was used.

Bead motility assays

Recombinant His_6-tagged Ndc80 complex was linked to 0.44 mm-diameter streptavidin-coated polystyrene beads (Spherotech, Lake Forest, IL) using biotinylated His_5-antibody (Qiagen, Valencia, CA) essentially as described in Asbury et al. (2006) and Franck et al. (2007). The amount of complex per bead was adjusted by incubating dilutions of 0.6 – 15 nM Ndc80 complex, prepared in BRB80 (80 mM PIPES, 1mM $MgCl_2$, 1mM EGTA at pH 6.9) plus 8 mg mL^{-1} bovine serum albumin (BSA) and 1 mM DTT, with a fixed amount of beads (5.6 pM) at 4° C for 90 min. Flow chambers were created by sandwiching two strips of double-sided sticky tape between a KOH-washed coverslip and a standard glass slide, and functionalized by coating with 5 mg mL^{-1} biotinylated BSA (Vector Labs, Burlingame, CA), washing, and then incubating with 0.3 mg mL^{-1} avidin DN (Vector Labs). Stable, biotinylated microtubule seeds were introduced and then washed with growth buffer (BRB80 plus 8 mg mL^{-1} BSA with 1 mM GTP) before introduction of Ndc80-coated beads, which were diluted 8-fold into growth buffer supplemented with 1.5 to 1.9 mg mL^{-1} tubulin, 1 mM DTT and an oxygen scavenging system consisting of 250 µg mL^{-1} glucose oxidase, 30 µg mL^{-1} catalase and 4.5 mg mL^{-1} glucose. Assays were performed at 22° C.

TIRF microscopy assay

Flow cells for TIRF experiments were prepared as described in Gestaut et al. (2008). After rinsing with ddH_2O, the coverslip was incubated with 'rigor' kinesin diluted in BRB20 (20 mM PIPES, 1 mM $MgCl_2$, 1 mM EGTA, pH 6.9) plus 200 mM KCl and 8 mg mL^{-1} BSA for 5 min. Taxol-stabilized Alexa-647-labeled microtubules were bound for ~1 min and washed with BRB20 plus 0, 30 or 60 mM KCl (for final concentrations of 30, 60 and 90 mM K^+, respectively) and 10 µM taxol. GFP-tagged Ndc80 complex, diluted in BRB20 with 10 µM taxol, an oxygen scavenger system (consisting of 200 µg mL^{-1} glucose oxidase, 35 µg mL^{-1} catalase, 25 mM glucose and 5 mM DTT) and the reported amount of K^+, was then introduced.

For experiments with dynamic microtubules, Alexa-647-labeled GMPCPP-stabilized seeds were bound and washed with growth buffer (BRB80 plus 8 mg mL^{-1} BSA and 1 mM GTP). Extensions were assembled in growth buffer plus 2 mg mL^{-1} tubulin (1% Alexa-647-labeled), and oxygen scavenger. After ~5 min the buffer was exchanged with BRB20 plus 1 mM GTP, 2 mg mL^{-1} tubulin (1% Alexa-647-labeled), oxygen scavenger. Then 1 nM GFP-labeled Ndc80 complex was introduced in a buffer lacking both free tubulin and GTP (BRB20 plus oxygen scavenger), to induce depolymerization. For antibody-induced oligomerization, 525 nM Ndc80 complex was pre-incubated with 250 nM biotin-conjugated His_5-antibody (Qiagen, Valencia, CA) for ~60 min. For all experiments the Ndc80 complex was passed through a 0.22 µm filter after dilution into the final buffer.

Instrumentation, data collection, and analysis

Our optical force clamp has been described previously (Asbury, Gestaut et al. 2006; Franck, Powers et al. 2007). Bead-trap separation was sampled at 40 kHz while stage position was updated at 50 Hz to maintain the desired load. Position data were decimated to 200 Hz before storing to disk. Records of bead position versus time were analyzed using custom software written in Igor Pro (Wavemetrics, Lake Oswego, OR). Periods of microtubule growth

and shortening were identified in the records by eye. Catastrophes were scored only when a bead moved in the direction of filament shortening by an amount that clearly exceeded the level of random noise (typically 5 – 10 nm rms during force clamping). Rescues were scored when an episode of rapid disassembly was clearly followed by slow growth. In assays without load, mean squared displacements versus time for individual traces were averaged to estimate the diffusion coefficient during microtubule assembly.

TIRF movies were analyzed using software developed in Labview (National Instruments, Austin, TX) for tracking the position and brightness of individual GFP spots. Association rates were estimated by dividing the total number of events by the total microtubule length, the total observation time and the concentration of free complex in solution. Matlab software (Mathworks, Natick, MA) was developed to calculate the average GFP intensity per pixel as a function of distance from disassembling MT tips. Only intervals when the tips appeared to accumulate more fluorescence than the lattice for > 4 s were included in the averages.

Computer simulations of the biased diffusion mechanism

Simulations of the biased diffusion model were performed in Igor Pro using standard iterative Monte Carlo methods. Briefly, for each iteration the rate constants for 'inward' and 'outward' movement, k_i and k_o, were first calculated based on the current state of the system, as described by Hill (1985). A random number between 0 and 1 was then generated and compared with these rates to determine whether the coupler moved during the iteration. The time interval corresponding to each iteration was kept very short (typically < 5 μsec) to avoid missing events. Shortening the interval further had no effect on the simulations, confirming that the fraction of missed events was negligible. We also verified that the program recapitulates the steady-state distributions shown in Hill's paper (i.e., Figure 3) when matching parameters are used.

SUPPLEMENTAL DISCUSSION

Uncertainty in the number of complexes required for a load-bearing coupler

We estimated the uncertainty in our calculation of the number of Ndc80 complexes required for load-bearing tip attachment by combining the uncertainties arising from three potential sources of error. First, we used BCA assays (Pierce, Thermo Fisher Scientific, Rockford, IL) to measure the concentrations of our Ndc80 preparations. Based on many replicate measurements, these assays are repeatable to within ± 6% in our hands. The manufacturer additionally reports protein-to-protein variation of ± 15%. Assuming uncorrelated errors, these can be combined (i.e., added in quadrature; Taylor 1982) to yield a total uncertainty due to protein quantification of ± 16%. The second potential error source is the counting assay used to measure the concentrations of our preparations of anti-His beads. Based on repeated counts, the uncertainty of this measurement is ± 11%. The third source arises from Poisson statistics, which govern the variability in the number of complexes bound to a small area on the bead surface when the binding density is low. In the present case, this source will contribute ± 27% (i.e., $N^{-½}$, where $N = 14$ is the expected number of bound complexes based on the average density). Combining all three sources (by adding them in quadrature) yields a total uncertainty of ± 33% or, equivalently, an estimate of 14 ± 5 complexes.

We considered the possibility that Ndc80 complexes might form clusters on the bead surface large enough to significantly increase the number interacting with the filament above our

estimate (i.e. clusters > 20 to 30 complexes). However, several observations indicate that such clustering was unlikely. First, beads incubated with ≤ 2 nM GFP-tagged Ndc80 were uniformly decorated and did not exhibit the large bead-to-bead variability in brightness that would occur if the complexes bound in large clusters (Figure S4A and B). Second, their fluorescence increased linearly with the concentration of the complex, which demonstrates an absence of the binding cooperativity that would be expected if clustering were occurring (Figure S4C and D). Third, gel filtration experiments carried out in the same buffer that was used for bead binding showed no evidence for large clusters. The complex elutes as a clean peak with an apparent Stoke's radius close to the predicted size for individual heterotetramers (Figure S1C). Thus the conditions used here for bead binding.

Estimation of kinetochore-microtubule forces *in vivo*

The most straightforward way to estimate the range of forces transmitted to kinetochores during normal movement of bi-oriented chromosomes is to measure the amount of stretching between sister kinetochores and then multiply by the elasticity of the chromatin that links them together. Nicklas (1988) used this method, after determining chromatin elasticity with a calibrated microneedle, to estimate a force of 7 pN per microtubule in meiotic grasshopper spermatocytes. Essentially the same calculation can be performed for budding yeast, yielding a very similar force estimate. Pearson et al. (2001) showed that the pericentric chromatin linking sister kinetochores is extended to between 0.08 and 0.15 $\mu m\ kb^{-1}$, depending on whether stretching of the lacO GFP marker contributes. A reasonable estimate for the elasticity of this pericentric chromatin is the elasticity measured for chromatin fibers *in vitro*, which varies between 5 and 50 pN kb μm^{-1} depending on histone density (Brower-Toland, Smith et al. 2002). Multiplying these values gives the range of forces, 0.4 to 8 pN.

Predictions of the biased diffusion mechanism

Although Hill imagined a sleeve-like coupler completely encircling the microtubule, the physical underpinnings of his model can apply more generally to any array of microtubule binding elements that are linked together. The mechanism he proposed is a form of biased diffusion where the kinetochore undergoes thermally driven movement in a corrugated free energy landscape, as shown schematically in Figure S5A and B. The speed of diffusion depends on the height of the corrugations, which arise because movement along the filament requires breaking some bonds. Moving from one lattice site to another (e.g., from i to ii in Figure S5A and B) results in no net change in energy because the broken bonds can re-form. Thus, lattice-bound couplers in the absence of external load will undergo an unbiased random walk. However, if the coupler begins to move past the tip of the filament (i.e., from ii to iii, where it hangs partially off the end) some binding elements will no longer be able to reach the filament. Thus the free energy increases (in proportion to the number of broken bonds that are unable to re-form), which presents a barrier that biases the diffusion and inhibits detachment. Additionally, the corrugations in the landscape become smaller as the coupler begins to move off the tip because fewer bonds mediate the linkage, so fewer must be broken for further movement. This effect locally increases the rate of diffusion and, as explained in the following paragraph, allows couplers that are nearly immobile on the lattice to track effectively with shortening tips. Tip tracking requires the diffusion of the coupler to be fast enough and biased enough at the tip to outrun disassembly.

Hill's model predicts several changes in behavior as the number of binding elements changes. The most obvious difference is that couplers with fewer elements are predicted to detach more frequently, owing to their reduced binding energy. Couplers with fewer elements will also diffuse more quickly on the lattice, because fewer bonds must be broken to allow movement. During microtubule shortening, another interesting difference is predicted. Small highly mobile couplers will tend to stay ahead of the disassembling tip by moving randomly on the lattice and only occasionally 'bouncing' off the tip (Figure 7A). Conversely, larger less mobile couplers will track closely with the tip, even if they are so large that their diffusion on the lattice is negligibly slow (Figure 7B). More unidirectional tracking occurs in these cases because the mobility is low on the lattice but increases when the tip begins to disassemble out from under the coupler (see above). This in turn promotes lattice-directed movement and formation of new bonds, resulting in a steady state where the rate of new bond formation is balanced by the loss due to disassembly.

SUPPLEMENTAL MATERIALS AND METHODS

Details of expression plasmid construction and protein purification

For expression of the *S. cerevisiae* Ndc80 complex, we used two dicistronic vectors encoding the Ndc80/Nuf2 and Spc24/Spc25 sub-complexes that have been described previously (Wei, Sorger et al. 2005). To create a fluorescent-tagged version of the complex, the Nuf2 gene was excised from one of these vectors and substituted with Nuf2-GFP, which was derived through PCR from yeast strain MSY107-5d (Shimogawa, Graczyk et al. 2006) with addition of a Spe1 restriction site at the 5' end of the 3' primer. The internal Kpn1 restriction site and Spe1 restriction site were used to ligate the Nuf2-GFP PCR product into the dicistronic vector. For the full-length human Hec1 complex, we created a new polycistronic vector encoding all four subunits. cDNA clones for human Spc25, Spc24 and Hec1 were purchased from ATCC (Manassas, VA), and a clone for human Nuf2 was kindly provided by Jennifer De Luca (Colorado State University). Human Spc25, Spc24, Hec1 and Nuf2 were cloned into cassettes 1, 2, 3, and 4 of the pST39 vector (Tan 2001) using restriction sites Xba1 & Apa1, EcoR1 & HindIII, EcoRV & Kpn1, and BspE1 & Mlu1, respectively. In addition, a Pac1 site (encoding leucine-isoleucine-asparagine) was added to the 3' end of Spc25 for future cloning. All versions of the complex included a C-terminal His_6-tag on Spc24 to allow affinity purification and bead binding.

Vectors were transformed into *E. coli* BL21 (Rosetta; Novagen, Madison, WI) and protein expression and purification were carried out as previously described (Asbury et al., 2006; Franck et al., 2007; Gestaut et al., 2008). Cells containing the target plasmid(s) were grown at 37˚ C until they reached a density of 30 Klett units, induced overnight (~12 hours) at 23˚ C with the addition of 0.2 mM IPTG, then pelleted. Fresh pellets were lysed using a French press in 50 mM HEPES (pH 7.6) containing 300 mM NaCl, 2.5 U mL^{-1} benzonase, and protease inhibitors (0.01 mg mL^{-1} chymostatin, 0.01 mg mL^{-1} aprotinin, 0.01 mg mL^{-1} leupeptin, 0.01 mg mL^{-1} pepstatin, 0.002 mg mL^{-1} benzamadine and 1 mM phenylmethylsulfonyl fluoride) and clarified by centrifugation. Protein was purified by affinity chromatography using TALON resin as described by the manufacturer (BD Biosciences). Peak elutions were concentrated using an Amicon Ultra 50 kD MWCO centrifugal filter (Millipore, Billerica, MA) and then subjected to gel filtration chromatography on an SDX200 16/60 (GE Healthcare, Pistcataway, NJ)

equilibrated with 50 mM HEPES (pH 7.6) containing 200 mM NaCl. Glycerol was added to a final concentration of 10% and aliquots were snap frozen and stored at -80˚ C.

FIGURES

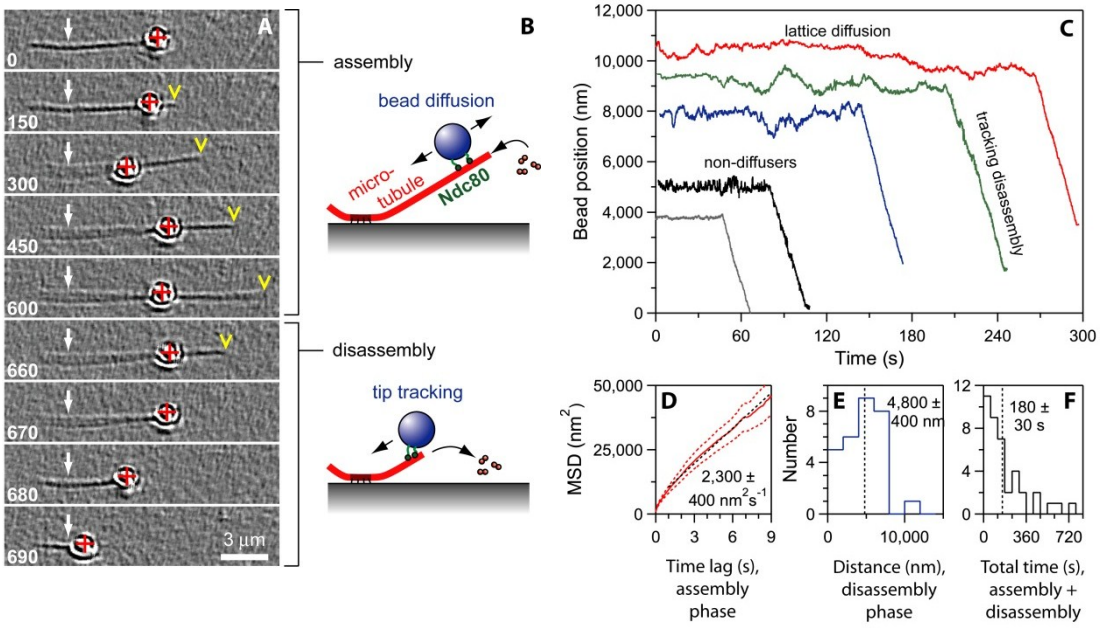

Figure 1: The Ndc80 complex couples cargo to dynamic microtubules

(**A**) An Ndc80-coated bead diffuses back-and-forth over the microtubule lattice and fails to track with the tip during filament growth (0 – 600 s). During filament shortening, it tracks with the disassembling tip (600 – 690 s). Selected frames from Movie S1 are shown. White arrows indicate the coverslip-anchored portion of the microtubule seed, red crosses indicate the bead center, and yellow arrowheads indicate the microtubule tip. Elapsed times are in seconds. (**B**) Schematic diagram of the Ndc80 bead motility assay. In the absence of tension, Ndc80-based linkages usually exhibit lattice diffusion as the filament grows by addition of tubulin subunits to the tip, and they remain tip-bound even as subunits are rapidly lost from the tip during shortening. (**C**) Records of bead position versus time, measured without applied force. Increasing position represents movement away from the anchored portion of the microtubule. For clarity, the records are offset vertically by an arbitrary amount. (**D**) Mean squared displacement plotted against time for the subset of beads that underwent lattice diffusion. Data are mean (solid red curve) ± s.e.m. (dotted red curves), computed from $N = 26$ records. Black line shows linear fit used to determine diffusion coefficient. (**E** and **F**) Histograms of bead displacement during microtubule shortening ($N = 29$ records) and total duration (including growth and shortening phases) of microtubule attachment ($N = 40$) for a population of beads. Dotted vertical lines indicate mean values. The data in (D – F) are pooled from experiments using beads prepared with 0.6 to 15 nM Ndc80 complex, corresponding to molar ratios of 110 to 2700 complexes per bead. (Figure layout is modified from original.)

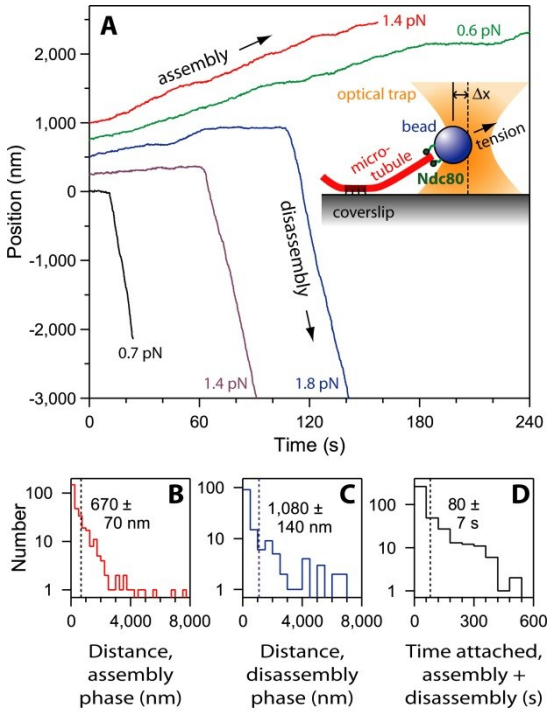

Figure 2: Ndc80-based couplers support tension

(**A**) Records of bead position versus time during continuous application of tensile load. Increasing position represents assembly-coupled movement in the direction of applied force, away from the anchored portion of the microtubule (e.g., blue trace < 120 s). Decreasing position represents disassembly-driven movement against the applied force (e.g., blue trace > 120 s). These data were recorded using beads prepared with ≤ 2 nM Ndc80 complex, corresponding to ≤ 360 complexes per bead. For clarity, the records are offset vertically by an arbitrary amount. The inset shows a schematic diagram of the force-clamp experiment. The bead is held by an optical trap (orange). As the microtubule grows and shortens, the coverslip is moved by computer to keep a fixed separation (Δx) between the bead and the trap, thereby keeping a constant level of tension on the Ndc80-based linkage.(**B** – **D**) Histograms of distance moved during assembly (*N* = 314 records), distance moved during disassembly (*N* = 142), and total attached time (including both assembly and disassembly phases; *N* = 392) for a population of tip-attached beads moving under 0.5 - 2.5 pN of tension. Dotted vertical lines indicate the average for each distribution. These data are pooled from experiments using beads prepared with 0.6 to 15 nM Ndc80 complex, corresponding to molar ratios of 110 to 2,700 complexes per bead.

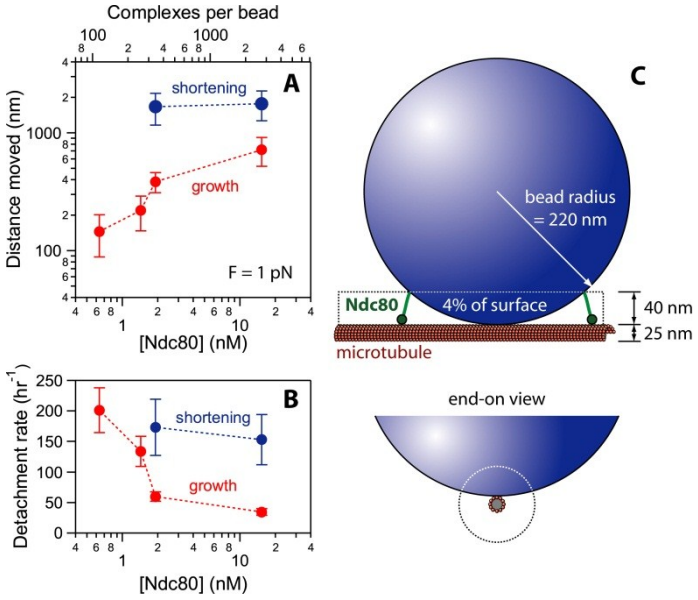

Figure 3: Low surface densities of Ndc80 are sufficient to form load-bearing couplers

(**A**) Mean displacement as a function of Ndc80 density for tip-attached beads under 1 pN of tension. The ratio of Ndc80 complexes to beads and the concentration of Ndc80 during incubation (with 5.6 pM beads) are shown on the top and bottom axes, respectively. At molar ratios of 360 complexes per bead and higher (i.e. ≥ 2 nM Ndc80 complex), tip attachments persisted for minutes and moved 400 to 1,000 nm during growth and shortening. Each red point represents the average of at least 30 events. Blue points are averages of at least 17 events. Uncertainties represent s.e.m. (**B**) Rate of bead detachment from growing and shortening tips, estimated by counting the number of detachment events and dividing by the total observation time in each phase. Each red point was calculated from at least 29 detachments during growth. Each blue point was calculated from at least 14 detachments during shortening. Uncertainties represent counting error. (**C**) Schematic diagram, drawn approximately to scale, showing that Ndc80 complexes on a small fraction of the bead surface, ≤ 4%, are capable of simultaneously binding to the microtubule. The configuration shown, where the bead rests against the side of a filament whose tip extends well past the point of contact maximizes the amount of bead surface in close proximity to the microtubule. Thus it provides an upper limit for the fraction of bead surface within 40 nm. The bead may instead adopt a more end-on configuration, which would reduce the number of complexes capable of binding.

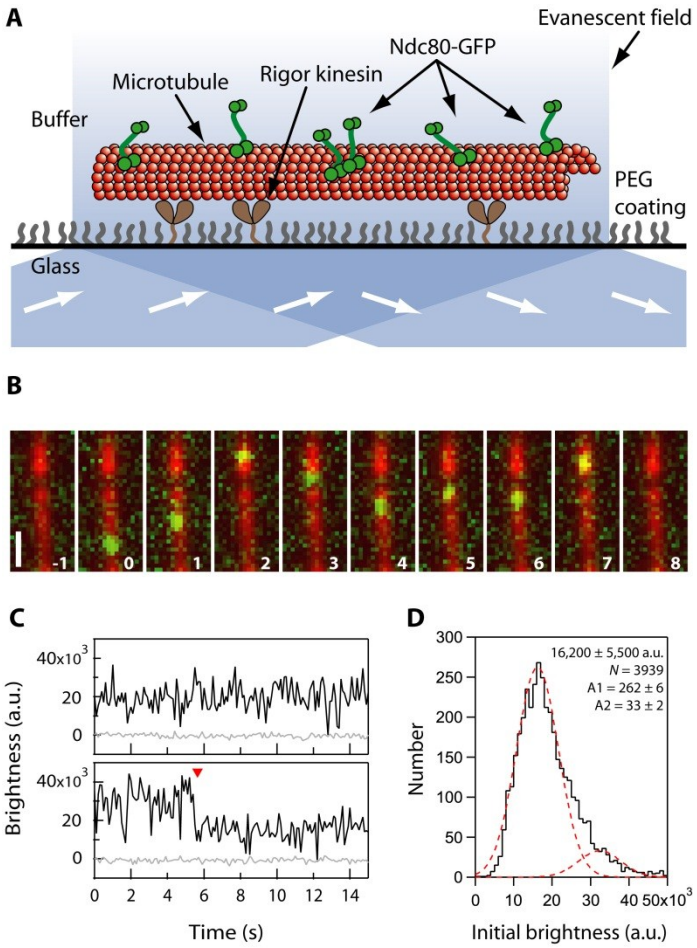

Figure 4: Ndc80 complexes exhibit one-dimensional diffusion along microtubules

(**A**) Schematic of the TIRF assay for observing GFP-tagged Ndc80 complexes (green rods) interacting with individual microtubules (red). Excitation by total internal reflection, in combination with a surface treatment that blocks non-specific adsorption, allowed movement of single Ndc80 complexes to be recorded in the evanescent field. (**B**) Selected frames from Movie S3 showing one-dimensional diffusion of the Ndc80 complex (green) along a microtubule (red). Elapsed times are in seconds. Scale bar, 1 μm.
(**C**) Records of brightness versus time for most diffusing particles were roughly constant over time (as in the upper trace). However, some particles showed a stepwise loss of half their intensity while they remained attached to the filament (red arrowhead, lower trace), consistent with photobleaching of one GFP molecule within a particle containing two GFPs. (**D**) Distribution of initial brightness values for particles of Ndc80-GFP diffusing on taxol-stabilized microtubules. Data are fit by the sum of two Gaussians (dashed red curves), corresponding to a large population (89%) with a unitary brightness of 16,200 ± 5,500 a.u. (mean ± s.d.) plus a small population (11%) with twice the brightness, 32,400 ± 5,500 a.u. (*N* = 3,939 events on 172 microtubules in 34 recordings).

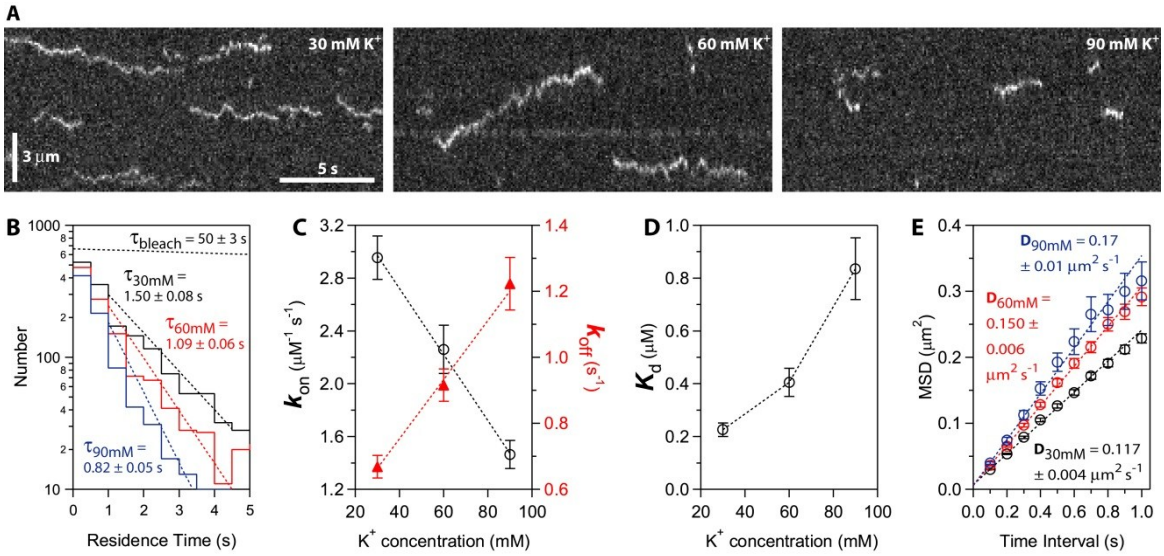

Figure 5: Binding of individual Ndc80 complexes to microtubules is sensitive to ionic strength

(**A**) Kymographs showing binding and diffusion of Ndc80-GFP on taxol-stabilized microtubules in buffers with varying ionic strength (30, 60 and 90 mM K^+). Position along the microtubule is depicted on the vertical axis while time changes along the horizontal axis. Long-duration events (> 3 s) were more common at lower ionic strength. Concentration of Ndc80 complex, 20 pM. (**B**) Residence time distributions for Ndc80 complexes in 30 mM K^+ (black histogram, N = 1,729 binding events on 61 microtubules in 12 recordings totaling 40 min), 60 mM K^+ (red histogram, N = 1,333 events, 57 microtubules, 11 movies, totaling 37 min) and 90 mM K^+ (blue histogram, N = 877 events, 54 microtubules, 11 movies, totaling 37 min). Dotted lines show weighted exponential fits used to determine mean residence times. The exponential distribution of bleach times for single GFP molecules in control experiments is depicted by the uppermost dotted black line, corresponding to a mean bleach time of t_{bleach} = 50 ± 3 s. (**C** and **D**) Raising the ionic strength lowered the association rate, k_{on} (left axis in C, open black circles), and increased the dissociation rate, k_{off} (right axis in C, filled red triangles). As a result, the apparent equilibrium dissociation constant, $K_d = k_{off} \cdot k_{on}^{-1}$, increased 4-fold (D). On-rates were calculated as the number of observed binding events per tubulin dimer per second, divided by the Ndc80 concentration. Off-rates were taken from t^{-1} in (B). Uncertainties represent s.e.m. (**E**) Raising the ionic strength speeds lattice diffusion of Ndc80 complexes. Mean squared displacement (MSD) is plotted against time for each ionic strength. Dotted lines show linear fits used to determine diffusion coefficients. Data are mean ± s.e.m., computed from N = 2,002 events for 30 mM K^+, N = 1,302 events for 60 mM K^+, and N = 664 events for 90 mM K^+.

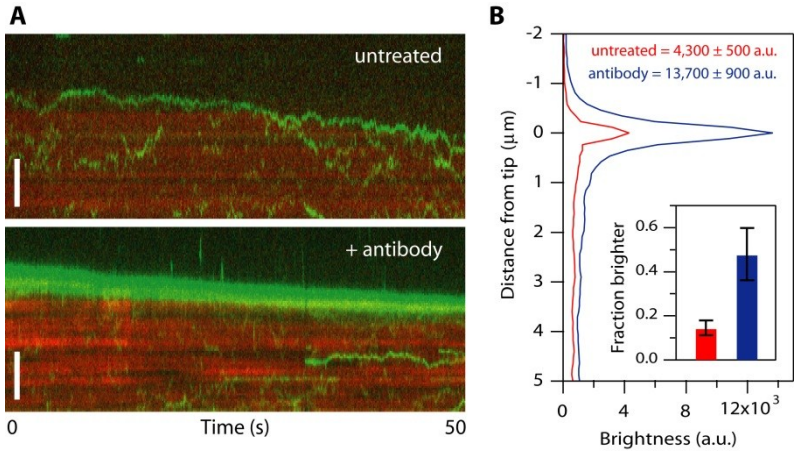

Figure 6: Small ensembles of Ndc80 complexes track with disassembling microtubule tips

(**A**) Kymographs showing movement of particles composed of Ndc80 complexes (green) on disassembling microtubules (red). At 1 nM Ndc80 complex the microtubules were crowded with diffusing particles, many of which encountered the disassembling tip. No clear tip tracking was evident. However, in some cases the density of particles became noticeably higher at a disassembling tip relative to the lattice. When individual particles could be discerned as they encountered a disassembling tip, they sometimes appeared to 'bounce' repeatedly off the tip (upper kymograph). After pre-treating the Ndc80 complex with anti-His antibody to drive oligomerization, more disassembling tips accumulated fluorescent particles, and some long episodes of processive tip tracking were observed (lower kymograph). Scale bars, 3 µm. (**B**) Profiles of average fluorescence versus position along the microtubule for a population of disassembling filaments decorated with Ndc80 complexes. Only intervals when the tip appeared to accumulate fluorescent particles were included in the averages. During these events, the disassembling tips became brighter if the Ndc80 complex had been pre-treated with antibody (blue curve, $N = 21$ events from 17 microtubules in 10 recordings) than without antibody pre-treatment (red curve, $N = 24$ events from 20 microtubules in 27 recordings). The fraction of disassembling tips that accumulated fluorescence was also increased after antibody pre-treatment (inset). Uncertainties in peak brightness represent s.d., and in the inset they represent counting error.

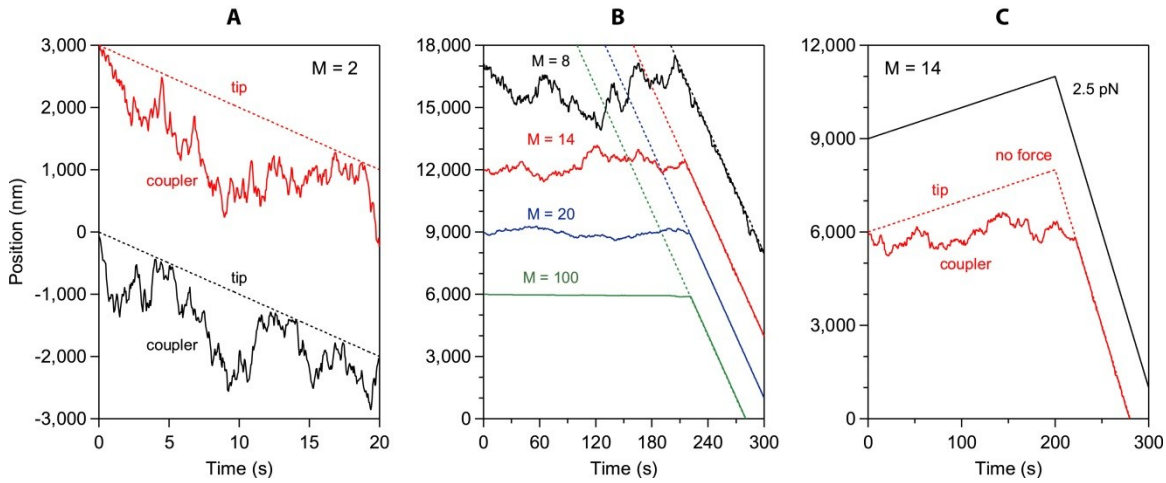

Figure 7: Simulated behavior of a diffusion-based coupler

(**A** – **C**) Output from Monte Carlo simulations with parameters defined as in Hill (1985) but chosen to match our observations. The number of binding elements in the coupler, *M*, was varied between 2 and 100, as indicated. In (A and B), no external load was applied. The couplers in (A) were initially located at a disassembling tip. In (B) they were initially located on the lattice, where they exhibited unbiased movement for several minutes until being captured and carried by the disassembling tip (denoted by dotted lines). In (C) the couplers were initially located at an assembling tip, which later began to disassemble (> 200 s). A load of 2.5 pN was applied in one case (black trace), whereas no load was applied in the other case (red trace). The other parameter values were held constant as follows: $r \equiv e^{-b/kT} = 0.75$, $s \equiv e^{-w/kT} = 10^{-6}$, $l = 0.62$ nm, $\kappa r l^2 = 0.170$ μm^2 s^{-1}, $\alpha c = 10$ nm s^{-1}, $\beta s = 100$ nm s^{-1}. Note that the parameters, s, l, $\kappa r l^2$, αc, and βs are constrained by the binding equilibrium for single Ndc80 complexes, the spacing of tubulin subunits in the microtubule lattice, the diffusion speed for single Ndc80 complexes, and the microtubule growth and shortening speeds, respectively. The only free parameter, r, was chosen to fall in the same range considered by Hill. The records are offset vertically by arbitrary amounts, for clarity.

SUPPLEMENTAL TABLE AND FIGURES

Table S1. Outcomes during force clamp experiments with yeast or human Ndc80 complex, under 0.5 to 2.5 pN of continuous tension.

		yeast Ndc80 complex	human Ndc80/Hec1 complex
A	total events observed	392	50
B	events with discernable assembly-coupled movement only	250 (64%)[1]	25 (50%)[1]
C	events with both assembly- and disassembly-coupled movement	64 (16%)[1]	21 (42%)[1]
D	events with discernable disassembly-coupled movement only	78 (20%)[1]	4 (8%)[1]
E	total events with discernable assembly-coupled movement (B+C)	314	46
F	'catastrophes' during assembly-coupled movement	64 (20%)[2]	21 (45%)[2]
G	detachments during assembly-coupled movement	226 (72%)[2]	15 (33%)[2]
H	other interruptions to assembly-coupled movement	24 (8%)[2]	10 (22%)[2]
I	total events with discernable disassembly-coupled movement (C+D)	142	25
J	'rescues' during disassembly-coupled movement	4 (3%)[3]	2 (8%)[3]
K	detachments during disassembly-coupled movement	83 (58%)[3]	23 (92%)[3]
L	other interruptions to disassembly-coupled movement	55 (39%)[3]	0 (0%)[3]

[1] expressed as a percentage of total events (row A)

[2] expressed as a percentage of total events with discernable assembly-coupled movement (row E)

[3] expressed as a percentage of total events with discernable disassembly-coupled movement (row I)

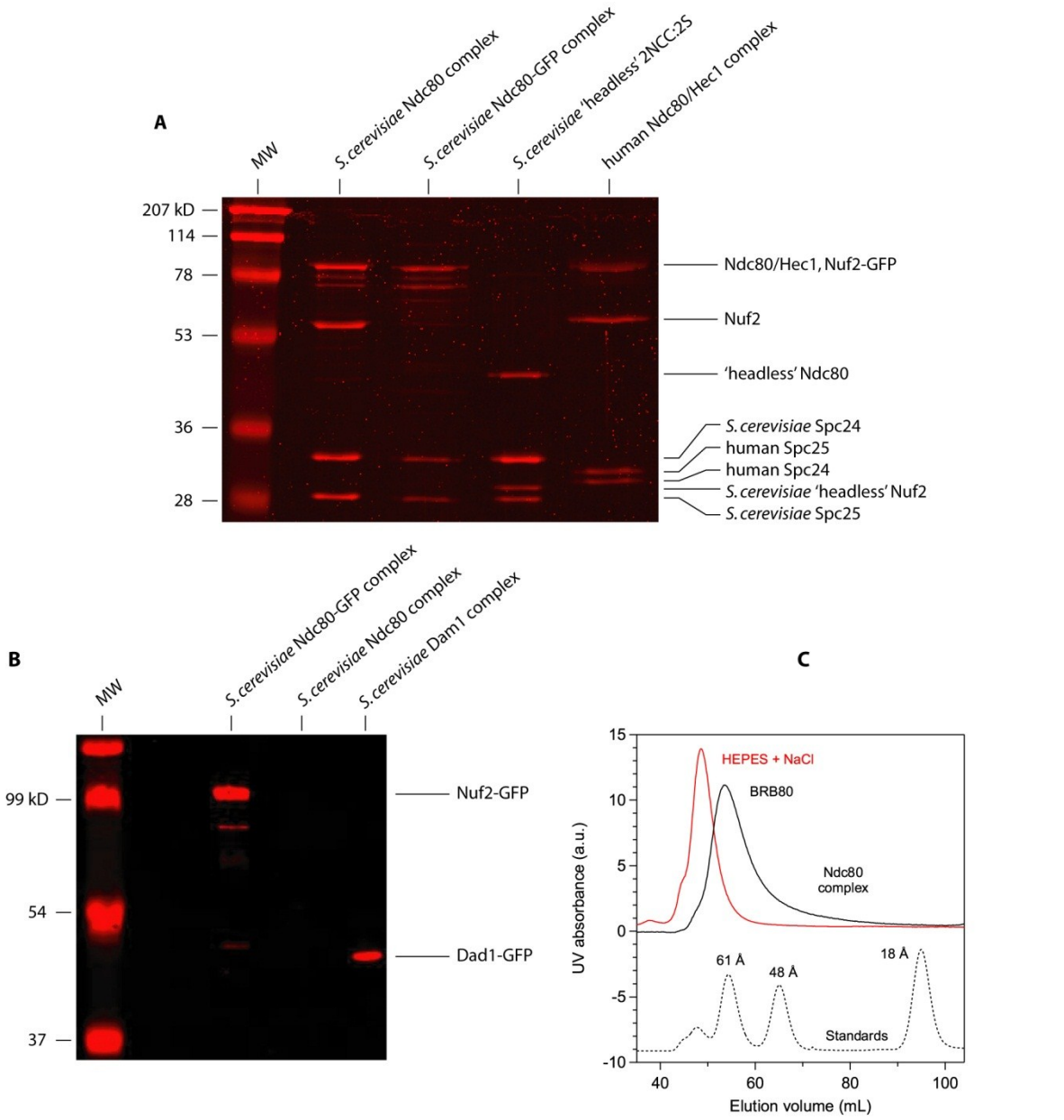

Figure S1: Purification of the Ndc80 complex

(**A**) Coommassie stained SDS-PAGE (12% acrylamide) showing the components of the *S. cerevisiae* Ndc80 complex, the GFP-tagged *S. cerevisiae* Ndc80 complex, the 'headless' 2NCC:2S complex and the human Ndc80/Hec1 complex. (**B**) Anti-GFP Western blot showing the GFP-tagged Nuf2 subunit of the *S. cerevisiae* Ndc80 complex. As negative and positive controls, untagged Ndc80 complex and GFP-tagged Dam1 complex (Gestaut, Graczyk et al. 2008) were run in adjacent lanes. (**C**) Gel filtration profile for the yeast Ndc80 complex in our standard purification buffer (50 mM HEPES pH 7.6 plus 300 mM NaCl; red trace) and in the buffer used for binding the complex to anti-His beads (BRB80; solid black trace). For comparison, the elution profile for a mixture of standard proteins in purification buffer is also shown (ferritin, Stoke's radius of 61 Å; aldolase, 48 Å; RNAse, 18 Å; dotted black trace, offset vertically for clarity).

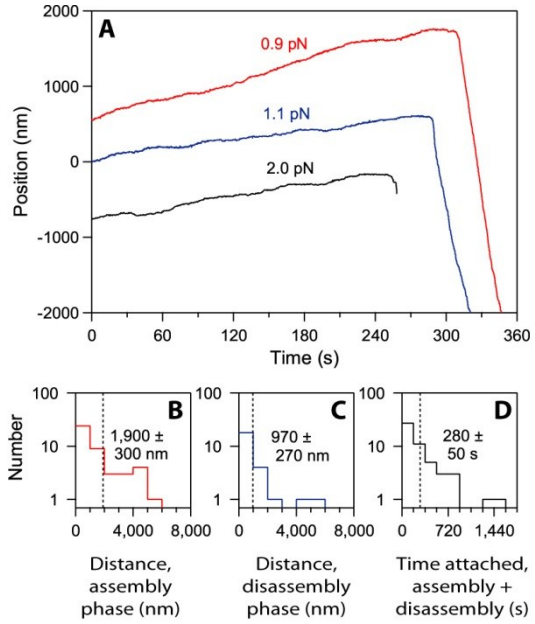

Figure S2: The human Ndc80/Hec1 complex couples force to dynamic microtubule tips

(**A**) Beads coated with the human Ndc80/Hec1 complex form persistent load-bearing attachments to growing and shortening microtubule tips, similar to attachments formed by the yeast Ndc80 complex. Records show bead position versus time during continuous application of tensile load, as in Figure 2A.
(**B** – **D**) Histograms of distance moved during assembly (*N* = 46 records), distance moved during disassembly (*N* = 25), and total attached time (including both assembly and disassembly phases; *N* = 50) for tip-attached beads moving under 0.5 - 2.5 pN of tension. Dotted vertical lines indicate the average (± s.e.m.) for each distribution.

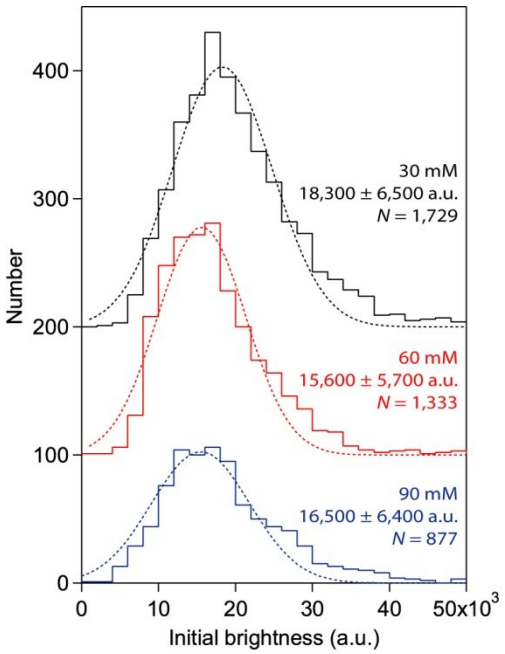

Figure S3: The brightness of diffusing Ndc80-GFP spots is unaffected by ionic strength

Distributions of initial brightness values for Ndc80-GFP particles diffusing on taxol-stabilized microtubules in 30 mM K^+ (black), 60 mM K^+ (red) or 90 mM K^+ (blue) buffer. Each histogram was fit by a Gaussian function (dotted lines) to determine the mean brightness values indicated (± s.d.). For clarity, the 60 mM K^+ and 90 mM K^+ distributions are offset vertically by 100 and 200 counts, respectively.

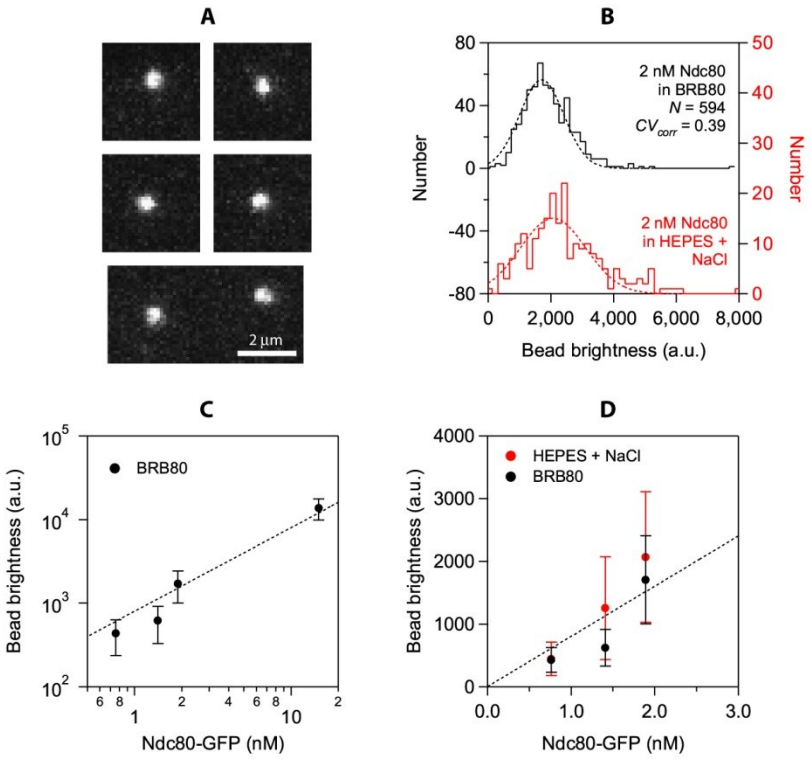

Figure S4: Quantification of GFP-tagged Ndc80 complex bound to anti-His beads

(**A**) Epifluorescence images of anti-His beads after incubation with 2 nM GFP-tagged Ndc80 complex in our standard binding buffer (BRB80 plus 8 mg mL^{-1} BSA and 1 mM DTT). (**B**) Brightness distributions for beads incubated with 2 nM GFP-tagged Ndc80 complex in our standard binding buffer (black histogram) or in the buffer used for purification of the complex (50 mM HEPES pH 7.6 plus 300 mM NaCl; red histogram).
(**C** and **D**) Mean brightness for beads incubated with GFP-tagged Ndc80 in our standard binding buffer (black symbols) or in purification buffer (red symbols) plotted against the concentration of the complex. Uncertainties represent s.d. The bead concentration was 5.6 pM for all incubations.

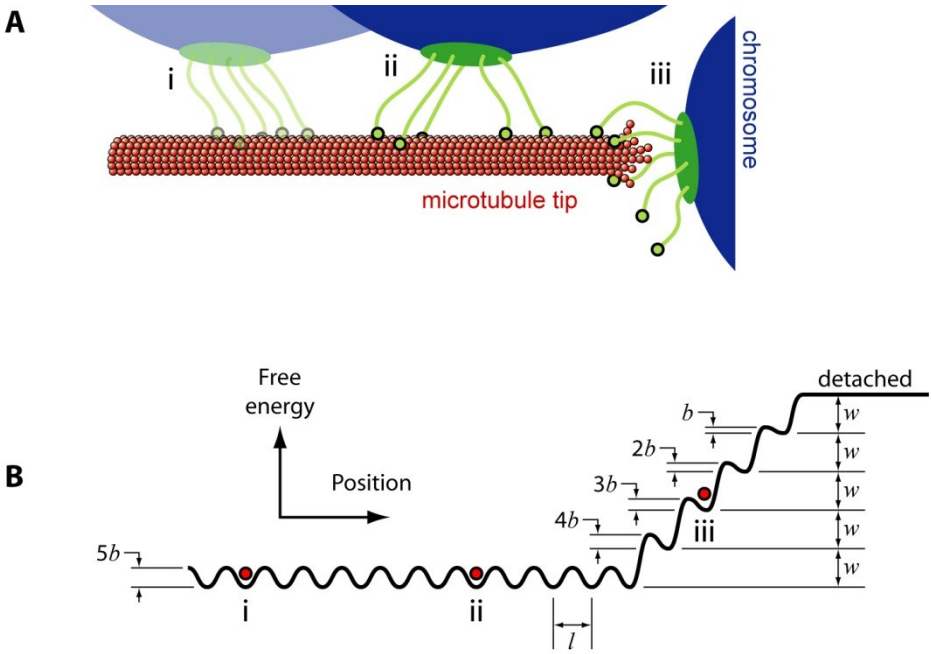

Figure S5: The biased diffusion model

(**A**) Schematic picture of a coupler composed of five microtubule binding elements attached to a microtubule at three different locations, two on the lattice (denoted i and ii) and one on the tip in a position where two of the elements are no longer bound (iii). (**B**) Free energy landscape for a five-element, biased diffusion-based coupler. Parameters are defined as in Hill (1985). The spacing of sites is denoted by *l*. The gradual increase in free energy on the right arises from the bond energies, *w*, that must be overcome to move the coupler past the filament tip. The corrugations in the landscape occur because movement along the filament requires breaking and reforming some bonds. Their heights, 5*b*, 4*b*, ..., *b*, decrease as the coupler begins to move past the tip. Red circles (i, ii, and iii) denote the landscape positions corresponding to the couplers shown in (A).

Chapter 5

Cooperation of the Dam1 and Ndc80 Kinetochore Complexes Enhances Microtubule Coupling and Is Regulated by Aurora B

Originally published in Journal of Cell Biology 189 (2010) 713-723.

ABSTRACT

The coupling of kinetochores to dynamic spindle microtubules is crucial for chromosome positioning and segregation, error correction, and cell cycle progression. How these fundamental attachments are made and persist under tensile forces from the spindle remain important questions. As microtubule-binding elements, the budding yeast Ndc80 and Dam1 kinetochore complexes are essential and not redundant, but their distinct contributions are unknown. Here we show that the Dam1 complex is a processivity factor for the Ndc80 complex, enhancing the ability of the Ndc80 complex to form load-bearing attachments to and track with dynamic microtubule tips in vitro. Moreover, the interaction between the Ndc80 and Dam1 complexes is abolished when the Dam1 complex is phosphorylated by the yeast Aurora B kinase Ipl1. This provides evidence for a mechanism by which Aurora B resets aberrant kinetochore-microtubule attachments. We propose that the action of the Dam1 complex as a processivity factor in kinetochore-microtubule attachment is regulated by conserved signals for error correction.

INTRODUCTION

During mitosis, kinetochores attach to assembling and disassembling microtubule tips while withstanding tensile forces from the mitotic spindle (Skibbens, Skeen et al. 1993; Skibbens, Rieder et al. 1995; Maddox, Straight et al. 2003). Kinetochores are able to harness energy from these disassembling microtubule tips to drive movement of chromosomes (for a review, see Inoue and Salmon 1995). Understanding how the kinetochore establishes microtubule attachments under force requires understanding the organization of the kinetochore components and how they bear and transmit load. Recent studies investigated the spatial organization of kinetochore components in vivo and how their arrangement changes throughout mitosis (Joglekar, Bloom et al. 2009; Wan, O'Quinn et al. 2009). Through systematic reconstitution of kinetochore components, we are pursuing a complementary approach with the ultimate goal of mapping the transmission of force across the kinetochore from the dynamic microtubule to the centromere. Here, we focus on the kinetochore-microtubule interface.

The kinetochores of all eukaryotes contain multiple microtubule-binding elements. The KMN network (KNL-1, Mis12 complex and Ndc80 complex) and the Ska1 complex both bind microtubules in higher eukaryotic cells (Cheeseman, Chappie et al. 2006; Gaitanos, Santamaria et al. 2009; Welburn, Grishchuk et al. 2009). Yeast also contain the KMN network and the Dam1 complex, possibly the functional homolog of the Ska1 complex (Hanisch, Sillje et al. 2006; Gaitanos, Santamaria et al. 2009; Raaijmakers, Tanenbaum et al. 2009; Welburn, Grishchuk et al. 2009). Cooperation of the three components of the conserved KMN network was shown by cosedimentation with taxol-stabilized microtubules (Cheeseman, Chappie et al. 2006), but how or whether any of the microtubule-binding components cooperate to achieve attachment to dynamic microtubules is unknown. We show for the first time that cooperation

between two kinetochore subcomplexes enhances processive, load-bearing coupling to dynamic microtubule tips.

In the budding yeast kinetochore, all four proteins of the Ndc80 complex and all ten proteins of the Dam1 complex are essential (Tanaka and Desai 2008). In vitro, both complexes independently form diffusive attachments to the microtubule lattice and track with disassembling microtubule tips, although the Ndc80 complex requires artificial oligomerization to tip-track (Westermann, Wang et al. 2006; Gestaut, Graczyk et al. 2008; Powers, Franck et al. 2009). When attached to beads, each complex also forms load-bearing attachments to dynamic microtubule tips (Asbury, Gestaut et al. 2006; Franck, Powers et al. 2007; Grishchuk, Efremov et al. 2008; Grishchuk, Spiridonov et al. 2008; Powers, Franck et al. 2009). Despite these similarities, the Ndc80 and Dam1 complexes are not redundant. The Ndc80 complex is required in vivo for attachment to microtubules (Kline-Smith, Sandall et al. 2005), and the Dam1 complex is required for attaching to the tips of microtubules and for establishing biorientation (Tanaka, Mukae et al. 2005; Shimogawa, Graczyk et al. 2006). Moreover, the Ndc80 complex is required for the assembly of Dam1 complex onto the kinetochore (Janke, Ortiz et al. 2002), and an interaction between the two complexes has been suggested by localization and two-hybrid studies (Shang, Hazbun et al. 2003; Joglekar, Bloom et al. 2009). Studying the combination of Ndc80 and Dam1 complexes in vitro will allow us to dissect their distinct roles in kinetochore-microtubule binding.

Kinetochores not only serve as physical bridges between chromosomes and spindle microtubules but also are regulatory hubs that ensure chromosome segregation fidelity during mitosis. For example, Aurora B kinase is responsible for resetting aberrant kinetochore-microtubule attachments to achieve biorientation (Cheeseman, Anderson et al. 2002; Tanaka, Rachidi et al. 2002; Hauf, Cole et al. 2003; Pinsky, Kung et al. 2006). Many of the microtubule-binding components of the kinetochore, including the Ndc80 and Dam1 complexes, are targets of Aurora B (Cheeseman, Anderson et al. 2002; Shang, Hazbun et al. 2003; Cheeseman, Chappie et al. 2006; DeLuca, Gall et al. 2006; Pinsky, Kung et al. 2006; Gestaut, Graczyk et al. 2008). In mammalian cells, Aurora B phosphorylation of the N-terminal tail of the Ndc80 protein (Hec1 in humans) abolishes kinetochore-microtubule attachment (DeLuca, Gall et al. 2006; Guimaraes, Dong et al. 2008). While the budding yeast Ndc80 protein also has an N-terminal tail, it is not essential (Akiyoshi, Nelson et al. 2009). Previously, we demonstrated that phosphorylation by the yeast Aurora B homolog Ipl1 at one target site within the Dam1 complex, Ser 20 of Dam1, reduces its affinity for the microtubule lattice (Gestaut, Graczyk et al. 2008). Two-hybrid assays and pull downs with in vitro translated proteins using phosphomimetic mutations at Ipl1 target sites in Dam1 also suggested that phosphorylation of the Dam1 complex modulates its interaction with the Ndc80 complex (Shang, Hazbun et al. 2003). Moreover, Ipl1 target sites on Dam1 are dephosphorylated as cells enter metaphase in a cohesin-dependent manner, which could prevent kinetochore-microtubule attachment turnover as biorientation is established (Keating, Rachidi et al. 2009).

Here we show that the Dam1 complex is a phosphoregulated processivity factor for the Ndc80 complex in kinetochore-microtubule coupling. Using techniques for tracking and manipulating single molecules in vitro, we demonstrate directly an interaction between the Ndc80 and Dam1 complexes on microtubules. Through this interaction, the Dam1 complex enhances the ability of the Ndc80 complex to maintain attachment to dynamic microtubule tips

even in the presence of external load. Finally, this interaction is regulated by Ipl1, further defining the mechanism for Aurora B-mediated corrective detachment in vivo.

RESULTS

The Dam1 and Ndc80 complexes interact on microtubules

We expressed recombinant *S. cerevisiae* Ndc80 and Dam1 complexes in *E. coli*, and purified each complex by affinity chromatography and gel filtration (Wei, Sorger et al. 2005; Gestaut, Graczyk et al. 2008; Powers, Franck et al. 2009). By velocity sedimentation analysis, we found weak interaction between the Ndc80 and Dam1 complexes free in solution (Fig. S1). Using total internal reflection fluorescence (TIRF) microscopy, we then quantified the interaction of GFP-tagged Ndc80 complexes with microtubules in the presence and absence of Dam1 complex (Fig. 1). In the absence of Dam1 complex, individual Ndc80 complexes formed transient and diffusive attachments to microtubules, as reported previously (Powers, Franck et al. 2009). We measured a dissociation rate constant (k_{off}) of 0.44 ± 0.03 s^{-1}, an association rate constant (k_{on}) of 0.60 ± 0.02 $\mu M^{-1} \cdot s^{-1}$, and a diffusion constant of 0.067 ± 0.003 $\mu m^2 \cdot s^{-1}$ (Fig. 1 C–E), values comparable to our previous study. We also simultaneously visualized GFP-tagged Ndc80 complexes and mCherry-tagged Dam1 complexes on microtubules. At concentrations affording single molecule resolution of each complex, interaction events were rare. When the two complexes did associate with each other, they appeared to diffuse more slowly (Fig. S2). However, interaction events between individual Ndc80 and Dam1 complexes were too infrequent to affect population behavior. To increase the frequency of interactions, we raised the concentration of Dam1 complex while maintaining low concentrations (10 pM) of the Ndc80 complex. Overall, Ndc80 complex transitioned gradually to a more persistent and more slowly diffusing behavior as the concentration of Dam1 complex was increased (Fig. 1 C–E). At 500 pM Dam1 complex, the Ndc80 complex dissociated two-fold more slowly from the microtubule (k_{off} = 0.23 ± 0.02 s^{-1}) and associated 1.6-fold faster onto the microtubule (k_{on} = 0.99 ± 0.02 $\mu M^{-1} \cdot s^{-1}$) as compared to Ndc80 complex alone. This corresponds to a three-fold decrease in the apparent equilibrium dissociation constant, $K_d = k_{off} \cdot k_{on}^{-1}$ (0.74 ± 0.06 μM to 0.23 ± 0.02 μM). At 500 pM Dam1 complex, the Ndc80 complex also diffused five-fold more slowly (0.013 ± 0.0006 $\mu m^2 \cdot s^{-1}$) as compared to Ndc80 complex alone. The Dam1 complex was unlikely to be acting as a simple barrier to diffusional motility, as the diffusive behavior of the Ndc80 complex was unchanged in the presence of phosphorylated Dam1 complex at the same lattice density (see below). The brightness distribution of the GFP signal remained unchanged across concentrations of the Dam1 complex, demonstrating that oligomerization of the Ndc80 complex did not contribute to its modified behavior in the presence of the Dam1 complex (Fig. 2). Even at 500 pM Dam1 complex, not all Ndc80 complexes bound persistently and diffused slowly. This indicates that not all Ndc80 complexes were associated with Dam1 complexes, so our calculated values describe a mixed population and likely underestimate Dam1 complex-mediated enhancement of Ndc80 complex-microtubule interactions.

In the presence of the Dam1 complex, diffusion of the Ndc80 complex is slowed far below the reported rate for a single Dam1 complex (Gestaut, Graczyk et al. 2008). Therefore, we hypothesized that at the concentrations required to observe significant changes in the population behavior of the Ndc80 complex, the Dam1 complex forms slowly diffusing oligomers. To test this, we measured the diffusion rate of GFP-tagged Dam1 complex on microtubules (Fig. S3 A, B). At 2 pM, single GFP-tagged Dam1 complexes diffused rapidly, at

0.060 ± 0.003 $\mu m^2 \cdot s^{-1}$, similar to the rates reported previously (Westermann, Wang et al. 2006; Gestaut, Graczyk et al. 2008). At 20 and 50 pM Dam1 complex, however, we observed slowly diffusing spots that exhibited fluorescence brighter than individual Dam1 complexes. To maintain single molecule resolution for quantifying the diffusion of Dam1 complex at higher concentrations, we mixed untagged Dam1 complex with a small amount of GFP-tagged Dam1 complex. At 500 pM, Dam1 complex diffused at least 60-fold more slowly than at 2 pM (Fig. S3 B). These observations indicate that oligomerization of the Dam1 complex slows its diffusion rate, as reported previously (Grishchuk, Efremov et al. 2008). Moreover, they imply that the enhanced binding of Ndc80 complex to microtubules that we have quantified here (e.g., in Fig. 1 C–E) occurs via interaction with Dam1 complexes that are primarily in an oligomeric state.

In vitro, the Dam1 complex forms rings of 16-25 complexes that encircle microtubules (Miranda, King et al. 2007; Wang, Ramey et al. 2007). To investigate whether rings are important for interaction with the Ndc80 complex, we used negative-stain electron microscopy to quantify ring formation on taxol-stabilized microtubules (at 36 nM tubulin) across a range of Dam1 concentrations (Fig. 3). At 500 pM Dam1 complex, the highest concentration used in our TIRF assays, rings were absent. Instead, we observed small particles scattered around or attached to the filaments. The dimensions of these particles were consistent with Dam1 complex dimers (Wang, Ramey et al. 2007). Rings first appear on microtubules at 1 nM Dam1 complex, substantially increase in density between 5 and 10 nM, and saturate at 100 nM (Table 1). These findings are consistent with a strong and cooperative binding of the Dam1 complex to microtubules as reported previously (Gestaut, Graczyk et al. 2008).

While 500 pM Dam1 complex did not assemble into rings on microtubules at 36 nM tubulin, reducing the amount of tubulin could promote ring formation by increasing the density of Dam1 complex bound to microtubules. To explore the magnitude of this effect, we imaged 500 pM Dam1 complex on microtubules at 5-fold lower tubulin (7 nM). Rings were again absent ($n = 8$ microtubules, 101 μm total). Further reductions in tubulin concentration were impractical because the microtubules became too sparse on the electron microscopy grids. Since the effective concentration of tubulin polymer in our TIRF assays was lower still (~1 nM), it remains possible that Dam1 complex rings contributed to the observed alterations in behavior of the Ndc80 complex. We note, however, that two observations suggest ring formation is not required for the initial interaction between the Ndc80 and Dam1 complexes. First, the Dam1 and Ndc80 complexes interact during velocity sedimentation, where the Dam1 complex is primarily in dimeric form (see Fig. S1). Second, interactions between individual Ndc80 and Dam1 complexes can be observed directly in TIRF assays (albeit rarely; see Fig. S2).

The Dam1 complex enhances attachment of the Ndc80 complex to dynamic microtubule tips

The Ndc80 complex has been shown to track efficiently with disassembling microtubule tips in vitro, but only when it is bound to beads or to antibodies (Powers, Franck et al. 2009). In contrast, the Dam1 complex tracks robustly with disassembling tips without artificial oligomerization (Westermann, Wang et al. 2006; Gestaut, Graczyk et al. 2008). We therefore tested whether the Dam1 complex enhances tip-tracking by the Ndc80 complex. We grew microtubules from non-hydrolyzable GMPCPP seeds in the presence of free fluorescent-labeled tubulin and GTP. We visualized the behavior of GFP-tagged Ndc80 complex as microtubules

disassembled after the free tubulin was removed. By itself, the Ndc80 complex localized only briefly to microtubule tips during disassembly (Fig. 4 A). Most binding events were transient and diffusive similar to those seen on taxol-stabilized microtubules (and as reported in Powers, Franck et al. 2009). In contrast, the addition of Dam1 complex, which accumulates at the disassembling microtubule tip (Fig. S3 C), substantially increased the tip-tracking behavior of the Ndc80 complex (Fig. 4 A). Ndc80 complexes bound preferentially at the microtubule tip, were more persistently attached, and moved with the disassembling tip.

For quantification, we defined tip-tracking as the colocalization of GFP-tagged Ndc80 complex with disassembling microtubule tips. In the presence of Dam1 complex, Ndc80 complex tracked with 78% (62 of 80) of disassembling microtubule tips over an average distance of 1.2 ± 0.2 μm, compared to only 27% (19 of 71) of tips over an average distance of 0.13 ± 0.09 μm in the absence of Dam1 complex (Fig. 4 B). In the presence of the Dam1 complex, tip-tracking events by the Ndc80 complex often continued until the tips reached the microtubule seeds. Therefore, we likely underestimate the effect of the Dam1 complex to enhance the ability of the Ndc80 complex to track disassembling tips.

We then used an optical trapping-based force clamp (Asbury, Gestaut et al. 2006; Franck, Powers et al. 2007; Powers, Franck et al. 2009; Franck, Powers et al. 2010) to test if the Dam1 complex enhances the tip-tracking ability of Ndc80 complex while under load. We attached beads decorated with Ndc80 complex to the tips of assembling microtubules in the presence and absence of free Dam1 complex. We applied constant tensile force until the attachment broke, the microtubule switched to disassembly or, in a few cases, the event was terminated by other causes (e.g., the bead became stuck to the coverslip). In the absence of Dam1 complex, bead-bound Ndc80 complex formed persistent load-bearing attachments to assembling and disassembling microtubule tips (Fig. 5), as reported previously (Powers, Franck et al. 2009). While bearing 1.8 ± 0.4 pN (mean ± s.d.) of continuous load, travel distances during assembly were broadly distributed with a mean of 350 nm ($n = 115$). Detachment from assembling tips occurred at a rate of 0.026 ± 0.003 s^{-1} (Fig. 5 B). To mimic the likely arrangement in vivo, we added free Dam1 complex lacking an affinity tag so that it interacted with the beads only via its interaction with Ndc80 complex (i.e., direct Dam1 complex-bead interactions were prevented – see Methods). In the presence of the Dam1 complex, the mean travel distance increased three-fold to 1,100 nm ($n = 42$, $P = 3 \cdot 10^{-8}$, KS test) and the detachment rate decreased five-fold to 0.005 ± 0.0008 s^{-1} (Fig. 5 B). Accordingly, plots of survival probability versus distance show that the couplers remained more persistently attached when Dam1 complex was present (Fig. 5 C).

We also developed a force ramp assay to test the coupling performance of bead-bound Ndc80 complex across a broader range of forces on both assembling and disassembling microtubule tips (Franck, Powers et al. 2010). After an initial 'preload' period at approximately 1 pN constant force, we gradually increased the force on a tip-attached bead at a constant rate (0.25 pN·s^{-1}) until the bead detached from the microtubule tip, the load limit of the trap (10-12 pN) was reached, or in the case of disassembling filaments, the microtubule switched from shortening to growth (Fig. 6). The maximum force achieved prior to any one of these termination points was recorded for each event. Without Dam1 complex present, all events recorded during microtubule assembly ended in detachment. Most events during disassembly also ended in detachment (93 of 96), but a few ended with a shortening-to-growth transition (2 of 96) or when the trap load limit was reached (1 of 96). The resulting maximum forces were

distributed narrowly, with means of 2.7 ± 0.1 pN (n = 101) during assembly and 2.7 ± 0.1 pN (n = 96) during disassembly (Fig. 6 E, F). The addition of Dam1 complex resulted in a clear improvement in the load-bearing capacity of the Ndc80 complex-coated beads. Most events recorded during assembly ended in detachment (112 of 131) but some persisted until the trap load limit was reached (19 of 131). Of the events recorded during disassembly, only about half ended in detachment (43 of 92). The remainder terminated when the microtubule switched to assembly (43 of 92) or, in a few cases, when the load limit was reached (6 of 92). The high frequency of shortening-to-growth transitions indicates that tension applied through linkages composed of both Ndc80 and Dam1 complexes promotes microtubule rescue, a phenomenon we saw previously using bead-bound Dam1 complex alone (Franck, Powers et al. 2007). The resulting maximum forces were distributed broadly with means of 5.2 ± 0.2 pN during assembly (n = 131) and 4.4 ± 0.2 pN during disassembly (n = 92), values that are two-fold higher than in the absence of Dam1 complex ($P < 1 \cdot 10^{-8}$ assembly; $P = 1 \cdot 10^{-8}$ disassembly). These observations, together with the force clamp results, show that interactions between Dam1 and Ndc80 complexes enhance coupling to both assembling and disassembling microtubule tips under load. This enhancement persists across a range of loads (up to 10 pN) and it occurs under conditions where the entire load is ultimately transmitted to the cargo through the Ndc80 complex.

Ipl1 phosphorylation regulates the interaction between Ndc80 and Dam1 complexes

We then asked if Ipl1 phosphorylation of the Dam1 complex regulates its interaction with the Ndc80 complex on microtubules. Phosphorylation of Ser 20 on the Dam1 protein weakens the interaction of the Dam1 complex with microtubules (Gestaut, Graczyk et al. 2008). To determine how phosphorylation at sites other than Ser 20 affects the interaction between the Dam1 and Ndc80 complexes, we used a modified Dam1 complex with a Ser 20 to Ala mutation (S20A). With the S20A substitution, the Dam1 complex interacts with microtubules in a manner that is indistinguishable from the wild-type complex, except that the interaction is insensitive to Ipl1 phosphorylation (Fig. S4 A, B). The phosphorylated S20A Dam1 complex also tracks with disassembling microtubule tips and is less diffusive at high concentrations, as expected for oligomers (Fig. S3). Phosphorylated S20A Dam1 complex also slows the disassembly of microtubules, as reported for wild-type Dam1 complex (Westermann, Wang et al. 2006; Franck, Powers et al. 2007; Grishchuk, Efremov et al. 2008).

In the presence of unphosphorylated S20A Dam1 complex, diffusion of the Ndc80 complex on microtubules is slowed, dissociation rate constant is decreased and tip-tracking is enhanced as described for the wild-type Dam1 complex (Fig. 7). However, Ipl1 phosphorylation of the S20A Dam1 complex abolished the ability of Dam1 complex to slow the diffusion and to decrease the dissociation rate constant of the Ndc80 complex (Fig. 7 B, C). Moreover, phosphorylated S20A Dam1 complex did not enhance the tip-tracking ability of the Ndc80 complex (Fig. 7 D). Control experiments were performed to ensure that after the initial Ipl1 phosphorylation reaction with the S20A Dam1 complex, residual Ipl1 activity was negligible (Fig. S5, see Methods). Furthermore, the ten proteins of the Dam1 complex do not dissociate from one another when the complex is phosphorylated by Ipl1 (Fig. S4 C). Since phosphorylation of the S20A Dam1 complex does not alter the behavior of the Dam1 complex alone but abolishes its ability to change the behavior of the Ndc80 complex, we conclude that Ipl1 phosphorylation of the Dam1 complex inhibits its interaction with the Ndc80 complex.

DISCUSSION

The Dam1 complex acts as a processivity factor for the Ndc80 complex

Many molecular machines require factors that enhance their processivity. For example, the proliferating cell nuclear antigen (PCNA) sliding clamp is required for efficient DNA replication by DNA polymerase ε (Kelman 1997). Likewise, dynactin is required for long-distance movement of cytoplasmic dynein along microtubules (King and Schroer 2000). Kinetochores are processive and form persistent attachments to dynamic microtubule tips over the times and distances required for chromosome biorientation and segregation. However, the contribution of individual components to the processivity of kinetochore-microtubule attachments is poorly understood. Here we show that the Dam1 complex enables the Ndc80 complex to track with disassembling microtubule tips over distances in excess of the length of the entire yeast spindle. We also show that the Dam1 complex strengthens the attachment of the Ndc80 complex to dynamic microtubule tips. In vivo, assembly of the Dam1 complex onto the kinetochore requires the Ndc80 complex (Janke, Ortiz et al. 2002). In our optical trap experiments, bead-bound Ndc80 complex was assayed with the Dam1 complex free in solution to mimic this arrangement in vitro. The increased ability of bead-bound Ndc80 complexes to bear load in the presence of free Dam1 complex indicates that tensile force can be transmitted through an Ndc80 complex-based linkage in a physiologically relevant arrangement.

We propose that the Dam1 complex acts as a processivity factor for the Ndc80 complex, and that the two complexes cooperate to form load-bearing kinetochore-microtubule attachments. In vivo, the Ndc80 complex forms lateral attachments to spindle microtubules prior to kinetochore association of Dam1 complex and biorientation (Tanaka, Mukae et al. 2005; Shimogawa, Graczyk et al. 2006). Our results are consistent with a model in which the Ndc80 complex initially mediates kinetochore attachment to microtubules. The Dam1 complex is later loaded onto the kinetochore to maintain attachment to dynamic microtubule tips. Association of the Dam1 complex is particularly important for these attachments to withstand the tensile forces required for biorientation. The existence of a distinct and separable processivity factor also provides a point of regulation for corrective detachment.

A mechanism for Aurora B-mediated corrective detachment

The regulatory mechanism that ensures chromosome biorientation has been proposed to respond to the level of tensile force on the kinetochore (Kelly and Funabiki 2009). When kinetochores make attachments that generate little tension, such as monotelic or syntelic attachments, progression to anaphase is blocked. Key to this regulation, the conserved Aurora B kinase is responsible for the release of aberrant kinetochore-microtubule attachments (Biggins, Severin et al. 1999; Tanaka, Rachidi et al. 2002; Hauf, Cole et al. 2003; Pinsky, Kung et al. 2006). We showed previously that phosphorylation by the yeast Aurora B kinase Ipl1 at Ser 20 of Dam1 decreases the affinity of the Dam1 complex for the microtubule lattice (Gestaut, Graczyk et al. 2008). We show here that Ipl1 phosphorylation of the Dam1 complex at sites other than Ser 20 weakens its interaction with the Ndc80 complex. Together these observations suggest that Ipl1 phosphorylation of the Dam1 complex promotes corrective detachment of kinetochores via two distinct mechanisms, decreasing the affinity of the Dam1 complex for both the Ndc80 complex and for microtubules. Regulation by Aurora B kinase is a conserved feature of kinetochore function in all eukaryotes. Therefore, we propose that regulation at both the

kinetochore-microtubule interface and between components of the kinetochore itself will extend to mechanisms of corrective detachment in higher eukaryotes.

MATERIALS AND METHODS

Protein Expression and Purification

The *S. cerevisiae* Ndc80 and Dam1 complexes were expressed from polycistronic vectors in *E. coli* as described (Wei, Sorger et al. 2005; Gestaut, Graczyk et al. 2008; Powers, Franck et al. 2009; Gestaut, Cooper et al. 2010). For TIRF microscopy, the Ndc80 complex Nuf2 subunit was tagged with GFP, and the Dam1 complex Dad1 subunit was tagged with GFP or mCherry. Complexes were purified by affinity chromatography and gel filtration as previously described (Asbury, Gestaut et al. 2006; Franck, Powers et al. 2007; Gestaut, Graczyk et al. 2008; Powers, Franck et al. 2009).

For optical trap bead assays, a TEV cleavage site was inserted adjacent to the His_6 affinity tag within the GFP-tagged Dam1 complex. The complex was purified by affinity chromatography and gel filtration as previously described (Gestaut, Graczyk et al. 2008). The cleavage reaction was carried out in 50 mM phosphate buffer, 350 mM NaCl, pH 6.9 with 1 mM DTT, 0.5 mM EDTA and recombinant TEV protease for 2 hrs at 4°C. TEV-cleaved Dam1 complex was isolated by gel filtration and cleavage was verified by immunoblot analysis.

Phosphorylation of the Dam1 complex

Dam1 complex was phosphorylated with purified GST-Ipl1 and GST-Sli15 as described (Gestaut, Graczyk et al. 2008). The reaction (50 µl) contained 4 µM GFP- or mCherry-tagged S20A Dam1 complex, 0.5 µM GST-Ipl1, 0.5 µM GST-Sli15 (residues 554-698), 200 mM NaCl, 10 mM ATP, 25 mM $MgCl_2$ and 50 mM HEPES buffer, pH 7.2. Reactions were incubated at 30°C for 90 min. Control reactions lacked GST-Ipl1 and GST-Sli15. Control reactions lacking ATP were also performed and gave similar results as previously reported (Gestaut, Graczyk et al. 2008). Ipl1 activity was not eliminated after the phosphorylation reaction. Therefore, to ensure that residual Ipl1 from the reaction did not affect our assays, we performed mock phosphorylation reactions using BSA in place of the Dam1 complex. The components of this mock reaction had no effect on the diffusion and dissociation rate constants of the Ndc80 complex either in the absence or presence of the Dam1 complex (Fig. S5).

TIRF Microscopy

A custom TIRF illumination system was constructed for simultaneous excitation of Alexa-647 and GFP (Gestaut, Graczyk et al. 2008; Powers, Franck et al. 2009; Gestaut, Cooper et al. 2010). Total internal reflection of a far-red laser (FTEC-635-0-25-PFQ, Blue Sky Research) and a blue laser (Sapphire 488-75, Coherent) was achieved using a through-the-objective lens arrangement (100 x 1.4 numerical aperture (NA) CFI Plan Apochromat, Nikon). Images from the far-red and green channels were projected side by side onto a cooled emCCD camera (iXon 887-BI, Andor Technology).

A custom flow cell construction method (Gestaut, Graczyk et al. 2008; Powers, Franck et al. 2009; Gestaut, Cooper et al. 2010) was employed. Glass slides (Gold Seal) were drilled with two holes along the short axis. Double-sided sticky tape (Scotch) was placed on either side of the holes to produce the walls of the flow channel. Silanized coverslips (Corning) were then

pressed firmly onto the tape and the ends of the channel were sealed with vacuum grease. To draw fluid through the channel, a peristaltic pump was used via a custom adaptor attached above one of the holes on the glass slide with adhesive transfer tape (3M).

Flow cells were washed with three 100 µl volumes of dH_2O. To bind taxol-stabilized microtubules, we flowed in a modified "rigor" kinesin (G234A) lacking motor activity (Rice, Lin et al. 1999) diluted in BRB80 containing 8 $mg \cdot ml^{-1}$ BSA (BB80). Flow cells were then washed with two 50 µl volumes of BB80, the second of which contained 10 µM taxol (BB80T). Alexa-647 labeled microtubules were diluted in BB80T and incubated in flow cells for 5 min. Flow cells were then washed with two 50 µl volumes of BB80T. Proteins were then introduced, diluted in BB80T containing 0.02 to 0.1 $mg \cdot ml^{-1}$ κ-casein, 200 $\mu g \cdot ml^{-1}$ glucose oxidase, 35 $\mu g \cdot ml^{-1}$ catalase, 25 mM glucose and 5 mM DTT. When assayed in combination, Ndc80 and Dam1 complexes were pre-mixed prior to their introduction into flow cells. After flowing in the protein mixture, 2000-frame movies were taken at 10 frames per second with iXon software (Andor Technology). All assays were performed at 26°C.

For disassembling microtubule assays, "rigor" kinesin was bound to flow cells and washed with 50 µl BB80, followed by 50 µl BB80 containing 0.1 mg ml^{-1} κ-casein and 1 mM GTP (GB). Alexa-647 labeled GMPCPP microtubule seeds were then bound and washed with two 50 µl volumes of GB. Microtubules were grown by incubating for ~15 min in GB containing 2 $mg \cdot ml^{-1}$ tubulin (Alexa-647 labeled 1:100), 200 $\mu g \cdot ml^{-1}$ glucose oxidase, 35 μg ml^{-1} catalase, 25 mM glucose and 5 mM DTT. Microtubule depolymerization was induced by buffer exchange removing free tubulin and simultaneously introducing proteins diluted in BB80 containing 0.1 $mg \cdot ml^{-1}$ κ-casein, 200 $\mu g \cdot ml^{-1}$ glucose oxidase, 35 $\mu g \cdot ml^{-1}$ catalase, 25 mM glucose and 5 mM DTT. Movies were started concomitantly with induction of depolymerization and taken at 10 frames per second for 2000 frames.

TIRF Microscopy Data Analysis

Software analysis of TIRF microscopy data was performed using Labview (National Instruments) as previously described (Gestaut, Graczyk et al. 2008; Powers, Franck et al. 2009; Gestaut, Cooper et al. 2010). The software generated the position and brightness of individual GFP-tagged complexes on microtubules over time. Custom Igor Pro (WaveMetrics) programs (available on request) were used to generate histograms of Ndc80 complex residence times on microtubules. A weighted single exponential fit was applied to determine the mean residence time, τ, and to calculate the dissociation rate constant, $k_{off} = \tau^{-1}$. Association rate constants, k_{on}, were estimated as the number of observed Ndc80 complex binding events per tubulin dimer per second, divided by the free concentration of Ndc80 complex. Standard diffusion plots of mean squared displacement versus time were generated in Igor Pro. A weighted linear fit was used to calculate the one-dimensional diffusion constant, D, of GFP-tagged complexes on microtubules.

To quantify Ndc80 complex tip-tracking, brightness profiles along disassembling tips were created in Labview. Fluorescent signals at the tips were averaged across seven frames (0.7 sec) and we required a minimum intensity threshold of 20% above background to score a tip-tracking event. For each individual frame, the instantaneous depolymerization rate was calculated as the change in tip position over 50 frames (5 sec). A microtubule disassembly event was defined to start at the first appearance of GFP-tagged Ndc80 complex at the tip, and to end when the rate of depolymerization dropped below 0.03 $\mu m \cdot s^{-1}$. Microtubule tips without tracking as defined by this criterion were omitted from further analysis. The total tracking

distance for each individual tip was determined and the average tracking distance per depolymerization event was calculated.

To quantify binding to microtubules, we created brightness profiles of 500 pM mCherry-tagged Dam1 complex using our TIRF assay. After 5 min incubation with taxol-stabilized microtubules, an image was recorded (6 or 7 images per condition). For each microtubule in the image, the integrated intensity of mCherry was measured in ImageJ (NIH) and the brightness per unit length was calculated. Brightness per unit length values were averaged across all microtubules within one image, and reported as averages from multiple images.

Electron Microscopy

Taxol-stabilized microtubules were made by polymerizing cleared tubulin in a total volume of 40 µl BRB80 containing 1.75 mM GTP, 1 mM $MgCl_2$, and 3.5% DMSO at 37°C for 30 min. Various concentrations of Dam1 complex were mixed with taxol-stabilized microtubules to a final concentration of 36 nM tubulin in BRB80 containing 10 µM taxol, and incubated for 15 min. Samples were prepared for analysis by electron microscopy as follows. Carbon coated copper grids were positively charged in a glow discharge device (EMS) for 2 minutes. A 2 µl drop of sample was applied onto a freshly discharged grid and incubated for 20 seconds. Excess solution was blotted off and the grid washed twice with water and once with 0.075% uranyl formate before staining with uranyl formate. The stain was blotted off and the grid air dried. The preparations were viewed on a transmission electron microscope (Spirit T12, FEI) operating at 120kV and images recorded on a 1k x1k Gatan bottom mount slow-scan charge coupled device camera at a nominal magnification of either 15,000x or 52,000x at the specimen level. For each preparation, the total number of Dam1 complex rings on microtubules were counted and divided by the total length of microtubules to generate an average number of Dam1 complex rings per microtubule micron. In control experiments performed in the presence of blocking proteins (8 $mg \cdot ml^{-1}$ BSA and 0.02 $mg \cdot ml^{-1}$ κ-casein), rings were still absent at 500 pM Dam1 complex.

Optical Trap Instrumentation and Bead Preparation

Our optical trap has been described previously (Franck, Powers et al. 2007; Powers, Franck et al. 2009; Franck, Powers et al. 2010). The instrument is built around an inverted microscope (TE2000, Nikon) equipped for video-enhanced differential interference contrast (DIC) imaging. Custom-mounted optics direct the infrared trapping laser (J20-BL10–106Q, Spectra Physics) through the objective lens (100 x 1.4 NA oil CFI Plan Apochromat IR, Nikon), through a high-NA oil immersion condenser, and onto a position sensitive detector. During force clamp experiments, a computer-feedback controlled piezo specimen stage (P-517.3CL, Physik Instrumente) was programmed (using Labview, National Instruments) to maintain a fixed offset between the tip-attached bead and the trap center by moving to accommodate changes in microtubule length, thereby keeping the tensile force constant. During force ramp experiments, the bead-trap separation was increased at a fixed rate, 0.25 $pN \cdot s^{-1}$, up to a preset maximum of 10-12 pN (just below the escape force of the trap). For both force ramp and force clamp experiments, the stage position was updated and stored to disk at 50 Hz. Bead-trap separation was sampled at 40 kHz but decimated to 200 Hz for storage.

Beads were prepared as previously described (Powers, Franck et al. 2009). Ndc80 complex was linked to 0.44 µm diameter streptavadin-coated beads (Spherotech) with

biotinylated His_5 antibody (Qiagen). Ndc80 complex was diluted to 13-15 nM in BB80 with 1 mM DTT, and incubated with 6 pM beads at 4°C for ~90 min. In some experiments, recombinant His_6-tagged GFP was used as a blocking agent. Here, Ndc80 complex was diluted to 30 nM in BB80 with 1 mM DTT, and incubated with 12 pM beads at 4°C for ~90 min. These beads were then mixed 1:1 with 6 μM GFP and incubated an additional 30 minutes before use. The amount of complex per bead and the final bead concentration was the same in both protocols. Both protocols yielded a molar ratio of Ndc80 complexes to beads of 2,200 to 2,500. Based on simple geometric considerations (Powers, Franck et al. 2009), we estimate that < 100 Ndc80 complexes could simultaneously interact with the filament. The Ndc80 complex:bead ratio was chosen to create tip-attachments of moderate strength, so the full force range of the optical trap could be used to assess the contribution of Dam1 complex to the Ndc80 complex-based attachments. Results obtained with and without the GFP block were statistically indistinguishable ($P = 0.3010$ Ndc80 complex during assembly; $P = 0.5518$ Ndc80 complex during disassembly; $P = 0.1663$ Ndc80 complex + Dam1 complex during assembly; $P = 0.8597$ Ndc80 complex + Dam1 complex during disassembly), so they were pooled and analyzed together.

Optical Trap Bead Assays, Data Collection and Analysis

Flow chambers were constructed and functionalized as previously described (Powers, Franck et al. 2009; Franck, Powers et al. 2010). Briefly, two lengths of double-sided sticky tape (Scotch) were placed across the width of a microscope slide (Gold Seal) to form an inverted chamber of 2-3 mm width. A cleaned coverslip (Corning) longer than the slide width was pressed firmly onto the tape to form the chamber bottom, the overhanging edges acting as reservoirs for pipetting and aspirating solutions through the chamber. The chamber was functionalized by introducing one volume of 1 $mg \cdot ml^{-1}$ biotinylated BSA (Vector Labs) and incubating for >10 minutes at room temperature. The chamber was then washed with ~20 volumes of BRB80, followed by ~20 volumes of 0.33 $mg \cdot ml^{-1}$ Avidin DN (Vector Labs). After a second wash with ~20 volumes of BRB80, stable biotinylated microtubule seeds were introduced and then washed with a growth and blocking buffer, BRB80 containing 1 mM GTP, 2 $mg \cdot ml^{-1}$ κ-casein and 2% pluronic F-187. Subsequently, we introduced Ndc80 complex-coated beads that were diluted 8-fold into growth buffer, BB80 containing 1 mM GTP, 1.4 $mg \cdot ml^{-1}$ tubulin, 1 mM DTT, 250 $\mu g \cdot ml^{-1}$ glucose oxidase, 30 $\mu g \cdot ml^{-1}$ catalase and 4.5 $\mu g \cdot ml^{-1}$ glucose. In assays with Dam1 complex, His_6-cleaved GFP-tagged Dam1 complex was used at a final concentration of 9-15 nM and added to the bead mixture just prior to introduction into the flow chamber. Microtubule disassembly events either occurred by a spontaneous switch from assembly to disassembly or were induced by laser scission (Franck, Powers et al. 2010). All trap assays were performed at 26°C.

Records of bead position versus time were analyzed using custom software written in Igor Pro (available on request). Periods of microtubule assembly and disassembly were visually identified in the records. Detachments were scored when the force on a bead under load suddenly dropped to zero and the stage exhibited open-loop ('run-away') movement. The maximum force was taken as the mean of the final ten data points prior to event termination (detachment or microtubule assembly/disassembly state switching). The survival probability was calculated by dividing the number of events that persisted beyond a given distance by the total number of events.

A bead-microtubule binding assay was used to verify that His_6-cleaved GFP-tagged Dam1 complex did not bind directly to the GFP-blocked beads. Taxol-stabilized microtubules were introduced into a flow chamber and given 1 minute to adhere nonspecifically to the coverslip. Following a wash and 10 minute incubation with surface block (BRB80 with 2 $mg \cdot ml^{-1}$ κ-casein and 10 μM taxol), free beads were introduced. After waiting 10 minutes to allow beads to bind, the number of microtubule-attached beads was counted across many fields of view (each 822 μm^2). Beads decorated with Ndc80 complex bound microtubules at a density of 7,800 $beads \cdot mm^{-2}$ (1,355 beads in 210 fields of view), whereas beads blocked with GFP in the presence of free Dam1 complex bound at only 24 $beads \cdot mm^{-2}$ (5 beads in 250 fields of view) under identical conditions.

FIGURES

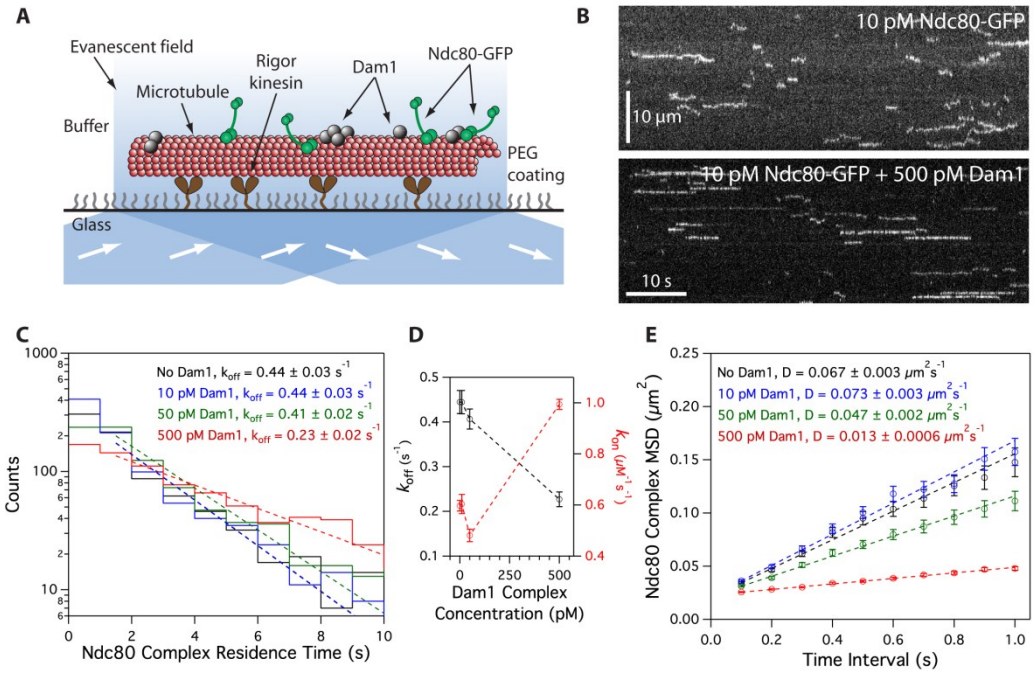

Figure 1: Dam1 complex enhances binding of individual Ndc80 complexes to microtubules

(**A**) Schematic of the TIRF assay developed to visualize the behavior of GFP-tagged Ndc80 complexes (green rods) in the presence of untagged Dam1 complexes (grey spheres) on microtubules. (**B**) Representative kymographs showing the binding and one-dimensional diffusion of 10 pM Ndc80 complexes on taxol-stabilized microtubules in the absence or presence of 500 pM Dam1 complex. Positions along the microtubule are shown on the vertical axis, while the passage of time is depicted along the horizontal axis. Concentrations are of free complexes in solution. (**C**) Residence time distributions of 10 pM Ndc80 complex on microtubules without Dam1 complex (black histogram, *n* = 883 events), with 10 pM Dam1 complex (blue histogram, *n* = 966), with 50 pM Dam1 complex (green histogram, *n* = 928), and with 500 pM Dam1 complex (red histogram, *n* = 1,003). Dotted lines show the weighted exponential fits used to determine dissociation rate constants, k_{off}. (**D**) Dissociation rate constants (k_{off}, left axis, black markers) for the Ndc80 complex, calculated from the data in (C), are plotted against the concentration of Dam1 complex. Association rate constants (k_{on}, right axis, red markers) of the Ndc80 complex are also plotted (without Dam1 complex, *n* = 1,103; with 10 pM Dam1 complex, *n* = 1,426; with 50 pM Dam1 complex, *n* = 1,179; with 500 pM Dam1 complex, *n* = 1,412). (**E**) Mean-squared displacement (MSD) is plotted against time for 10 pM Ndc80 complex on microtubules without Dam1 complex (black markers, *n* = 803 events), with 10 pM Dam1 complex (blue markers, *n* = 859), with 50 pM Dam1 complex (green markers, *n* = 883), and with 500 pM Dam1 complex (red markers, *n* = 968). Dotted lines show the weighted linear fit used to determine diffusion constant, D. Markers are mean values ± s.e.m.

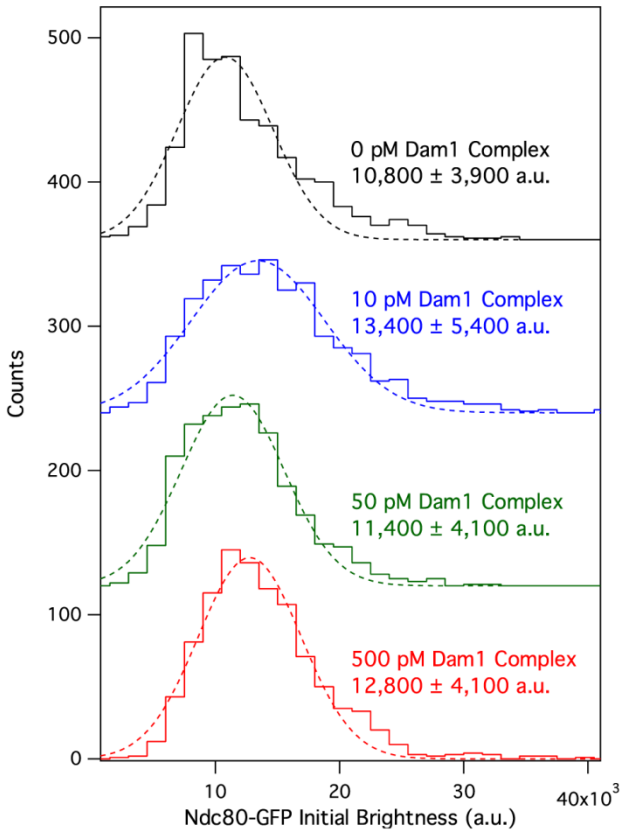

Figure 2: Dam1 complex does not affect the oligomerization state of the Ndc80 complex on microtubules

Average initial brightness distributions of GFP-tagged Ndc80 complex (10 pM) binding events on microtubules without Dam1 complex (black histogram, *n* = 883 events), with 10 pM Dam1 complex (blue histogram, *n* = 966), with 50 pM Dam1 complex (green histogram, *n* = 928), and with 500 pM Dam1 complex (red histogram, *n* = 1,003). Dotted lines show Gaussian fits used to determine mean values ± s.d. These values are similar to the average brightness from rare single bleach steps of GFP-tagged Ndc80 complex (9,300 ± 3,200 a.u., *n* = 11). For clarity, green, blue, and black histograms are offset vertically by 120, 240, and 360 counts respectively.

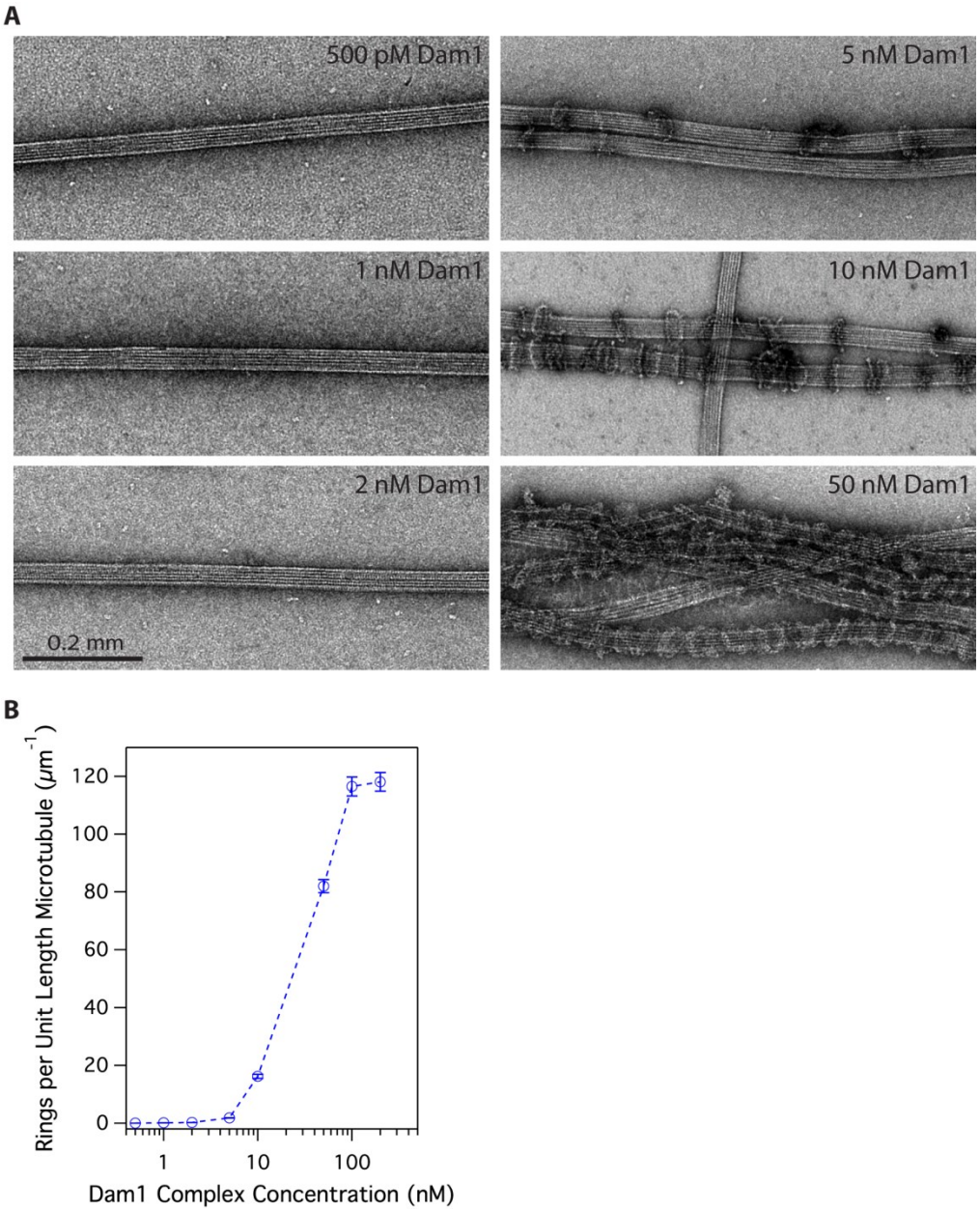

Figure 3: Assembly of oligomeric rings of the Dam1 complex around microtubules

(**A**) Negative-stain electron micrographs of oligomeric rings formed by the Dam1 complex around taxol-stabilized microtubules. (**B**) The number of rings observed per unit length (μm) of microtubule was quantified (statistics shown in Table 1) and plotted against the total concentration of Dam1 complex. Error bars represent counting uncertainties.

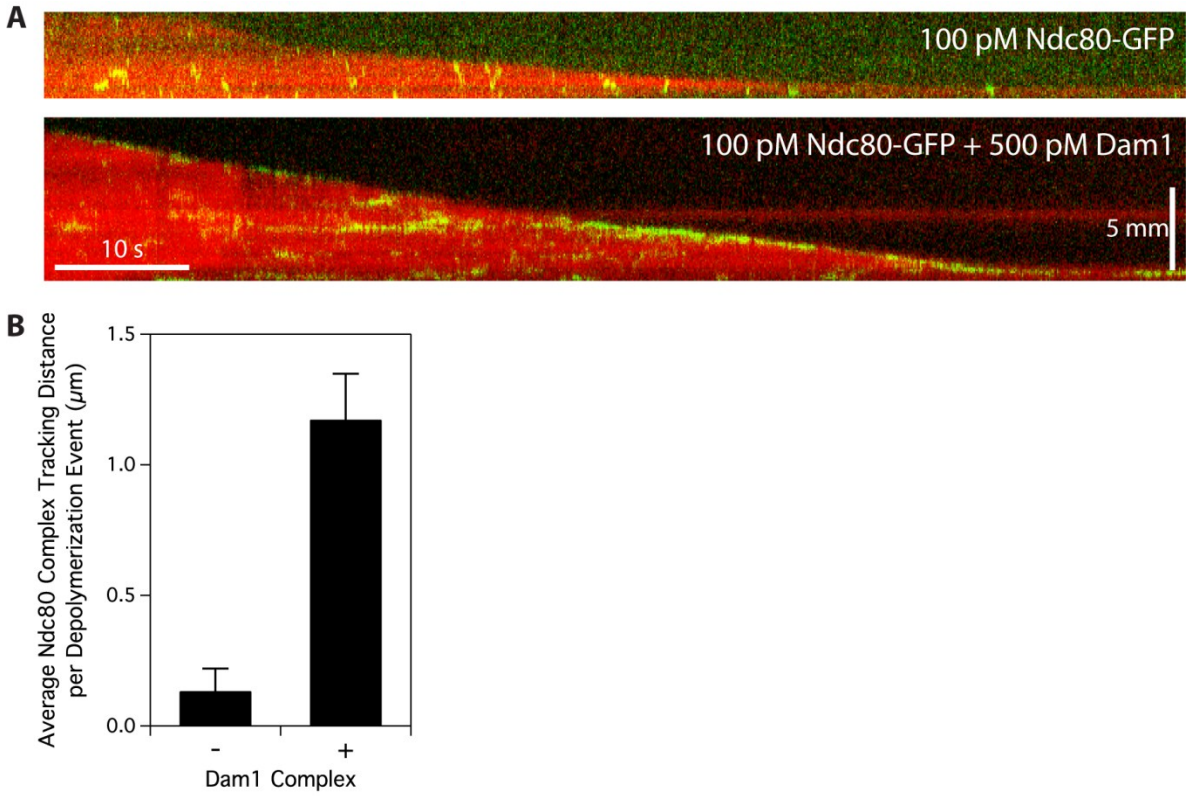

Figure 4: Ndc80 complex tracks with disassembling tips in the presence of Dam1 complex

(**A**) Representative two-color kymographs showing the tip-tracking ability of Ndc80 complex (100 pM) in the presence or absence of Dam1 complex (500 pM). Movement of GFP-tagged Ndc80 complex (green) is shown on disassembling microtubules (red). Concentrations are of free complexes in solution. (**B**) Average tracking distance of Ndc80 complex per depolymerization event in the absence of Dam1 complex (n = 19) or in the presence of 500 pM Dam1 complex (n = 62). Bars are mean values ± s.e.m.

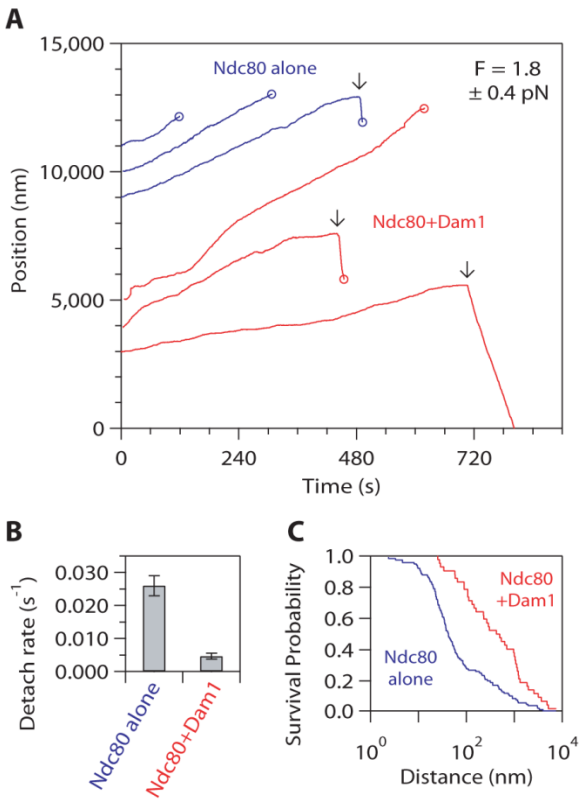

Figure 5: Dam1 complex enhances the coupling of bead-bound Ndc80 complex to assembling microtubule tips under fixed load

(**A**) Representative records of bead position versus time for microtubule tip attachments by bead-bound Ndc80 complex in the absence (blue traces), or presence (red traces) of free Dam1 complex during continuous application of tensile load. Increasing position represents assembly-coupled movement in the direction of applied force. Arrows mark transitions from assembly to disassembly. Decreasing position represents disassembly-driven movement against the applied force. Circles indicate detachment. For clarity, each record is offset vertically by an arbitrary amount. (**B**) Rates of bead detachment from assembling microtubule tips, estimated by counting the number of detachment events and dividing by total observation time. Error bars represent uncertainty based on Poisson statistics. (**C**) Survival probability versus distance for attachments composed of bead-bound Ndc80 complex in the absence (blue trace), or presence (red trace) of free Dam1 complex. The survival probability is the number of events that persisted beyond a given distance divided by the total number of events.

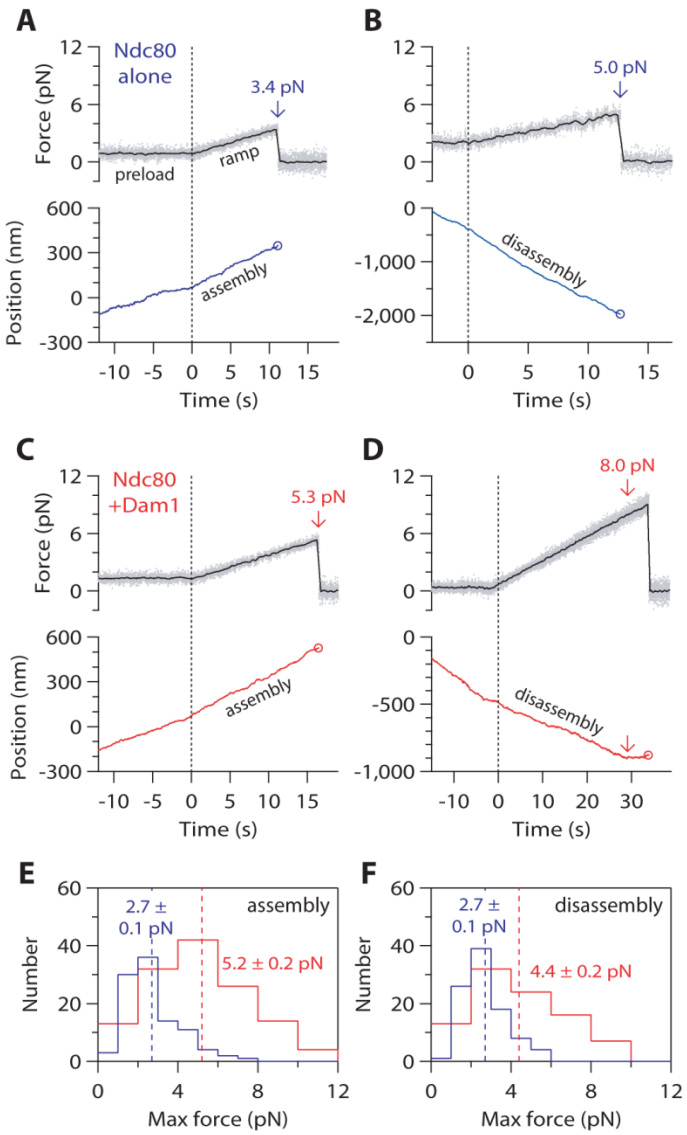

Figure 6: Dam1 complex enhances the coupling of bead-bound Ndc80 complex to assembling and disassembling microtubule tips across a range of loads

(**A**-**D**) Representative records showing tensile force (upper plots) and bead position (lower plots) versus time for bead-bound Ndc80 complexes attached to assembling and disassembling microtubule tips in the absence (A, B) or presence (C, D) of free Dam1 complex. The instrument was programmed to automatically increase the force at a constant rate (0.25 pN·s^{-1}) after ~500 nm of movement occurred. Arrows mark maximum forces, recorded either at rupture or when the microtubule switched from disassembly to assembly. Circles mark ruptures. (**E**) Distributions of maximum force for bead-bound Ndc80 complexes attached to assembling tips in the absence (blue histogram, *n* = 101), or presence (red histogram, *n* = 131) of free Dam1 complex. (**F**) Distributions of maximum force for bead-bound Ndc80 complexes attached to disassembling tips in the absence (blue histogram, *n* = 96), or presence (red histogram, *n* = 92) of free Dam1 complex. Dotted vertical lines indicate the average for each distribution. Uncertainties represent standard errors.

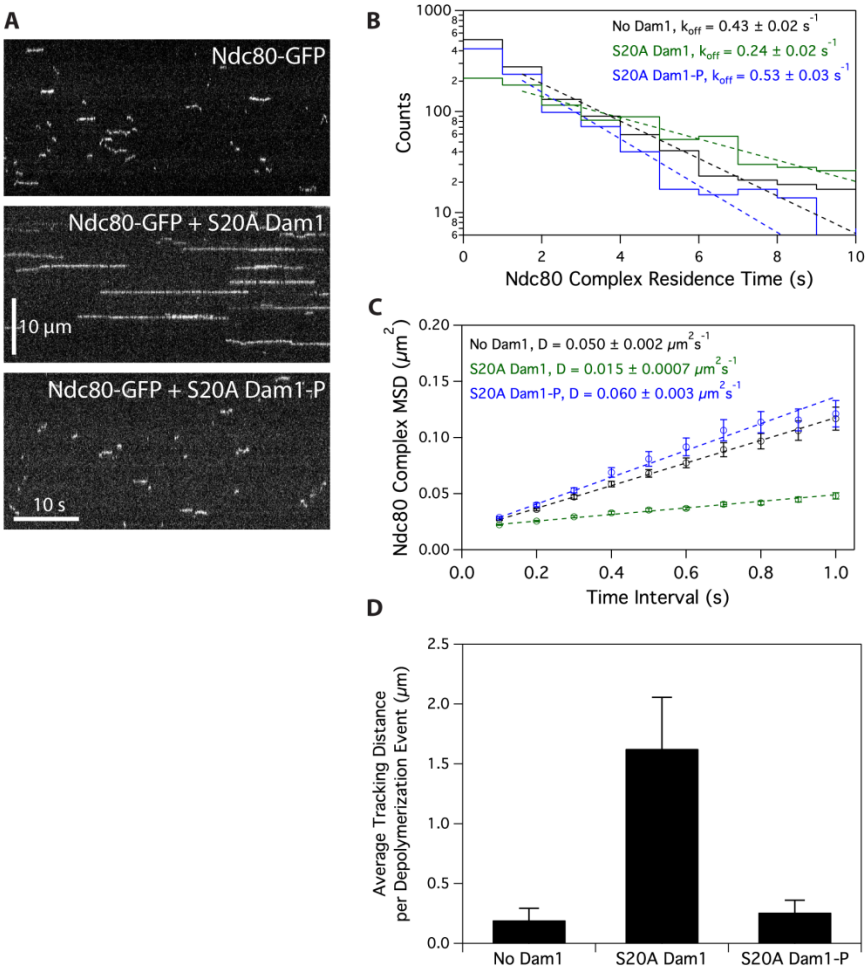

Figure 7: Ipl1 phosphorylation of the Dam1 complex regulates its interaction with the Ndc80 complex

(**A**) Representative kymographs showing changes in behavior of the Ndc80 complex (10 pM) with the addition of S20A Dam1 complex (500 pM) with or without Ipl1 phosphorylation. Concentrations are of free complexes in solution. (**B**) Residence time distributions of Ndc80 complex (10 pM) on microtubules without Dam1 complex (black histogram, *n* = 1,266 events), with 500 pM S20A Dam1 complex (green histogram, *n* = 1,081), and with 500 pM Ipl1 phosphorylated S20A Dam1 complex (blue histogram, *n* = 974). Dotted lines show the weighted exponential fits used to determine dissociation rate constants, k_{off}. (**C**) Mean-squared displacement (MSD) is plotted against time for Ndc80 complex (10 pM) on microtubules without Dam1 complex (black markers, *n* = 1,102), with 500 pM S20A Dam1 complex (green markers, *n* = 1,030), and with 500 pM Ipl1 phosphorylated S20A Dam1 complex (blue markers, *n* = 860). Markers are mean values ± s.e.m. Dotted lines show the weighted linear fit used to determine diffusion constant, D. (**D**) Average tracking distance of 100 pM Ndc80 complex per depolymerization event in the absence of Dam1 complex (*n* = 19), in the presence of 500 pM S20A Dam1 complex (*n* = 28), or in the presence of 500 pM Ipl1 phosphorylated S20A Dam1 complex (*n* = 39). Bars are mean values ± s.e.m.

SUPPLEMENTAL FIGURES

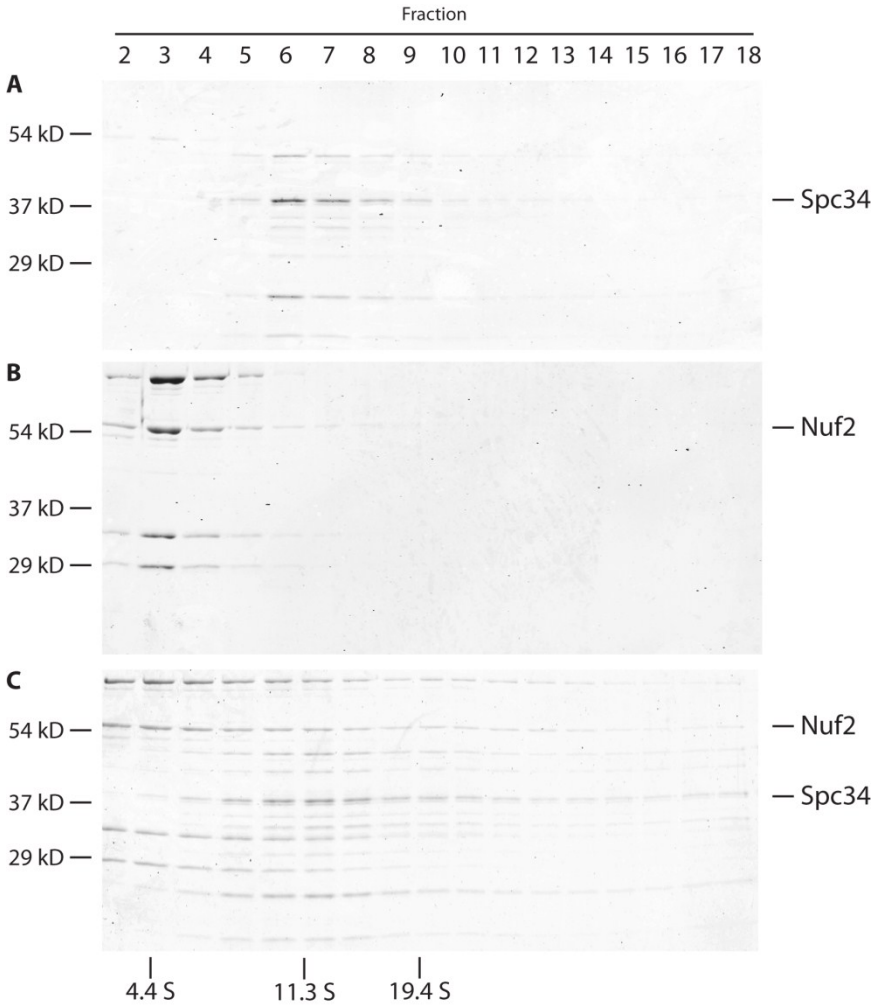

Figure S1: Ndc80 and Dam1 complexes interact weakly free in solution
The interaction between Ndc80 and Dam1 complexes free in solution was assayed by velocity sedimentation. Samples (240 µl) were layered onto 4.75 ml linear sucrose gradients (8 – 32%). Gradients were centrifuged at 189,000xG at 4°C for 6 hrs and fractions (265 µl) were collected. Fraction 1 is the top of the gradient. BSA (4.4S), catalase (11.3S), and thyroglobulin (19.4S) were used as standards. When assayed alone and together, Ndc80 complex and Dam1 complex had a sedimentation coefficient of 4.4S and 11.3S respectively. Based on a Stokes radius of 9.9 nm as determined by gel filtration, the molecular weight of Dam1 complex was calculated to be ~470 kD (Siegel and Monty, 1966). Therefore, at the concentration in this assay, the 204 kD Dam1 complex exists primarily as a dimer free in solution. The positions of the Dam1 complex component Spc34 and the Ndc80 complex component Nuf2 are indicated on the right. (**A**) 2 µM Dam1 complex, (**B**) 1 µM Ndc80 complex and (**C**) 2 µM Dam1 complex and 1 µM Ndc80 complex in combination.

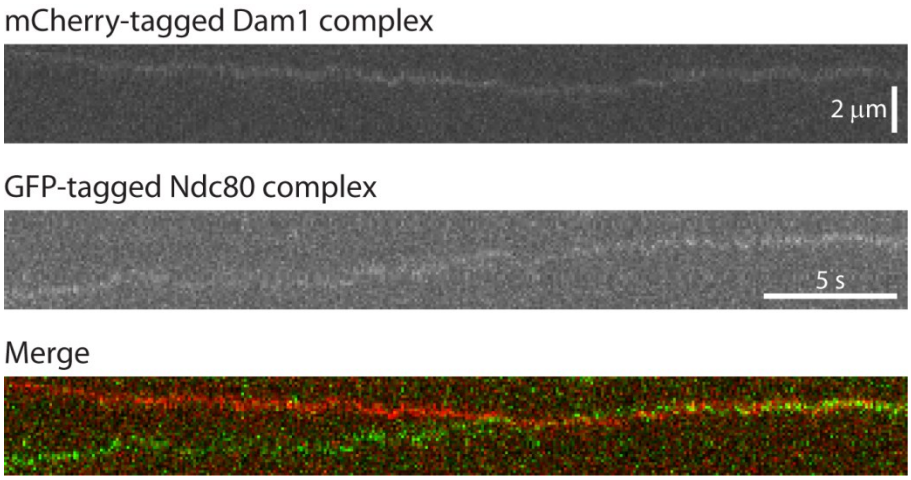

Figure S2: Ndc80 complex and Dam1 complex interact on microtubules

Representative kymograph showing the diffusion of GFP-tagged Ndc80 complex (10 pM) and mCherry-tagged Dam1 complex (2 pM) on microtubules. Both complexes are diffusive alone, but appear to diffuse more slowly when they interact on microtubules.

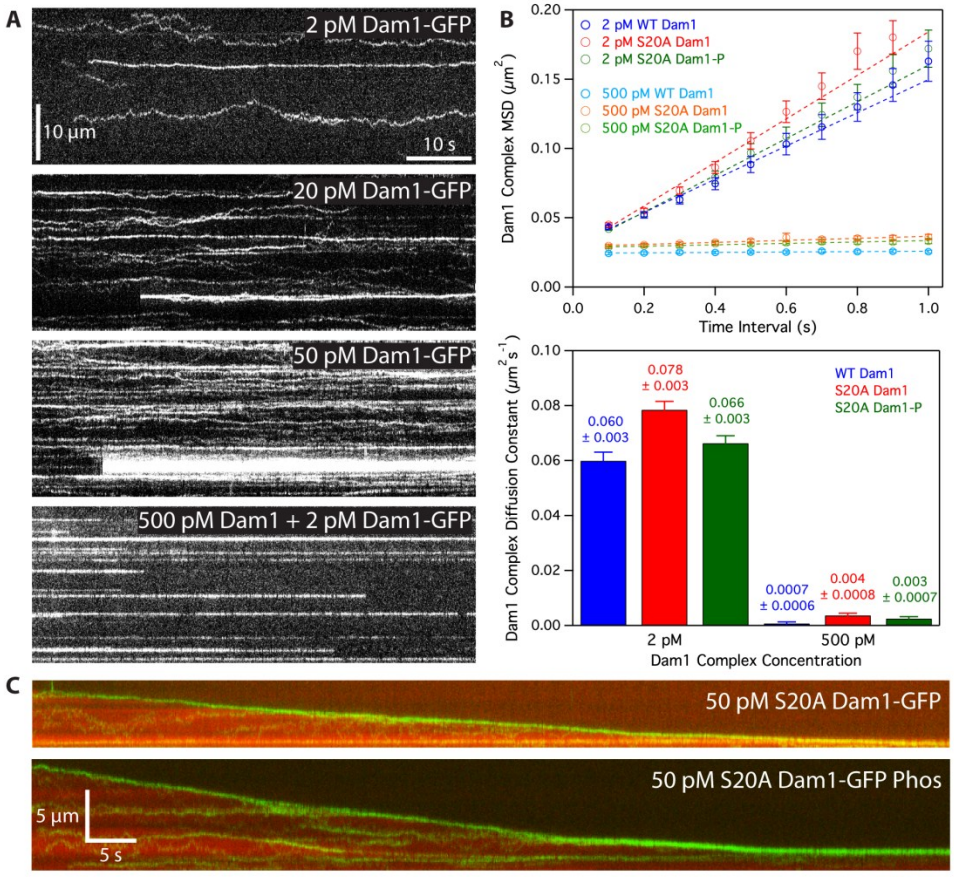

Figure S3: The Dam1 complex oligomerizes on microtubules and tracks with disassembling tips
(**A**) Representative kymographs showing changes in Dam1 complex behavior as it oligomerizes on microtubules. At 2 pM GFP-tagged Dam1 complex, single monomers were discernable. At 20 and 50 pM, slowly diffusing oligomers were seen as lines. At 500 pM Dam1 complex, the behaviors of individual oligomers were traced by visualizing a small proportion of labeled complex. Concentrations are of free complexes in solution. (**B**) Oligomerization of Dam1 complex slows its diffusion on taxol-stabilized microtubules and oligomerization of S20A Dam1 complex is not abolished by Ipl1 phosphorylation. Top: Mean-squared displacement (MSD) is plotted against time for 2 pM WT Dam1 complex (blue markers, n = 188), 2 pM S20A Dam1 complex (red markers, n = 327), 2 pM Ipl1 phosphorylated S20A Dam1 complex (green markers, n = 346), 500 pM wild-type (WT) Dam1 complex (light blue markers, n = 129), 500 pM S20A Dam1 complex (orange markers, n = 188) and 500 pM Ipl1 phosphorylated S20A Dam1 complex (light green markers, n = 231). At 500 pM Dam1 complex, the behaviors of individual oligomers were traced by visualizing a small proportion of labeled complex. Markers are mean values ± s.e.m. Dotted lines show the weighted linear fits used to determine diffusion constants, D. Bottom: Diffusion constants derived from MSD versus time plots are summarized as a bar graph. WT Dam1 complex (blue bars), S20A Dam1 complex (red bars), and Ipl1 phosphorylated S20A Dam1 complex (green bars). Error bars denote s.e.m. (**C**) Representative two-color kymographs demonstrating the tip-tracking ability of Ipl1 phosphorylated S20A Dam1 complex. Movement of 50 pM GFP-tagged unphosphorylated and phosphorylated S20A Dam1 complex (green) is shown on disassembling microtubules (red).

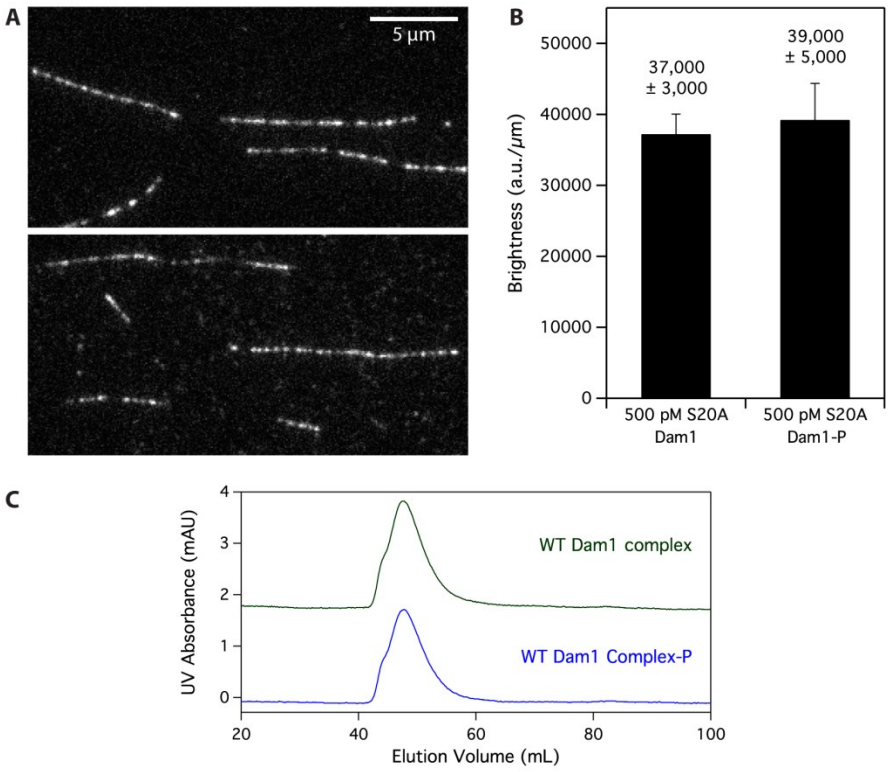

Figure S4: Phosphorylation does not affect microtubule binding of S20A Dam1 complex, and does not cause disassembly of wild-type Dam1 complex

(**A**) Representative images of mCherry-tagged S20A Dam1 complex on microtubules. Top: 500 pM S20A Dam1 complex. Bottom: 500 pM Ipl1 phosphorylated S20A Dam1 complex. (**B**) Image averages of mCherry brightness per unit length microtubules for unphosphorylated (*n* = 6 images representing 68 microtubules, totaling 790 µm) and phosphoryated (*n* = 7 images representing 51 microtubules, totaling 754 µm) S20A Dam1 complex. Bars are mean values ± s.e.m. (**C**) Unphosphorylated and Ipl1 phosphorylated wild-type Dam1 complexes each migrate as a single peak during gel filtration, and elute at a volume consistent with previously reported values (Gestaut et al., 2008). The elution profile for unphosphorylated Dam1 complex is offset vertically by 2 mAU.

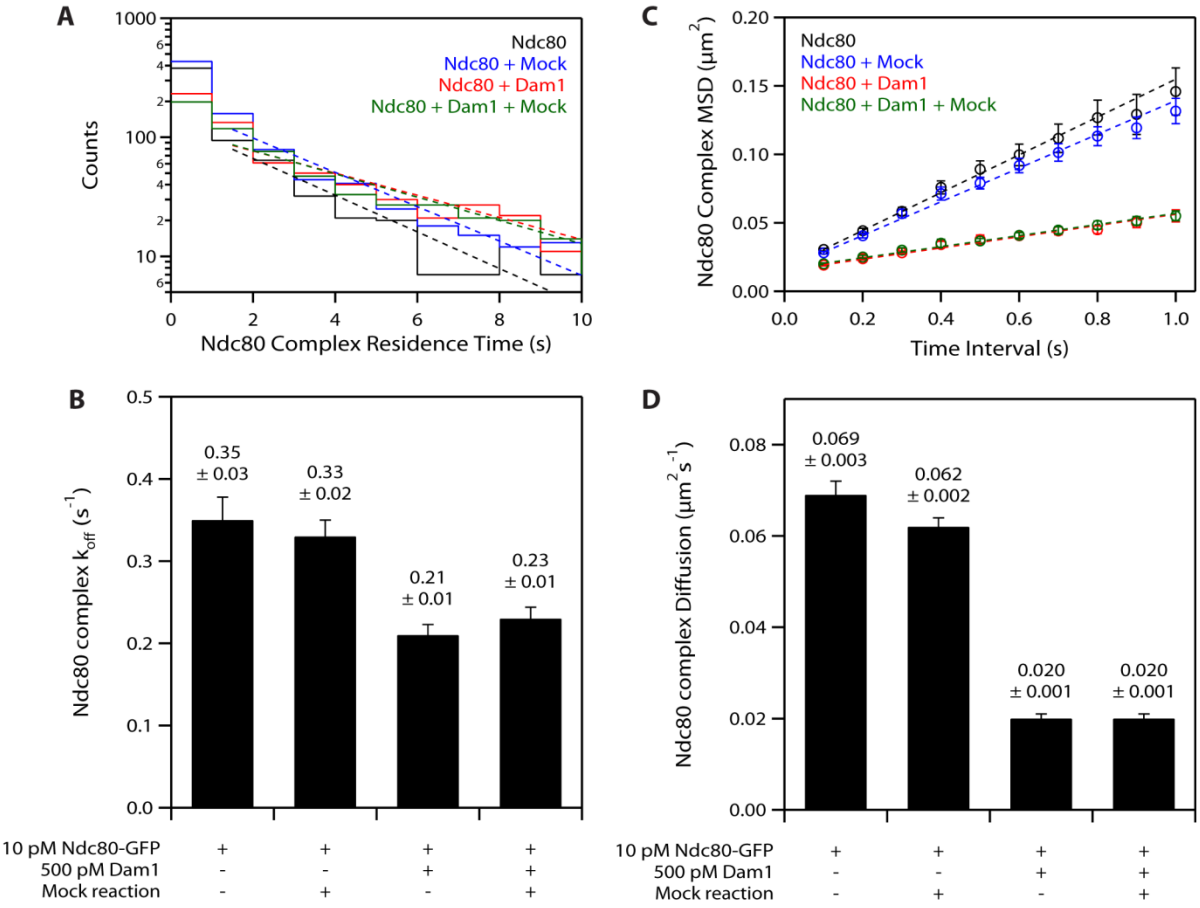

Figure S5: Residual components of Ipl1 phosphorylation reactions have no effect on the behavior of the Ndc80 complex on microtubules

Mock Ipl1 phosphorylation reactions were performed with BSA in place of Dam1 complex, and added to TIRF assays at concentrations as in Fig. 6 (63 pM Ipl1, 63 pM Sli15, and 1.3 μM ATP). (**A**) Residence time distributions of GFP-tagged Ndc80 complex (10 pM) on microtubules alone (black histogram, *n* = 692), with mock reaction (blue histogram, *n* = 869), with 500 pM Dam1 complex (red histogram, *n* = 752), and with 500 pM Dam1 complex and mock reaction (green histogram, *n* = 699). Dotted lines show the weighted exponential fits used to determine dissociation rate constants, k_{off}. (**B**) Dissociation rate constants derived from histograms are summarized as a bar graph. Bars are mean values ± s.e.m. (**C**) Mean-squared displacement (MSD) is plotted against time for GFP-tagged Ndc80 complex (10 pM) on microtubules alone (black markers, *n* = 472), with mock reaction (blue markers, *n* = 670), with 500 pM Dam1 complex (red markers, *n* = 636), and with 500 pM Dam1 complex and mock reaction (green markers, *n* = 586). Markers are mean values ± s.e.m. Dotted lines show the weighted linear fits used to determine diffusion constants, D. (**D**) Diffusion rate constants derived from MSD versus time plots are summarized as a bar graph. Bars are mean values ± s.e.m.

Chapter 6

A Combination of Biased Diffusion and Conformational Wave Mechanisms Can Quantitatively Explain Kinetochore-Microtubule Coupling

ABSTRACT

To orchestrate mitosis, multi-protein assemblies called kinetochores form tension-bearing attachments between chromosomes and the tips of dynamic microtubule filaments, coupling chromosome movement to microtubule growth and shortening. Models for kinetochore-microtubule coupling must explain how kinetochores remain attached to both assembling and disassembling tips. Two types of mechanisms have been proposed, one based on biased thermal diffusion and another based on a 'conformational wave' or power stroke exerted by the microtubule tip. Here we describe a predictive mathematical model that can incorporate both mechanisms. Model predictions are compared with actual detachment rates measured for reconstituted couplers as the number of binding elements in the couplers is varied, and across different levels of applied tension. The data recorded during assembly-coupled movement are well-fit by pure biased diffusion models, in which the random movement of individual binding elements on the microtubule lattice becomes biased only at the terminal tubulin subunits. However, such models predict detachment rates during disassembly-driven movement that are at least and order of magnitude faster than measured. Globally matching the data from both assembly and disassembly requires a hybrid model, with an extra force representing the spring-like protofilament curls found at disassembling tips. These considerations suggest that kinetochore-microtubule coupling occurs through a combination of the biased diffusion and conformational wave mechanisms.

INTRODUCTION

Chromosomes are organized and segregated during mitosis by the mitotic spindle, an array of dynamic microtubule filaments organized between two poles. Kinetochores are macromolecular assemblies that mechanically couple chromosome movement to microtubule growth and shortening. They also serve as signaling modules, sensing and correcting errors in attachment and forestalling progression through mitosis until each paired chromosome is fully and properly coupled to microtubules emanating only from its proximal pole. Improper and lost attachments create aneuploidy, a disastrous gain or loss of chromosomes strongly correlated with many cancers and birth defects. A better understanding of how kinetochores maintain persistent, load-bearing attachments at the tips of assembling and disassembling microtubules is paramount, not only for basic science but also for research on the development and treatment of cancer. Although several attractive models for kinetochore-microtubule attachment have been proposed, the underlying mechanism remains poorly understood and largely untested. We can, however, reconstitute and observe kinetochore-like attachments in vitro, permitting the construction and testing of quantitative models for microtubule coupling using motility assays, a capability presently lacking in living cells. Here, using a combination of theory and experimentation, we propose a simple, flexible model for kinetochore-microtubule attachment that fully describes our data. The model addresses long-standing questions about not only kinetochore-microtubule coupling, but also the biophysical nature of multivalent attachment.

Models for kinetochore-microtubule attachment can be classified by the energy source responsible for chromosome movement. In the first class, coupling is based on ATP-powered motor enzymes. Motors localized at kinetochores contribute to microtubule coupling in many organisms and some are capable of forming attachments to disassembling microtubules in vitro (Lombillo, Stewart et al. 1995; Sharp, Rogers et al. 2000; Yang, Tulu et al. 2007). However, other non-enzymatic kinetochore components, including the Dam1 and Ndc80/Hec1 (hereafter Hec1) complex are indispensable for kinetochore-microtubule coupling (Cheeseman, Enquist-Newman et al. 2001; Jones, He et al. 2001; Li, Bachant et al. 2002; Tanaka and Desai 2008). In vitro studies have shown that these complexes bind directly to microtubules, implicating the microtubule itself as an important energy source. Hydrolysis of GTP –containing subunits drives the non-equilibrium microtubule growth and shortening termed "dynamic instability", harnessed by the kinetochore to produce force and motion (Mitchison and Kirschner 1984; Inoue and Salmon 1995). Energy transduction may occur by mechanical motion or by the establishment of a free-energy potential in binding or both. The tip of a disassembling microtubule is typically a frayed collection of curling protofilaments, suggesting that a contiguous peeling of subunits could generate a "conformational wave" or power stroke of mechanical force (Koshland, Mitchison et al. 1988). The high binding affinity of kinetochore complexes for microtubules may also play role in attachment. A free-energy potential is generated when microtubule disassembly releases previously bound complexes, creating a thermodynamic driving force that could bias diffusive motion toward the microtubule filament, even against an opposing load (Hill 1985). Evidence for microtubule-generated motion comes primarily from in vitro studies. A bead tightly bound to disassembling microtubule via biotin-strepavidin linkage can exert a brief pulling force before detaching, a motion attributed to the peeling of the tip (Grishchuk, Molodtsov et al. 2005). Since the Dam1 complex forms rings and spirals around microtubules, we and others thought that Dam1-based attachments might be based exclusively on structures encircling the filament, acted upon by the conformational wave (Miranda, De Wulf et al. 2005; Asbury, Gestaut et al. 2006; Franck, Powers et al. 2007; Grishchuk, Spiridonov et al. 2008). But, in the absence of rings Dam1 still forms persistent attachments to shortening microtubules (Gestaut, Graczyk et al. 2008; Grishchuk, Spiridonov et al. 2008). So does Hec1, which has not been shown to form ring-like structures at all (Powers, Franck et al. 2009). Several groups, including our own, have shown that individual Dam1 and Ndc80 complexes diffuse freely along stabilized microtubule filaments, but exhibit biased motion away from disassembling tips (Westermann, Wang et al. 2006; Gestaut, Graczyk et al. 2008; Powers, Franck et al. 2009). Since the two complexes interact with microtubules in a qualitatively similar manner, we wondered whether a common mechanism based on biased diffusion could account for their microtubule coupling ability.

RESULTS

The classic model for biased diffusion was proposed by Terrell Hill on purely theoretical grounds (Hill 1985). By expanding the model to make quantitative predictions, we tested whether it could describe the average lifetime for a microtubule attachment in vitro under a constant force, mediated by a fixed number of either Dam1 or Hec1 complexes. We adapted a motility assay used previously to show that Dam1 or Hec1 can couple a bead to the tip of growing or shortening microtubule (Asbury, Gestaut et al. 2006; Franck, Powers et al. 2007; Powers, Franck et al. 2009). A His6 tag was added to both complexes to facilitate purification

and bead binding. To vary the surface density of bead-bound complex, we incubated beads with molar ratios of complex ranging from 200:1 to 2000:1. Fluorescence intensity measurements of GFP-Dam1 coated beads show that surface density varies in linear proportion to the labeling ratio (fig. S1A). Simple geometric considerations show that approximately 1% of bead-bound complexes can simultaneously interact with the microtubule, providing an estimate for the number of complexes mediating coupling (fig. S1B). Bead decorated with Dam1 complex were introduced into a chamber containing dynamic microtubules grown from stable, coverslip-bound seeds. The filaments exhibited the dynamic instability characteristic of microtubules in vitro, stochastically switching between growth (~10 nm s^{-1}) and shortening (~150 nm s^{-1}). Transitions from growth to shortening were relatively rare, so we also induced disassembly by laser scission of growing filaments. To bind beads to microtubules, we captured beads in solution with a laser trap and held them near the tip. Binding occurred spontaneously and was seen as a reduction of Brownian motion along the microtubule axis, viewed by high spatiotemporal resolution, back focal plane interferometry. We employed a laser-trapping based force clamp to apply force to attachments (Fig 1A). Constant tension was applied in the direction of microtubule growth with a software-controlled piezoelectric stage programmed to maintain a fixed offset between the bead and the trap center. During phases of microtubule assembly, beads under tension remained attached to the growing tip until the coupling failed, the tip spontaneously switched to rapid shortening, or the event was interrupted (e.g. bead stuck to coverslip). Some beads remained tip-attached during transitions from growth to shortening, but others were bound to the microtubule filament and held at a low force (0.5 pN) until disassembly generated ≥500 nm of directed motion, whereupon the force was increased. During shortening, beads underwent disassembly-coupled movement until the attachment failed, the tip switched to growth, or the event was otherwise interrupted.

Similar to what we had observed for Ndc80/Hec1 previously, we found that the lifetime for Dam1-based attachment increases with the molar ratio of complex per bead and decreases with applied force (Fig 1B and C). By collecting many individual events, we were able to calculate an average detachment rate for each surface density and force by counting the number of detachments and dividing by the total observation time (Fig. 1D and E). Detachment rates from growing and shortening microtubules are plotted against the molar ratio of complex to bead or an equivalent estimate of the total number of binding elements contributing to coupling. The most striking feature is the scaling behavior of the data. Curves of detachment rate display an initial, rapid decrease followed by a prolonged, gradual reduction as the number of binding elements increase. Across levels of force, differences in detachment rate are always more pronounced at low surface densities. The rate of detachment from shortening microtubules is approximately ten-fold higher than those from growing microtubules.

Reasoning that different models would produce different scaling behaviors, we used this data to test quantitative models for kinetochore-microtubule coupling. We only considered simple models where individual complexes or binding elements act independently, excluding scenarios such as cooperative binding and ring formation as these have been treated in elegant detail elsewhere. For an attachment consisting of a fixed, finite number of binding elements N_t one can imagine the system performing a random walk along a one-dimensional graph (Fig. 2A). Each state represents only the number of bound elements, so all particular combinations are assumed to have the same free energy. Rightward and leftward steps correspond to the unbinding and rebinding of single elements. The final leftward step is to an absorbing boundary

representing irreversible detachment, equivalent to a bead breaking free from the microtubule tip. Transition rates between states are model-dependent. Since the process involves only the discrete gain or loss of bonds, the stochastic dynamics of the attachment can be described by a one-step master equation (Erdmann and Schwarz 2004; Erdmann and Schwarz 2004)

$$\frac{dp_i}{dt} = r_{i+1}p_{i+1} + g_{i-1}p_{i-1} - (r_i + g_i)p_i$$

where $p_i(t)$ is the probability that i elements are bound at time t and r_i and g_i are the reverse and forward rates between states $0 \leq i \leq N_t$. The complete time dependent solution for all states $p_i(t)$ may be calculated using matrix methods, but of principle interest here is the mean first passage time (MFPT) of the system. The MFPT is the average amount of time a random walker which starts at some site n takes to arrive at the absorbing boundary, i.e. to detach. The inverse of the MFPT is a detachment rate analogous to those we measure in our experimental system. For a graph of a given length with rate constants r_i and g_i the MFPT starting from any lattice point n is (Bar-Haim and Klafter 1998)

$$\tau(n) = \sum_{i=1}^{N_t} \rho_i + \sum_{r=1}^{n-1} \frac{1}{\rho_r g_r} \sum_{s=r+1}^{N_t} \rho_s$$

where

$$\rho_i = \frac{g_1 g_2 \ldots g_{i-1}}{r_1 r_2 \ldots r_{i-1} r_i}$$

and

$$\rho_1 = \frac{1}{r_1}$$

In his original model for biased diffusion, Hill treats the kinetochore as a rigid sleeve of binding elements (Hill 1985). The loss and gain of elements are tightly coupled to the position of the sleeve with respect to the microtubule tip, forcing elements to detach and reattach in a fixed order. Using simple physical reasoning, Hill proposed rate constants for biased diffusion of the sleeve and showed that, on a shortening microtubule, the system would reach a steady-state corresponding to a persistent attachment. To make quantitative predictions about attachment lifetime, we made numerical estimates for Hill's rate constants using parameters constrained by single-molecule data for the Dam1 complex. Incorporating these rate constants into the analytical calculation for the MFPT allows us to plot predicted detachment rates for a Dam1-based coupler versus the total number of binding elements (Fig 2 F and G). On both growing and shortening microtubules the model predicts very steep exponential drops in detachment rate, a scaling behavior not seen in the experimental data.

With standard fixation techniques, electron micrographs depict kinetochores as tri-laminar plates with electron-dense inner and outer layers. Microtubules embedded in the outer plate would appear to be surrounded by a sleeve of kinetochore material. However, milder fixation procedures have shown that the outer layer of the kinetochore is actually a labile network of fiber-like structures (O'Connell, Khodjakov et al. 2012). Given this view, we questioned the once-reasonable assumption that the kinetochores resemble rigid sleeves. Instead, we treat the kinetochore as an array of independent binding elements. Rather than binding and

unbinding in a fixed order, any bound element is permitted to unbind and any unbound element is free to rebind. To further simplify our model, we assume that load is shared equally amongst the bound elements and that the rate of rebinding is independent of force and position. However, the unbinding rate is both position and force-dependent. Elements located distal to the microtubule tip unbind at a constant rate, whereas elements at the tip unbind at a rate given by Bell's law and also, on a shortening filament, a rate proportional to tubulin subunit loss (Bell 1978). Thus the transition rates for the gain and loss of binding elements can be written as

$$g_i = k_{on}(N_t - i)$$
$$r_i = i\left(P_{lattice}k_{off} + P_{tip}k_{off}e^{f/i} + \varepsilon\right)$$

where N_t and i are the total number of binding elements and the number of elements presently bound, k_{on} and k_{off} are single molecule rates for binding and unbinding in the absence of force, $P_{lattice}$ and P_{tip} are steady-state probabilities of being on the microtubule lattice or tip with $P_{lattice} + P_{tip} = 1$, f is a dimensionless force and ε the unbinding rate due to subunit loss. The dimensionless force is related to the loading force by

$$f = \frac{Fx_b}{k_BT}$$

where F is the loading force, x_b is the physical distance between the bound and unbound states and k_BT is Boltzmann's constant multiplied by temperature. To calculate the unbinding rate due to tubulin subunit loss, we assume that the tip of a shortening microtubule is comprised of curls of fixed length. This length is discrete, given by number of subunits in the curl N_{curl} multiplied by the subunit length of 8 nm. Portions of a curl can break anywhere along its length with equal probability, resulting in a loss rate per subunit given by

$$k_{loss} = \frac{v_d}{8\text{ nm}\cdot\sum_{j=1}^{N_{curl}} j}$$

where v_d is force-dependent shortening speed. The loss rate is larger for longer curls since there are more potential sites for breakage. The total unbinding rate due to subunit loss is

$$\varepsilon = k_{loss}\sum_{j=1}^{N_{curl}} P(j)(N_{curl} + 1 - j)$$

where $P(j)$ is the steady-state probability that a binding element is located j subunits from the microtubule tip. In the case where binding elements are always at the tip ($P_{tip} = 1$) and the microtubule is growing or stationary, the model is identical to those proposed for cell to cell and cell to substrate adhesion. We assume that, even bound to a bead, kinetochore complexes can diffuse on the microtubule tip with diffusion coefficients similar to those measured by single molecule TIRF microscopy. This translates into an unloaded "hopping rate", given by the diffusion coefficient divided by the length of a subunit squared (64 nm^2). The effect of the force

per bond is split equally between the forward and backward rate constants, favoring movement toward the tip. By specifying a maximal diffusion length of 160 nm or 20 tubulin subunits, we calculate the steady-state occupation probabilities for a binding element at discrete, subunit-length distances from the microtubule tip using standard methods (Kampen 1992). For growing microtubules the occupation probability is highest at the tip, decaying as a simple force-dependent exponential (Fig. 2D). On shortening microtubules we were compelled to add a position-dependent reverse bias to the rate constants, starting a fixed distance from the tip given byN_{curl}. The bias takes the form of a harmonic potential with a constant term α, whose contribution is split equally between the forward and backward rate constants, creating a force-dependent probability distribution that peaks some distance away from the microtubule tip. Although this may seem ad hoc, some form of reverse bias is required to account for the detachment rate of kinetochore couplers on shortening microtubules (see below).

We fitted the model to all of our Dam1 data, allowing only the global parameters k_{on} , k_{off} and x_b and α to vary freely. Since it must be integer-valued, the parameter N_{curl} was varied manually to obtain best fits to data acquired during disassembly. Overall, the model captured the unique scaling behavior of the data, but the best-fit parameters surprised us (Fig 1 D and E, Table 1). During episodes of microtubule growth, values for k_{on} and k_{off} determine the scaling behavior of the model (Fig 2 F). The unbinding rate for a single Dam1 complex is very slow, corresponding to residency time of 21.7 s on a microtubule. Even more striking was the binding rate, suggesting that a single Dam1 complex typically remains unbound from the microtubule for 250 s before rebinding! To test the sensitivity of the model to perturbations of k_{on} and k_{off} , we compared our best-fit curve to theoretical curves in which k_{on} or k_{off} were increased by an order of magnitude (Fig 2 F). A 10-fold increase in k_{off} generated a curve with similar scaling behavior as the best fit curve but shifted upward, while a 10-fold increase in k_{on} produced a curve of much steeper descent, suggesting that the data constrains the model to a restricted parametric space. Since k_{off} is slow, the higher rates of detachment observed during microtubule shortening must be driven by the loss of tubulin subunits. But, if the position probabilities of binding elements were identical in assembly and disassembly (i.e. α=0), the predicted detachment rate would be much higher than measured (Fig 2 G). We reasoned that there must be some entity near the tip of disassembling microtubule that slows detachment due to subunit loss. Here we invoke the idea that a curl acts as a spring with stiffness α, capable of pushing subunits away from the disassembling tip. Microtubule shortening slows as more force is applied to the tip, so the spring effect must decrease as the loading force increases, otherwise the model would predict detachment rates that decrease with increased force. Since stiffness is an inherent material property, we assume that the effect of force is to reduce the rest-length of the spring. This increases the probability that elements are located near the microtubule tip, counteracting force-dependent slowing of subunit loss.

The best-fit parameters to the data make predictions that we are able to test using independent means. The value for k_{off} is an order of magnitude smaller than previously measured using single-molecule total internal reflection (TIRF) microscopy. This projected value serves as a key first test of the model because, as shown in the previous section, a larger k_{off} would produce a curve that fails to fit the measured data (Fig 2F). Since the discrepancy was likely due to differences in buffer condition, we repeated the single molecule Dam1 measurements in our standard trap assay buffer and a buffer containing higher [K^+] used

previously. In both buffers, particles of Dam1-GFP bound and diffused along taxol-stabilized microtubule filaments (Fig 3A). Coefficients of diffusion were estimated by linear fits to plots of mean-squared displacement versus time and found to be similar between buffers (Fig 3D). However, the dissociation rate was much lower in our trap buffer than in the high K^+ buffer and in good agreement with the predicted off-rate. Next, we considered explanations as to why the single-molecule on-rate was so slow. In most TIRF assays, higher concentrations of kinetochore complex are required for adequate decoration of microtubule filaments when free tubulin is present. This suggests that a kinetochore complex can also bind free tubulin which, in turn, prevents it from rebinding to the microtubule. To test this hypothesis, we measured the detachment rate of Dam1-decorated beads at different concentrations of free tubulin. Detachment rates rose with increased tubulin concentration during both episodes of microtubule growth and shortening (Fig 3 F and G), consistent with a tubulin-dependent slowing of rebinding.

DISCUSSION

Incorporating key ideas from models for kinetochore attachment and cell adhesion, our model describes the behavior of reconstituted, kinetochore-like microtubule attachments in vitro. We have shown that the model can also make useful quantitative and qualitative predictions amenable to experiment. Now with this capability, we can begin to address several outstanding questions about kinetochore-microtubule interactions. Recently our collaborators isolated what appear to be intact kinetochores from budding yeast. Our lab showed that these putative kinetochore-microtubule attachments were far more robust that attachments based on Dam1 and Ndc80 alone (Akiyoshi, Sarangapani et al. 2010). The model suggest several reasons why this might be so. These include, but are not limited to, a larger number of binding elements proximal to the microtubule tip, a slower off-rate for composite binding elements (e.g. a super complex of Dam1 and Ndc80), or more rapid rebinding of unbound elements. More work is needed to test whether this simple model will apply to kinetochores and how kinetochores create and maintain such persistent attachments. Although the model does not speak to the mechanism that activates the spindle checkpoint, it could offer insight into how attachments are weakened and lost during episodes of corrective detachment. For instance, it is already well established that phosphorylation of kinetochore components by the Ipl1 kinase somehow weakens attachment. The effects of phosphorylation at specific sites on kinetochore complexes can be measured at the single molecule level in TIRF, and with the model, one can predict what effect specific phosphorylation events will have on kinetochore attachment lifetime and strength. Finally, this model may serve a general framework capable of describing how all microtubule associated proteins, including motors, form attachments to dynamic microtubule tips. If kinetochore-associated motors had a low duty cycle and were capable of diffusive movement independent of microtubule binding, they may be able to form persistent attachments to microtubules by a mechanism similar to that described above. In summary, this model offers much potential insight into previously hidden mechanisms underlying kinetochore-microtubule attachment and suggests simple ways to test for them.

MATERIALS AND METHODS

Protein Expression and Purification of Dam1 and Dam1-GFP complexes

Dam1 and Dam1-GFP complex polycistronic vectors were transformed into BL21 Rosetta (Novagen, Darmstadt, Germany). Protein expression and purification were carried out as previously described (25). Briefly, Cultures were grown to about 30 Klett units, and the temperature was reduced to 23 °C. Cultures were induced overnight (~12 hrs). Pellets were lysed using a French press in 50 mM sodium phosphate buffer (pH 6.9) containing 350 mM NaCl and protease inhibitors (0.01 mg/mL chymostatin, 0.01 mg/mL aprotinin, 0.01 mg/mL leupeptin, 0.01 mg/mL pepstatin 0.002 mg/mL benzamadine, 1 mM phenylmethylsulfonyl fluoride). Protein was purified by affinity chromatography using Talon resin as described by the manufacturer (BD Biosciences). Peak elutions were concentrated using an Amicon Ultra 50 kDa MWCO (Millipore, Billerica, MA) to about 1 mL and then subjected to gel filtration chromatography on an SDX200 16/60 column (GE Healthcare, Pistcataway, NJ). Peak fractions were concentrated using an Amicon Ultra 50 kDa MWCO, and cleared at 13,000×g. Glycerol was added to a final concentration of 10% and aliquots were snap frozen and stored at -80 °C.

Protein Expression and Purification of Hec1 and Hec1-GFP complexes

Vectors for Hec1 and Hec1-GFP were transformed into electrocompetent E. coli BL21 cells (Rosetta; Novagen). Protein expression and purification were carried out as previously described (25). In brief, cells containing the appropriate expression plasmids were grown at 37° C until they reached a density of 30-60 Klett units. The temperature was then lowered to 20° C, and protein expression was induced with the addition of 0.2 mM IPTG. Induced cells were incubated at 20° C overnight (12-16 hours), and then pelleted. A French press was used to lyse pelleted cells resuspended in 50 mM HEPES buffer (pH 7.6) containing 300 mM NaCl, 8 mM imidazole, 2.5 U ml^{-1} benzonase, and protease inhibitors (0.01 mg ml^{-1} chymostatin, 0.01 mg ml^{-1} aprotinin, 0.01 mg ml^{-1} leupeptin, 0.01 mg ml^{-1} pepstatin, 0.002 mg ml^{-1} benzamadine, and 1 mM phenylmethylsulfonyl fluoride). Cell lysate was clarified by centrifugation at 30,000 x g for 20 minutes at 4°C. Protein was purified by affinity chromatography in 50 mM HEPES buffer (pH 7.6) containing 300 mM NaCl using TALON resin (BD Biosciences) or Bio-Scale Mini Profinity IMAC cartridges (Bio-Rad) as described by the manufacturer. Peak elutions were concentrated using an Amicon Ultra 50-kDa MWCO centrifugal filter (Millipore) and further purified by gel filtration chromatography on a Superdex 200 16/60 (GE Healthcare) equilibrated with 50 mM HEPES buffer (pH 7.6) containing 200 mM NaCl. As necessary, the peak fraction(s) were concentrated using a centrifugal filter, as above. Glycerol was added to a final concentration of 5-10% and aliquots were snap frozen and stored at -80°C.

Bead Motility Assays

Recombinant His6-tagged Dam1 or Hec1 complex was linked to 0.44 mm diameter streptavidin-coated polystyrene beads (Spherotech, Lake Forest, IL) using biotinylated His5 antibody (QIAGEN, Valencia, CA). The ratio of antibody to bead was varied to achieve a 1:1 ratio of antibody to kinetochore complex during incubation, otherwise the labeling procedure was as described previously (ref). The amount of complex per bead was adjusted by incubating dilutions of 1–10 nM complex, prepared in BRB80 (80 mM PIPES, 1 mM MgCl2, and 1 mM EGTA [pH 6.9]) plus 8 mg ml^{-1} bovine serum albumin (BSA) and 1 mM DTT, with a fixed amount of beads (~5 pM) at 4°C for 90 min. Any remaining free complex was removed from

the beads by centrifugation before introducing them into the flow chamber. Flow chambers were created
by sandwiching two strips of double-sided sticky tape between a KOH-washed coverslip and a standard glass slide and functionalized by coating with 5 mg ml^{-1} biotinylated BSA (Vector Labs, Burlingame, CA), washing, and then incubating with 0.3 mg ml^{-1} avidin DN (Vector Labs). Stable, biotinylated microtubule seeds were introduced and then washed with a blocking buffer (BRB80 containing 2 mg·ml^{-1} κ-casein and 2% pluronic F-187) before introduction of Dam1- or Hec1-coated beads, which were diluted 8-fold into growth buffer (BRB80 containing 8 mg·ml^{-1} BSA and 1 mM GTP) supplemented with 1.0–1.8 mg ml^{-1} tubulin, 1 mM DTT, and an oxygen scavenging system consisting of 250 mg ml^{-1} glucose oxidase (CalBiochem), 30 mg ml^{-1} catalase (CalBiochem), and 4.5 mg ml^{-1} glucose. Assays were performed at 24.5 °C.

TIRF microscopy assays

Flow cells for TIRF experiments were prepared as described previously. After rinsing with ddH2O, the coverslip was incubated with ‘‘rigor’’ kinesin diluted in assay buffer (BRB80 plus 8 mg ml^{-1} bovine serum albumin (BSA) , 1 mM DTT and 10 mM Taxol) for 5 min. After washing away free kinesin with assay buffer, Taxol-stabilized Alexa-647-labeled microtubules were bound for ~1 min and washed with assay buffer. GFP-tagged Dam1 or Hec1 complex, diluted in assay buffer containing an oxygen scavenger system consisting of 200 mg ml^{-1} glucose Oxidase (Sigma), 35 mg ml^{-1} catalase (Sigma), 25mM glucose and 5mM DTT was then introduced.

Instrumentation, Data Collection, and Analysis

Our optical force clamp has been described previously. Records of bead position versus time were analyzed using custom software written in Igor Pro version 6.22A (Wavemetrics, Lake Oswego, OR). Periods of microtubule growth and shortening were identified in the records by eye. Only events lasting >0.1 s were retained for analysis. Detachments during growth and shortening were scored by observing a marked decrease in bead-trap separation corresponding to a loss of coupling. The model was globally fit to the detachment rate data using non-linear least squares analysis in Igor Pro. TIRF movies were analyzed using software developed in Labview (National Instruments, Austin, TX) for tracking the position and brightness of individual GFP spots.

Computer Simulations of the Biased Cluster Model

Model predictions were calculated using Matlab (Natick, MA) software. Simulations of the model were performed using a Matlab-specific implementation of the stochastic simulation algorithm (also known as the SSA or Gillespie algorithm) (Gillespie 1977; Ullah, Schmidt et al. 2006).

TABLE AND FIGURES

Table 1 Model Parameters for Detachment Rate Data						
Fixed Parameters	**Dam1 Assembly**		**Dam1 Disassembly**		**Hec1 Assembly**	**Hec1 Disassembly**
Force (pN)	0.8	1.8	0.8	1.8	1.8	1.8
Bead-Microtubule Contact Area (%)	1	1	1	1		
Diffusion Coefficient ($\mu m^2 s^{-1}$)	0.12	0.12	0.12	0.12	0.8	0.8
Step Size (nm)	8	8	8	8	8	8
Number of probability states	40	40	40	40	40	40
Number of subunits in Tip, N_{curl}	-	-	5	2	-	
Microtubule Shortening Speed (nm/s)	-	-	170	70		
Fit Parameters						
Single-Molecule Off Rate, k_{off} (s^{-1})	0.046	0.046	0.046	0.046		
Single-Molecule On Rate, k_{on} (s^{-1})	0.0041	0.0041	0.0041	0.0041		
Distance to Unbound State, x_b (nm)	1.6	1.6	1.6	1.6		
Harmonic Potential Constant, α ($pN \cdot nm^{-1}$)	-	-	0.36	0.36		

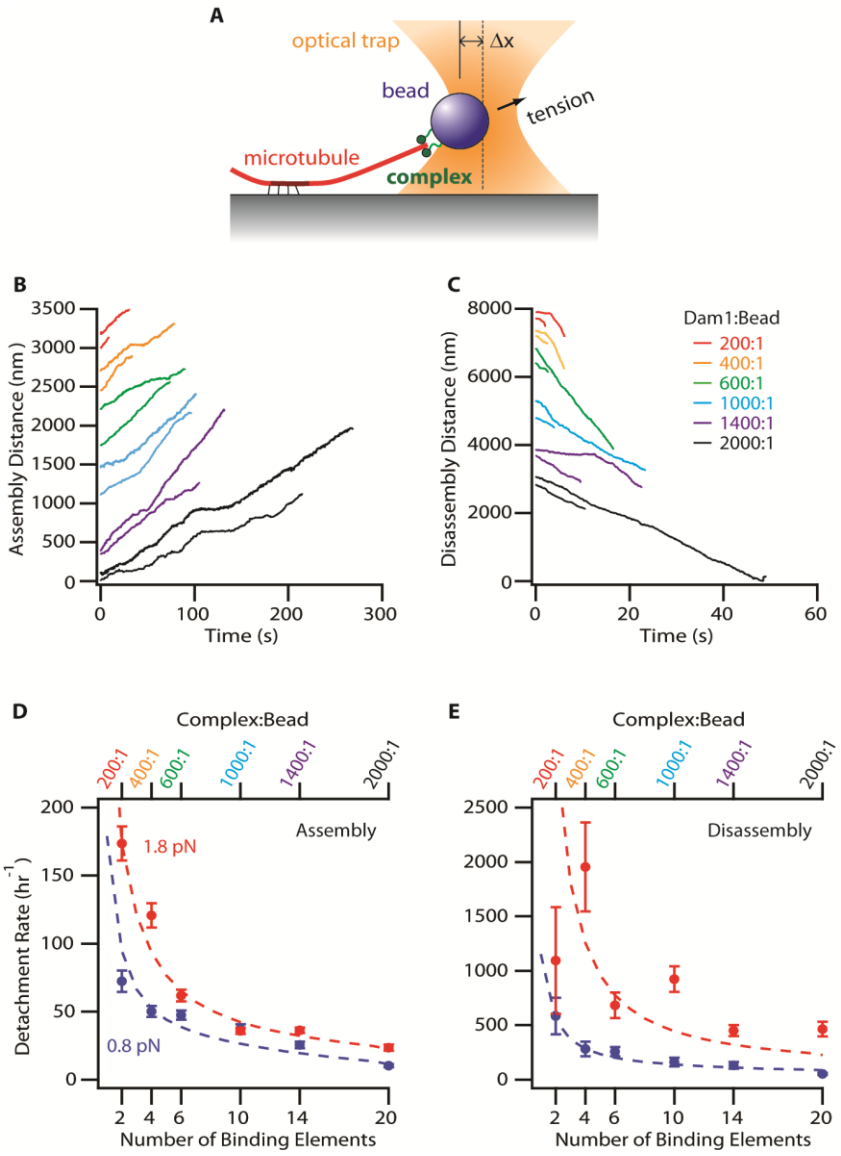

Figure 1: Quantitative measurements of detachment rate as function of surface density and force.

(**A**) Schematic representation showing experimental geometry and force-clamp operation. A polystyrene bead (blue) is held by an optical trap (orange). The Dam1 complex (green) on the bead surface mediates attachment to the tip of a dynamic microtubule (red). A portion of the microtubule (dark red) is anchored to the coverslip. As the microtubule grows and shortens, the coverslip is moved by computer to keep a fixed separation (Δx) between the bead and trap, thereby maintaining a constant level of tension. (**A** and **B**) Representative records showing position versus time for tip-attached beads under tension. (A) Increasing position represents bead movement away from anchored portion of filament during microtubule growth. (B) Decreasing position represents bead movement toward the anchored filament during shortening. Color represents surface density of Dam1 complex on beads (see legend, Fig 1B). For each color pair, bead is under 0.8±0.2 pN tension in upper trace and 1.8±0.2 pN tension in lower trace. Traces are offset vertically for clarity. (**C** and **D**) Rates of bead detachment on growing (C) and shortening (D) tips at 0.8 pN (blue) and 1.8 pN (red) of tension as a function of surface density (top) or the equivalent number of binding elements (bottom). Detachment rates are estimated by counting the number of detachment events and dividing by the total observation time. Dashed lines are global non-linear least squares fits to the data using the biased cluster model.

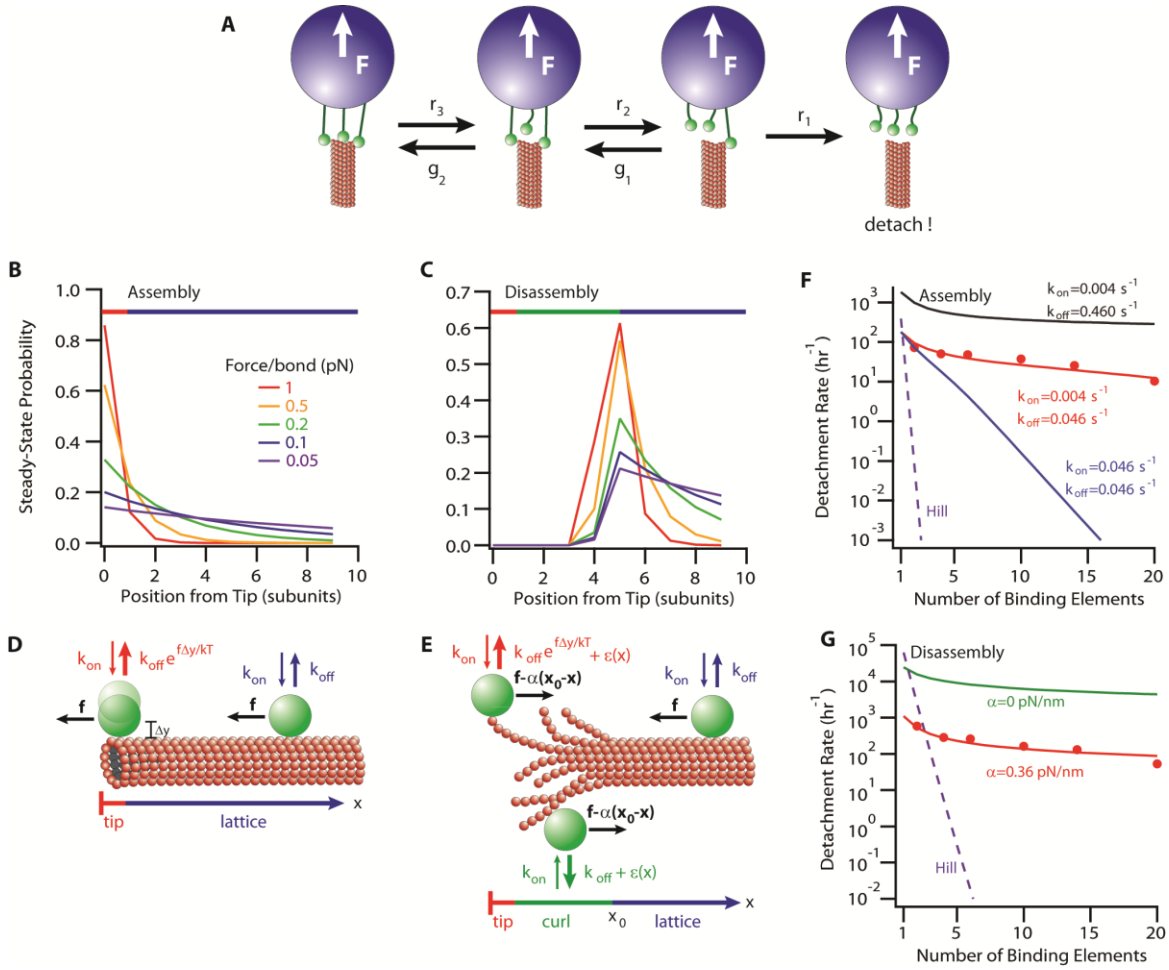

Figure 2: A biased cluster model for kinetochore-microtubule attachment.

(**A**) Schematic depicting loss and gain of bound elements in a cluster. Individual elements bind and unbind independently from the filament. For a number of bound elements i the loss rate for the next element is given by r_i and the gain rate is given by g_{i-1}. Unbinding of the final element is irreversible and results in detachment of the cluster. (**B** and **C**) Steady-state occupation probabilities versus tip position for a single biased diffuser on an assembling (B) or disassembling (C) microtubule. Trace color represents the magnitude of the trap-applied force exerted on the diffuser (see legend, Fig 2C.). Upper color bar represents regions of the microtubule with different unbinding rates at: the tip (red), curling protofilaments (disassembly only, green) and the lattice (blue). (**D**) Binding and unbinding rates for a single element under a trap-applied force f on an assembling microtubule at the tip (red) and on the lattice (blue). Δy is the distance between the bound and unbound states. (**E**) Binding and unbinding rates for a single element on disassembling microtubule at the tip (red) and along a protofilament curl (green) and on the lattice (blue). The element is under the trapping-force f all along the filament, but is also subject to a position-dependent force $\alpha(x_0\text{-}x)$ starting at x_0 due to protofilament peeling. This reversal force lowers the occupation probability at the disassembling tip. See text for details regarding unbinding rates. (**F** and **G**) Measured (red circles, replotted from Fig. 1D and E.) and predicted (dashed and solid lines) rates of detachment as a function of the number of binding elements for clusters on assembling (F) and disassembling (G) microtubules under 0.8 pN of tension. Dashed purple lines (F and G) represent detachment rates predicted by Hill's sleeve model using single molecule data for Dam1 as input parameters. Solid red lines (F and G) are best fits to the data using the biased cluster model (replotted from Fig. 1D and E.) with best-fit values for model parameters k_{on} and k_{off} and α. Solid blue line (F) represents the detachment rate predicted by the biased cluster model for a k_{on} equal to the fitted k_{off}. Solid black line (F) represents the detachment rate predicted by the biased cluster model for a k_{off} ten-fold larger than the fitted value. Solid green line (G) represents the detachment rate predicted by the biased cluster model when α=0.

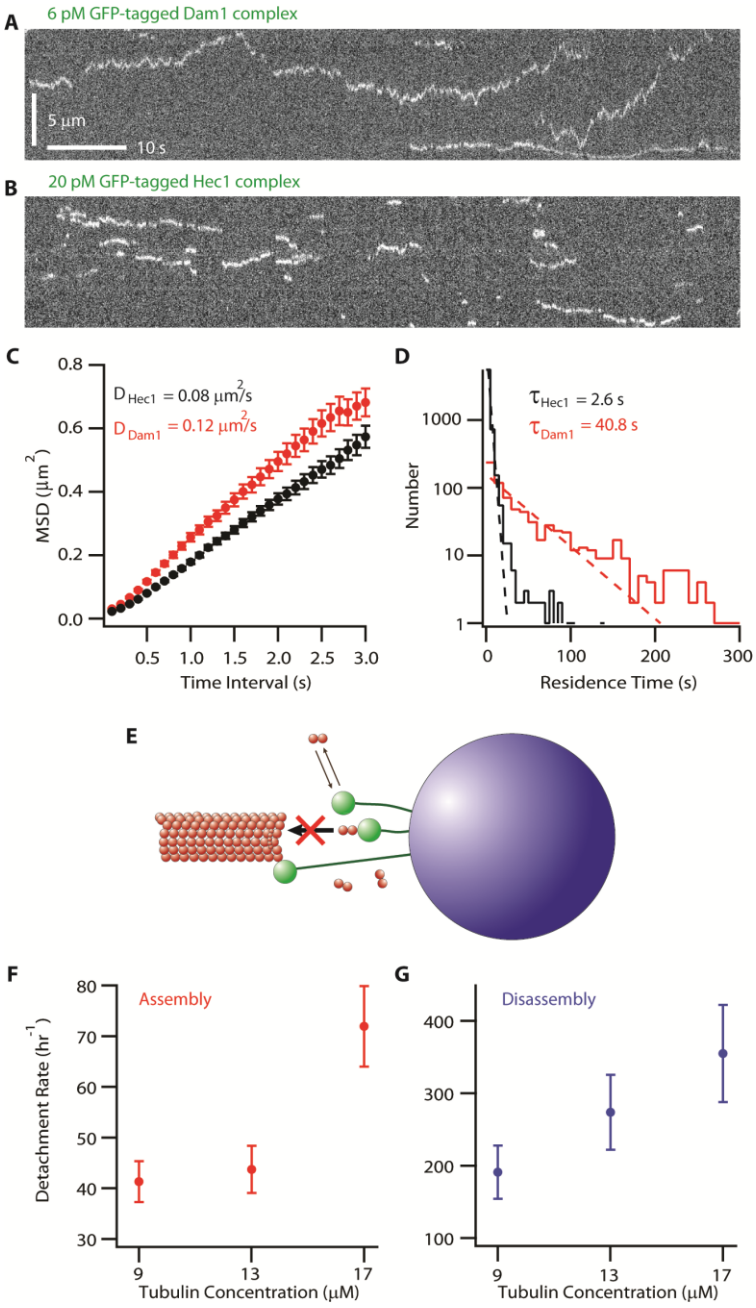

Figure 3: Independent verification of biased cluster model predictions.

(**A** and **B**) Kymographs showing binding and diffusion of Dam1-GFP (A) and Hec1-GFP (B) on taxol stabilized microtubules in a buffer similar to that using in the optical trapping trap-based assays. Positions along the microtubule are depicted on the vertical axis while time changes along the horizontal axis. Under these conditions long duration events for Dam1-GFP (>10 s) are common. (**C**) Mean-squared displacement (MSD) is plotted against time for Dam1 (red) and Hec1 (black). Data are mean ± SEM, computed for n = 770 for Dam1 and n = 6423 for Hec1. (**D**) Residence time distributions for Dam1 complexes (red histogram, n = 771 events) and Hec1 (black histogram, n = 6547 binding events) in recordings totalling 348 minutes). Dotted lines show weighted exponential fits used to determine mean residence times. (**E**) Schematic depicting binding of free tubulin subunits to kinetochore complexes. Complexes cannot rebind to the microtubule lattice until free tubulin dissociates, slowing the rebinding rate in a tubulin concentration-dependent manner. (**F** and **G**) Rates of detachment for beads with a surface density of 1000 Dam1 complexes per bead on growing (F) and shortening (G) microtubule tips under a constant load of 0.8 pN at free tubulin concentrations equivalent to 70%, 100% and 130% of the standard used throughout the remainder of the text.

Chapter 7

Tension Applied Through the Dam1 Complex Promotes Microtubule Elongation: A Direct Mechanism for Length Control in Mitosis

Originally published in Nature Cell Biology 9 (2007) 832-837.

ABSTRACT

In dividing cells, kinetochores couple chromosomes to the tips of growing and shortening microtubule (MT) fibers(Koshland, Mitchison et al. 1988; Inoue and Salmon 1995) and tension at the kinetochore-MT interface promotes fiber elongation(Nicklas 1988; Skibbens, Rieder et al. 1995; Khodjakov and Rieder 1996; Skibbens and Salmon 1997). Tension-dependent MT fiber elongation is thought to be essential for coordinating chromosome alignment and separation(Nicklas 1988; Skibbens, Skeen et al. 1993; Inoue and Salmon 1995; Gardner, Pearson et al. 2005; Goshima, Wollman et al. 2005; Civelekoglu-Scholey, Sharp et al. 2006), but the mechanism underlying this effect is unknown. Using optical tweezers, we applied tension to a model of the kinetochore-microtubule interface composed of the yeast Dam1 complex(Cheeseman, Drubin et al. 2002; Miranda, De Wulf et al. 2005; Westermann, Avila-Sakar et al. 2005) bound to individual dynamic microtubule tips(Asbury, Gestaut et al. 2006). Higher tension decreased the likelihood that growing tips would begin to shorten, slowed shortening, and increased the likelihood that shortening tips would resume growth. These effects are similar to the effects of tension on kinetochore-attached microtubule fibers in many cell types, suggesting that we have reconstituted a direct mechanism for microtubule length control in mitosis.

INTRODUCTION

For decades, a central problem for biologists has been to understand how MT lengths are controlled during mitosis(Inoue and Ritter 1975; Nicklas 1983). MTs are protein polymers that switch stochastically between phases of assembly and disassembly, during which tubulin subunits are added or lost from the filament tips(Inoue and Salmon 1995). This behavior, called 'dynamic instability', can be described by four parameters: the speeds of growth and shortening, and the rates of switching from growth to shortening and from shortening to growth, transitions known as 'catastrophes' and 'rescues'(Walker, O'Brien et al. 1988; Inoue and Salmon 1995) In dividing cells, chromosomes are linked to the tips of MT fibers through specialized structures called kinetochores and their movements are coupled to fiber growth and shortening(Koshland, Mitchison et al. 1988; Inoue and Salmon 1995). Remarkably, kinetochores maintain persistent, load-bearing attachments to microtubule tips even as the filaments assemble and disassemble under their grip(Koshland, Mitchison et al. 1988; Inoue and Salmon 1995; Maddox, Straight et al. 2003). Classic micromanipulation experiments show that tension at the kinetochore-MT interface promotes MT fiber elongation(Nicklas 1988; Skibbens, Rieder et al. 1995; Khodjakov and Rieder 1996; Skibbens and Salmon 1997), and this effect is widely believed to be essential for controlling fiber lengths and thereby coordinating chromosome alignment and separation(Nicklas 1983; Nicklas 1988; Skibbens, Skeen et al. 1993; Inoue and Salmon 1995; Gardner, Pearson et al. 2005; Goshima, Wollman et al. 2005; Civelekoglu-Scholey, Sharp et al.

2006). Very little is known about the mechanism underlying this tension-dependent length control. However, the dynamic behavior of kinetochore-attached MT tips(Maddox, Straight et al. 2003) implies that the mechanism underlying tension-dependent length control *in vivo* may act by altering one or more of the parameters of dynamic instability in response to load.

A key unanswered question is whether tension promotes elongation via an *indirect* mechanism, where force transmitted through load-bearing kinetochore components regulates the activity of separate MT-modifying components, or by a *direct* mechanism, where the load-bearing components themselves modulate MT behavior. Indirect regulation through MT-modifying enzymes has been implicated in corrective detachment of aberrant kinetochore-MT attachments(Andrews, Ovechkina et al. 2004; Cimini, Wan et al. 2006; Pinsky, Kung et al. 2006), but it is unknown whether an analogous indirect mechanism also controls the lengths of MTs that remain persistently attached. Evidence for a simpler direct mechanism comes from cell-free assays showing that compressive force caused by pushing MT tips against glass barriers slows filament growth(Dogterom and Yurke 1997; Janson, de Dood et al. 2003), and that brief pulses of tension < 1 pN transmitted through avidin-biotin linkages can delay detachment of terminal subunits(Grishchuk, Molodtsov et al. 2005). However, these approaches do not allow measurement of MT dynamic parameters under continuous tension, so their relevance to length control of kinetochore MTs—which are usually under tension(Khodjakov and Rieder 1996; Waters, Skibbens et al. 1996)—is uncertain.

RESULTS

To overcome these limitations, we relied on a motility assay using the Dam1 complex(Cheeseman, Drubin et al. 2002) (also known as DASH, or DDD), a putative load-bearing component of kinetochores in yeast(Cheeseman, Drubin et al. 2002; Miranda, De Wulf et al. 2005; Westermann, Avila-Sakar et al. 2005; Asbury, Gestaut et al. 2006; Westermann, Wang et al. 2006). Like kinetochores, pure recombinant Dam1 complex forms robust connections to growing and shortening MT tips that remain attached even when tension is applied(Asbury, Gestaut et al. 2006). This persistent tip tracking has enabled us to measure the effects of continuous tension on MT dynamic parameters in a reconstituted system for the first time. In our assay, beads coated with the Dam1 complex are attached to the tips of individual dynamic MTs grown from stabilized seeds anchored to a glass coverslip(Dogterom and Yurke 1997; Janson, de Dood et al. 2003; Asbury, Gestaut et al. 2006) (Fig. 1a). Tension is applied to the filament tip using an optical trapping-based force clamp that moves the specimen stage under feedback control(Asbury, Gestaut et al. 2006). Changes in MT length are accommodated while keeping a fixed offset between the tip-attached bead and the center of the optical trap, thus maintaining a constant tensile force. MT growth and shortening is recorded by monitoring the position of the stage.

When a Dam1-coated bead is attached to a growing MT tip and placed under tension, it moves slowly away from the coverslip-anchored seed as the intervening portion of the filament lengthens (840 ± 80 nm on average, $N = 298$ records). Sometimes the bead detaches from the growing MT (Fig. 1b, red trace). However, as reported previously(Asbury, Gestaut et al. 2006), it will sometimes remain attached long enough for the filament to undergo catastrophe. After catastrophe, the shortening MT carries the bead back toward the seed (1400 ± 330 nm, $N = 72$), performing work against the tension applied by the optical trap (Figs. 1b and 2, Movie 1). To allow frequent catastrophes to be observed, we operated at relatively low tubulin concentration

(9 – 12 μM). Under these conditions, the filament usually disassembles completely back to the seed after catastrophe and the bead usually detaches during shortening. However, occasionally the filament will rescue and the bead will resume assembly-coupled movement (Fig. 1b, green trace, Fig. 2b, Movie 2). These observations show that growth, shortening, catastrophe and rescue can all be recorded with continuous tension using our Dam1-based motility assay.

To determine whether MT dynamic parameters are sensitive to tension, we recorded movement of tip-attached beads at two levels of force, either 0.5 ± 0.2 pN or 2.0 ± 0.2 pN (Fig. 3, Table 1). Growth and shortening speeds were obtained for each record by plotting traces of position over time and fitting lines to the appropriate segments. The distributions of growth speed were very similar at the two levels of force (Fig. 3a), with mean values consistent with previous *in vitro* measurements(Walker, O'Brien et al. 1988). The mean growth speed at 0.5 pN was 6.0 ± 0.8 nm s^{-1}, not significantly different ($p = 0.42$) from the mean speed at 2.0 pN, 5.8 ± 0.3 nm s^{-1} (Fig. 3c). The insensitivity of growth speed to tension indicates that the effective binding rate of free tubulin to the MT tip is load-independent under the conditions of our assay. In contrast, the distribution of MT shortening speeds at 2.0 pN was shifted towards lower values compared to 0.5 pN (Fig. 3b). The mean shortening speed at 2 pN was 56 ± 10 nm s^{-1}, significantly slower ($p = 0.00022$) than the mean speed at 0.5 pN, 158 ± 26 nm s^{-1} (Fig. 3d). The observation that, on average, filaments under higher tension shorten more slowly suggests that MT disassembly is sensitive to tension.

If the effect of tension on disassembly is direct, then abrupt changes in the level of tension should cause immediate changes in shortening speed. To test this hypothesis, we programmed our force clamp to automatically switch the level of tension during episodes of MT disassembly. After a specified amount of shortening occurred at the initial tension, the force was either increased (Fig. 4a,c) or decreased (Fig. 4b). Switching the force required ~0.2 s, during which elastic elements (e.g. seed-coverslip linkage, Dam1-bead linkage, etc.) stretched or relaxed depending on whether the force was increased or decreased. Thereafter, disassembly continued at the new, constant level of force. Fig. 4c shows an example where the force was increased from 0.5 to 2.0 pN, causing an immediate reduction in shortening speed, from 100 to 63 nm s^{-1}, which persisted > 25 s before bead detachment. Fig. 4b shows an example where the force was decreased from 1.9 to 0.3 pN, and the speed increased from 104 to 322 nm s^{-1}. To estimate the sensitivity of shortening speed to force we collected many records ($N = 27$) where the force was switched between 0.5 ± 0.2 and 2.0 ± 0.2 pN. For each record we quantified the sensitivity by computing $\Delta speed\ \Delta force^{-1}$, the change in shortening speed divided by the change in tension. The distribution of sensitivity values was broad, with a mean sensitivity of -40 ± 7 nm s^{-1} pN^{-1} (Fig. 4c, inset). This average agrees well with the mean sensitivity estimated from our prior measurements at constant force, -68 ± 28 nm s^{-1} pN^{-1} (Fig. 3d, Table 1), and indicates that shortening speeds are reduced when tension is increased. The observation that force can cause an immediate and persistent change in shortening speed confirms that tension affects MT disassembly in a direct manner.

MT length distributions are exquisitely sensitive to catastrophe and rescue frequencies (Belmont, Hyman et al. 1990; Verde, Dogterom et al. 1992; Kinoshita, Arnal et al. 2001), so we sought to determine whether these switching rates are also altered by changes in tension. To estimate catastrophe and rescue rates, we counted the number of switching events observed under constant force and divided by the total observation time. At 0.5 pN we recorded 44 catastrophes during 87 episodes of MT growth with a combined duration of 4.594 hrs. On this

basis, we estimate a catastrophe frequency of 9.6 ± 1.4 hr^{-1} (Table 1). At 2.0 pN we recorded 28 catastrophes during 211 growth episodes lasting 7.888 hrs, giving a catastrophe frequency of 3.5 ± 0.7 hr^{-1}, significantly lower (p = 0.00008) than at 0.5 pN (Fig. 3e). Rescues were comparatively rare in our experiments, partly due to frequent bead detachment during disassembly (Fig. 3h). Nevertheless, we recorded 7 rescue events in 0.068 hrs of shortening at 2.0 pN, whereas at 0.5 pN we recorded only 3 events in 0.212 hrs (Table 1). From these observations we estimate a rescue frequency of 14 ± 8 hr^{-1} at 0.5 pN and a 7-fold higher frequency, 103 ± 39 hr^{-1}, at 2.0 pN (p = 0.013, Fig. 3f).

The lower catastrophe and higher rescue frequencies at 2 pN imply that for a population of MTs, the proportion of time spent in the growth phase increases as tension increases. The lower shortening speed will also reduce the extent of disassembly during episodes of shortening. Numerous other studies have shown that similar changes, particularly reductions in the catastrophe frequency, dramatically promote microtubule elongation(Belmont, Hyman et al. 1990; Verde, Dogterom et al. 1992; Kinoshita, Arnal et al. 2001). Depending on switching frequencies and growth and shortening speeds, a population of MTs polymerized from stable seeds can exhibit two very different classes of behavior: steady state, where the average MT length reaches a constant value, and unbounded growth, where the population grows indefinitely (until the free tubulin is depleted)(Verde, Dogterom et al. 1992). The rate parameters we measured at 0.5 pN are consistent with the steady state scenario, with an average length of 2400 ± 500 nm. In contrast, the rates at 2.0 pN are consistent with unbounded growth, with an average length for the population that increases by 3.7 ± 1.0 nm s^{-1}. (These population-average values are calculated from the measured growth, shortening, catastrophe, and rescue rates as described in Methods.) In light of these considerations, our observations indicate that the microtubules in our assay are strongly biased toward elongation at higher levels of tension.

The tension dependent behavior we observed here with Dam1 and individual MTs is strikingly similar to the behavior of kinetochores and their attached MT fibers in a wide variety of cells(Rieder, Davison et al. 1986; Nicklas 1988; Skibbens, Skeen et al. 1993; Skibbens, Rieder et al. 1995; Khodjakov and Rieder 1996; Skibbens and Salmon 1997). For example, tugging on chromosomes in grasshopper spermatocytes using microneedles causes the kinetochore-attached fibers opposing the load to lengthen(Nicklas 1988), consistent with our central conclusion that tension promotes net MT elongation. Likewise, our observation that tension inhibits catastrophe and promotes rescue is consistent with observations of kinetochore 'directional instability' in PtK_1 and newt lung cells(Rieder, Davison et al. 1986; Skibbens, Skeen et al. 1993; Skibbens, Rieder et al. 1995; Khodjakov and Rieder 1996; Skibbens and Salmon 1997), where increased tension causes kinetochore-attached fibers to switch from shortening to growth(Skibbens and Salmon 1997), and loss of tension causes switching from growth to shortening(Skibbens, Rieder et al. 1995; Khodjakov and Rieder 1996; Skibbens and Salmon 1997). These similarities suggest that tension at kinetochore-MT interfaces *in vivo* modulates the dynamics of attached MTs in a direct manner analogous to our *in vitro* experiments. We note, however, that an alternative explanation for the above-mentioned experiments with animal cells, in which each kinetochore binds multiple MTs, is theoretically possible(Joglekar and Hunt 2002). Kinetochore switching could occur without tension-dependent changes in MT dynamic rates if shortening filaments under high tension detach and are subsequently replaced by new, growing filaments. But this detachment-driven mechanism is untenable in budding yeast, where each kinetochore binds a single MT tip (Pearson, Yeh et al. 2004) and tension-dependent control of MT dynamics is

strongly implicated(Pearson, Yeh et al. 2004; Gardner, Pearson et al. 2005). Our experiments show that such control can be exerted directly, through the Dam1 complex or other load-bearing kinetochore components, perhaps acting in concert with indirect mechanisms mediated by additional MT-modifying agents.

It is instructive to compare our results with previous measurements of MT dynamics under compressive force. MT tips growing against rigid barriers can generate a few pN of compressive force, which is enough to reduce their growth speed ~3-fold(Dogterom and Yurke 1997; Janson and Dogterom 2004) and to promote catastrophe(Janson, de Dood et al. 2003). The catastrophe frequency in such experiments scales with the reciprocal of growth speed over a range of tubulin concentrations independently of whether compressive force is applied, suggesting that compression promotes catastrophe only by limiting the rate of tubulin addition(Janson, de Dood et al. 2003). This relatively simple interpretation, however, cannot explain our results. Whereas forces of similar magnitude are sufficient to alter MT dynamics in either experiment (2 pN of tension versus 2 – 4 pN of compression(Dogterom and Yurke 1997; Janson and Dogterom 2004)), the net effect of tension in our assay is to promote MT growth by altering filament behavior, including the catastrophe frequency, without significantly changing the speed of growth. This difference suggests that the two methods of applying force differ not only in the direction of force, but also in the underlying mechanism by which force alters MT dynamics.

Understanding the structural basis for coupling between the Dam1 complex and MT tips is of great interest, and it is critical for understanding mechanistically how tension transmitted through the complex affects filament dynamics. The data presented here provide some clues about the nature of this interaction, but considerable uncertainty remains. The tips of shortening MTs are frayed because individual rows of tubulin subunits, called protofilaments, curl outward and peel away from the main filament before breaking off(Mandelkow, Mandelkow et al. 1991). The Dam1 complex may transmit tension to these outwardly curling protofilaments, tending to straighten them. Disassembly would be slowed in this interpretation because the protofilaments must overcome the tension as they peel away from the main filament. The same scenario could explain how tension affects catastrophe and rescue frequencies, since these transitions may also involve protofilament curling and straightening, respectively. The ring model proposed recently for Dam1-based coupling to MT tips(Miranda, De Wulf et al. 2005; Westermann, Avila-Sakar et al. 2005; Asbury, Gestaut et al. 2006; Westermann, Wang et al. 2006) is consistent with this picture. When pure recombinant Dam1 complex is mixed with stabilized MTs it oligomerizes into rings encircling the filaments(Miranda, De Wulf et al. 2005; Westermann, Avila-Sakar et al. 2005). To drive movement, peeling protofilaments may act as a ‘conformational wave’(Koshland, Mitchison et al. 1988) that propagates in the direction of shortening and pushes continuously against a ring of Dam1 and also against any external tension applied to the ring. We have confirmed that under the buffer conditions of our experiments free Dam1 complex (i.e. not bead-bound) is capable of forming rings (Fig. S1). Additional experiments will be required to determine if the bead-bound Dam1 complex in our assays can also form rings and if so, whether they are necessary for the tension-dependent effects reported here.

Tension-induced MT elongation is widely believed to be essential for controlling mitotic chromosome movements in organisms as diverse as yeast(Pearson, Yeh et al. 2004; Gardner, Pearson et al. 2005), insects(Nicklas 1988; Goshima, Wollman et al. 2005; Civelekoglu-Scholey, Sharp et al. 2006), and vertebrates(Skibbens, Skeen et al. 1993; Skibbens, Rieder et al. 1995).

Our work demonstrates that this effect can be reconstituted in a simple system. The effect is direct, in the sense that pure recombinant Dam1 complex without additional factors is sufficient to form load bearing attachments that also modify MT dynamics in response to the load. Important questions remain about the underlying mechanism, particularly regarding the structure of Dam1-based MT attachments. Regardless of the structural basis, however, our finding that a load-bearing kinetochore component alters filament dynamics in a tension-dependent manner suggests a general mechanism for MT length control *in vivo*. In principle, such a mechanism could operate wherever dynamic MTs form tension-bearing tip attachments (e.g., at kinetochores, spindle poles and the cell cortex).

METHODS

Protein purification

All 10 subunits of the Dam1 complex were expressed in *E. coli* (BL21 Rosetta, Novagen) from a single plasmid (gift of J.J. Miranda, Harvard) and purified essentially as described(Miranda, De Wulf et al. 2005; Westermann, Avila-Sakar et al. 2005; Asbury, Gestaut et al. 2006). The gene for one subunit (Spc34p) included a His_6-tag to facilitate purification and bead binding. Cells harboring the plasmid were induced to express the complex in mid-log phase by addition of 0.2 mM IPTG, grown for 5 hrs at 37 °C, pelleted, and snap frozen. Pellets were re-suspended in PB (20 mM phosphate, pH 7.0, 500 mM NaCl, 1 mM PMSF and Complete protease inhibitors without EDTA, (Roche)), lysed in a French press, and clarified by centrifugation. The supernatant was mixed with metal-affinity resin (Talon, BD Biosciences), washed in PB, and eluted with 200 mM imidazole. The eluate was purified on a size-exclusion column (Superdex 200 10/300GL, Amersham Biosciences), equilibrated with PB, and snap frozen in PB plus 10% glycerol.

Motility assays

To bind the His_6-tagged complex, 0.44-μm-diameter streptavidin-coated polystyrene beads (Spherotech) were further functionalized by incubation with biotinylated penta-His antibody (Qiagen) and washed in BRB80 (80 mM Pipes, 1 mM $MgCl_2$, 1 mM EGTA, pH 6.9) plus 8 mg ml^{-1} bovine serum albumin (BSA), included as a blocking protein. Dilute suspensions of anti-His beads (0.01% solids) were coated with Dam1 by mixing with 24 nM of the heterodecameric complex in BRB80 plus BSA and incubating 90 min. Free Dam1 was then removed by centrifugation before introducing the beads into the flow chamber. Stable MT seeds were grown by incubating 68 μM bovine brain tubulin, 1 μM biotinylated tubulin (Cytoskeleton), and 1 mM GMPCPP (Jena Bioscience) in BRB80 plus 10% glycerol at 37 °C for > 30 min. KOH-cleaned coverslips were fixed with double-stick tape to glass slides to create flow chambers, which were functionalized by incubation with 5 mg ml^{-1} biotinylated BSA (Vector Labs) followed by 0.3 mg ml^{-1} avidin DN (Vector Labs). Seeds were bound and then washed with GB (BRB80 plus BSA with 1 mM GTP) prior to introduction of Dam1 beads and 9 – 12 μM tubulin in GB supplemented with 1 mM DTT and an oxygen scavenging system consisting of 250 μg ml^{-1} glucose oxidase, 30 μg ml^{-1} catalase, and 4.5 mg ml^{-1} glucose. After MT growth, thermal fluctuations tended to bend the extensions slightly away from the coverslip, making them distinguishable from the seeds and their tips accessible for bead binding. Beads were attached exclusively to MT plus ends, identified by their greater extension length as compared to minus ends. The accuracy of this assignment was > 98%, judging from control

experiments in which kinesin-coated beads were used to determine unambiguously which end was the plus end (data not shown). We chose to work at low tubulin concentration in order to maximize the catastrophe frequency while still allowing MT extensions of sufficient length to grow from the coverslip-anchored seeds. The data in Table 1 and Fig. 3 were generated using two different preparations of tubulin. Because the fraction of active tubulin typically varies slightly between preparations(Walker, O'Brien et al. 1988; Janson and Dogterom 2004), we adjusted the relative concentrations to match MT growth rates. With this adjustment, all MT dynamic parameters measured with applied tension for the two preparations were statistically indistinguishable, so the data were combined. Assays were performed at 22 °C.

Instrumentation and data collection

The optical trap was essentially as described previously(Asbury, Gestaut et al. 2006). Position sensor response was mapped using the piezo stage to raster-scan a stuck bead through the beam, and trap stiffness was calibrated along the two principle axes using the drag force, equipartition, and power spectrum methods. Feedback was implemented with custom LabView software. During clamping, bead-trap separation was sampled at 40 kHz while stage position was updated at 50 Hz to maintain the desired load. Bead and stage position data were decimated to 200 Hz before storing to disk. For experiments where force was changed during microtubule-driven movement, the instrument was programmed to automatically switch to the new level of tension after the bead traveled a user-specified distance in the direction of disassembly (typically 250 – 500 nm).

Data analysis

Periods of slow MT growth and rapid shortening were easily identified in the records of relative bead position versus time. Growth and shortening speeds were obtained from best-fit lines to portions of these records. For constant force experiments (Figs. 1 – 3), shortening speeds were obtained from fits to the last half of the disassembly-driven movement to avoid brief periods of acceleration, usually lasting ~1 s, which sometimes occurred just after the onset of shortening. Catastrophes were scored and shortening speeds were recorded only when a bead moved in the direction of disassembly by an amount that clearly exceeded the level of random noise in the trace (i.e., by > 40 nm). Similarly, rescues were scored only when a clear episode of disassembly-driven movement (> 40 nm) was followed again by slow growth. For the force-switch experiments (Fig. 4), shortening speeds immediately before and after the change in tension were obtained by fitting 100 nm of movement on either side of the switch. Uncertainties reported for mean speeds represent s.e.m. and corresponding significance levels were estimated using both the one-tailed student's t-distribution and the Kolmogorov-Smirnov test. Both methods yielded essentially the same results, so only p-values from the t-tests are reported here. Uncertainties reported for catastrophe and rescue rates represent counting errors, computed as $\delta r = t^{-1}\sqrt{N}$ where t is the total observation time and N is the number of transition events. These uncertainties were used to calculate the corresponding significance levels, assuming normally distributed rates with standard deviations given by δr.

Two formulas from the literature were used to estimate how the tension-dependent changes in MT dynamic parameters we measured would affect net length for a population of MTs. Depending on parameter values, a MT population can exist in either a steady state regime, where the average length reaches a constant value, or an unbounded growth regime, where the

population grows indefinitely (until the free tubulin is depleted)(Verde, Dogterom et al. 1992). The first formula, adapted from Verde et al. (ref (Verde, Dogterom et al. 1992)), represents the mean length, $\langle L \rangle$, for a population of MTs in the steady state regime:

$$\langle L \rangle = v_s\, v_g\, (v_s f_c - v_g f_r)^{-1}$$

The second formula, adapted from Walker et al. (ref (Walker, O'Brien et al. 1988)), represents the mean rate of growth, $\langle J \rangle$, for a population in the unbounded growth regime:

$$\langle J \rangle = (v_g\, f_c^{-1} - v_s\, f_r^{-1})\, (f_c^{-1} + f_r^{-1})^{-1}$$

Here, v_g and v_s are the growth and shortening speeds, and f_c and f_r are the catastrophe and rescue frequencies, respectively.

Electron microscopy

Dam1 complex was mixed with taxol-stabilized MTs to final concentrations of 20 nM Dam1 and 80 nM tubulin in motility buffer (BRB80 supplemented with 8 mg ml^{-1} BSA, 1 mM GTP, 1 mM DTT, and an oxygen scavenging system consisting of 250 µg ml^{-1} glucose oxidase, 30 µg ml^{-1} catalase, and 4.5 mg ml^{-1} glucose) plus 10 µM taxol, incubated 10 min, and fixed by addition of 3 volumes of 2% glutaraldehyde. Samples were then negatively stained and viewed on a transmission electron microscope, as follows. Carbon coated electron microscopy cupper grids (EMS) were positively charged on a plasma cleaner (EMS-100, EMS). A 4 µl droplet of each sample was pipetted onto a clean grid, washed with water and stained with 2% uranyl acetate in water. Grids were air-dried and viewed on a 120kV JEM 1230. Images were recorded on a 2k x 2k Gatan slow-scan charge coupled device camera.

TABLE AND FIGURES

Table 1 Microtubule dynamic parameters measured at different levels of tension

Tensile force (pN)	0.5 ± 0.2	2.0 ± 0.2
Number of growth events	87	211
Mean growth speed (nm s^{-1})	6.0 ± 0.8	5.8 ± 0.3
Total growth time (hr)	4.594	7.888
Number of catastrophes	44	28
Catastrophe frequency (hr^{-1})	9.6 ± 1.4	3.5 ± 0.7
Number of shortening events	44	28
Mean shortening speed (nm s^{-1})	158 ± 26	56 ± 10
Total shortening time (hr)	0.212	0.068
Number of rescues	3	7
Rescue frequency (hr^{-1})	14 ± 8	103 ± 39

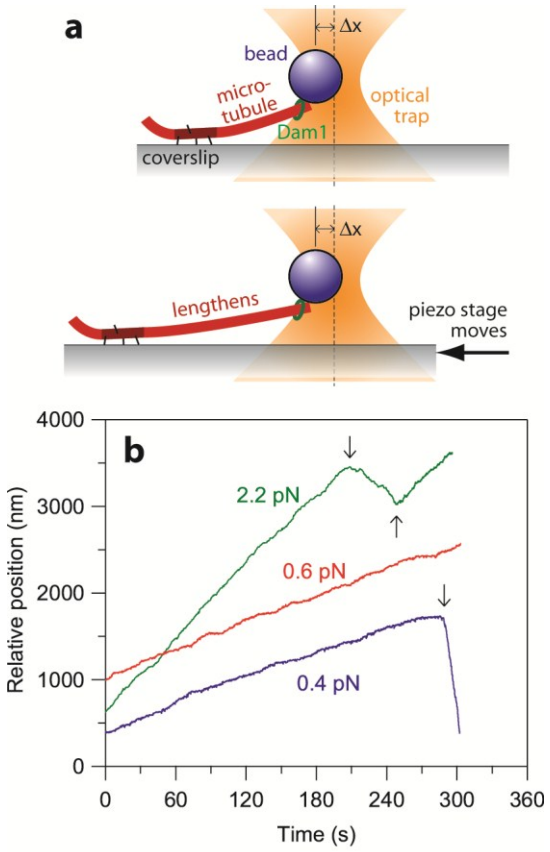

Figure 1: Recording microtubule dynamics with tension applied by an optical trapping-based force clamp.

(**a**) Schematic showing experimental geometry and force clamp operation. A polystyrene bead (blue) is held by an optical trap (orange). Dam1 complex (green) on the bead surface mediates attachment to the tip of a dynamic microtubule (red). A portion of the microtubule (dark red) is anchored to the coverslip. As the microtubule grows and shortens, the coverslip is moved via computer to keep a fixed separation (□x) between the bead and trap, thereby maintaining a constant level of tension. (**b**) Three (of *N* = 298) representative records showing position against time for tip-attached beads under tension. Increasing position represents bead movement away from the anchored portion of the filament during microtubule growth. Decreasing position represents movement toward the anchored seed during filament shortening. Arrows mark catastrophe and rescue events. More example records are shown in Fig. 2.

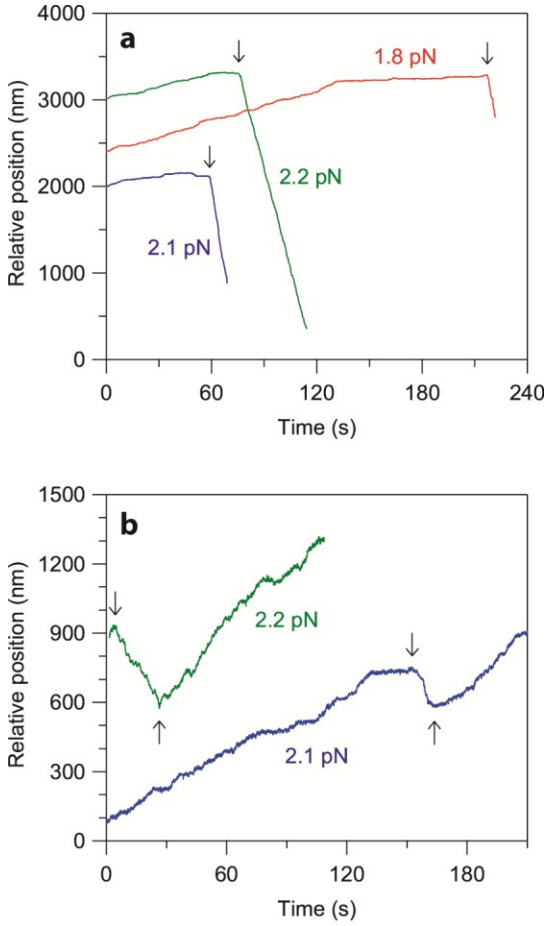

Figure 2: Additional records showing microtubule dynamics with applied tension.

(**a**) Three records showing growth, catastrophe (arrows), and shortening at the indicated levels of tension. (**b**) Two records showing growth, catastrophe (downward arrows), shortening, and rescue (upward arrows).

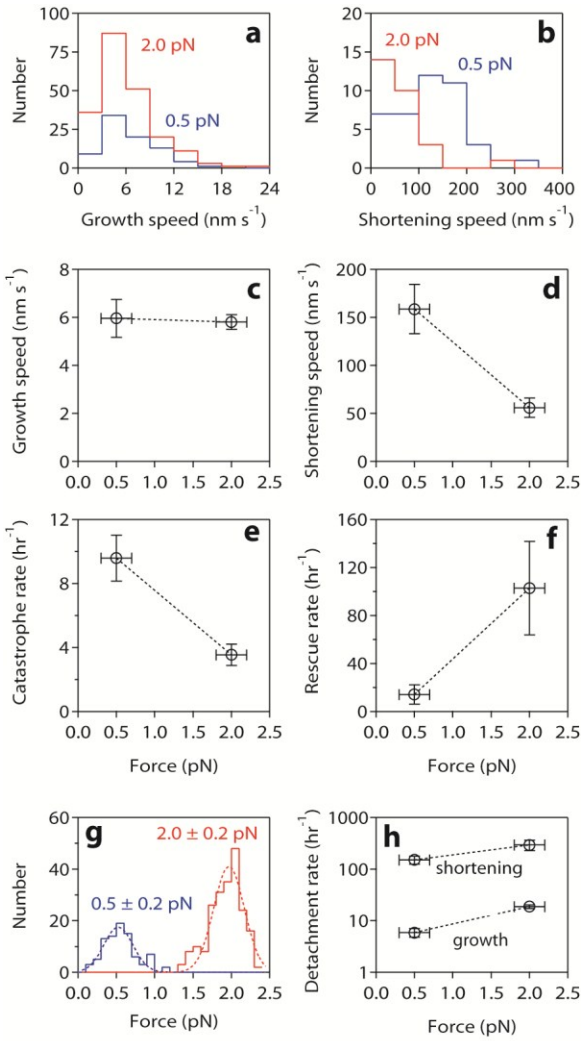

Figure 3: Tension slows shortening, inhibits catastrophe, and promotes rescue.

(**a**, **b**) Distributions of growth and shortening speeds at two levels of tension. Growth speed distributions at 2.0 pN (**a**, red histogram) and 0.5 pN (**a**, blue histogram) are similar in shape. The distribution of shortening speeds, however, is shifted toward lower values at 2.0 pN (**b**, red histogram) as compared to 0.5 pN (**b**, blue histogram). (**c**, **d**) Mean growth (**c**) and shortening speeds (**d**) plotted against tensile force. Uncertainties in speed and force represent s.e.m. and s.d., respectively. (**e**, **f**) Catastrophe (**e**) and rescue (**f**) rates plotted against tensile force. Uncertainties in transition rates represent counting errors. (**g**) Distributions of tensile force for the dataset. (**h**) Rates of bead detachment from shortening and growing tips, estimated by counting the number of detachment events and dividing by the total observation time in each phase. Uncertainties in detachment rate represent counting errors.

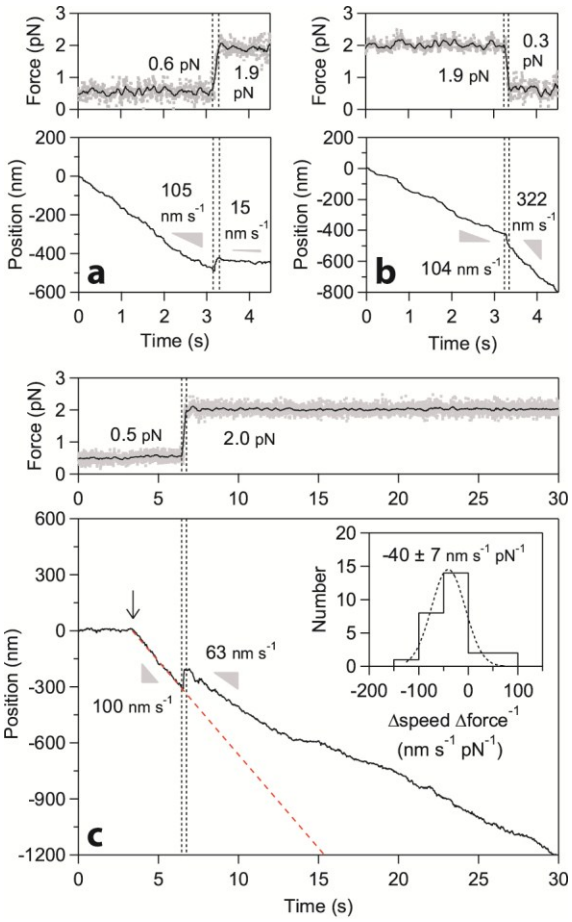

Figure 4: Changing the level of tension during movement immediately alters shortening speed.

(**a** – **c**) Three (of *N* = 27) representative records showing tensile force (upper plots) and bead position (lower plots) against time during disassembly-driven movement. In these force-switch experiments, the instrument was programmed to automatically change the level of tension after a pre-specified amount of movement occurred. Dashed vertical lines denote intervals (~0.2 s duration) when the force was changing. Shortening speeds before and after the change in force are indicated (gray triangles). In **c**, the arrow marks a catastrophe and the dashed red line shows a least-squares fit to the portion of the trace preceding the change in force. The inset shows the distribution of sensitivities, $\Delta speed\ \Delta force^{-1}$, computed from each record by dividing the change in speed by the change in force.

SUPPLEMENTAL FIGURE

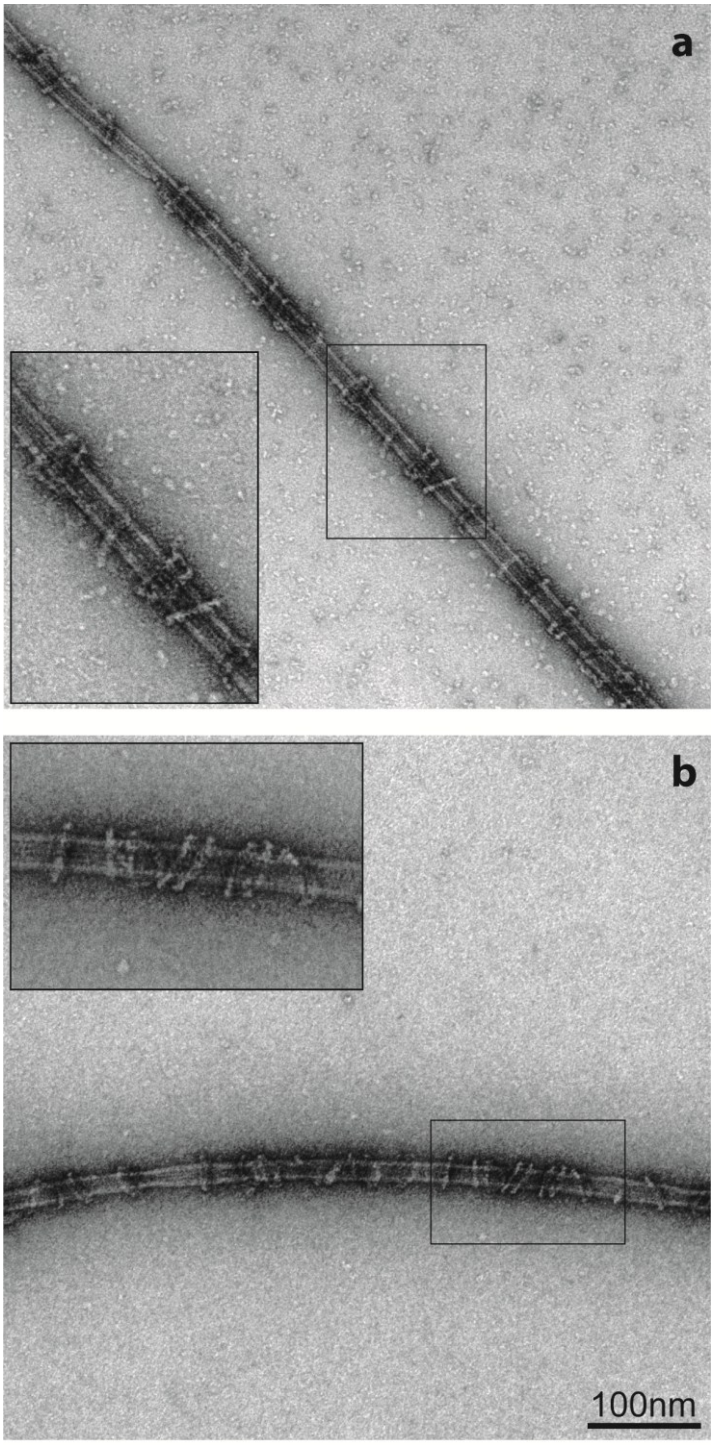

Figure S1: Electron microscopy of negatively stained preparations confirms that free Dam1 complex forms rings encircling MTs under the conditions of our *in vitro* motility experiments.
(**a**) A taxol-stabilized MT decorated with 20 nM Dam1 complex in motility buffer (BRB80 supplemented with 8 mg ml^{-1} BSA, 1 mM GTP, 1 mM DTT, and an oxygen scavenging system consisting of 250 µg ml^{-1} glucose oxidase, 30 µg ml^{-1} catalase, and 4.5 mg ml^{-1} glucose). Rings encircling the MT are clearly visible. The high concentration of BSA is apparent in the background in the form of small particles. (**b**) A taxol-stabilized MT decorated with 20 nM Dam1 complex in motility buffer without BSA. Note the cleaner background.

REFERENCES

Akiyoshi, B., C. R. Nelson, et al. (2009). "Analysis of Ipl1-mediated phosphorylation of the Ndc80 kinetochore protein in Saccharomyces cerevisiae." Genetics **183**(4): 1591-1595.

Akiyoshi, B., K. K. Sarangapani, et al. (2010). "Tension directly stabilizes reconstituted kinetochore-microtubule attachments." Nature **468**(7323): 576-579.

Andrews, P. D., Y. Ovechkina, et al. (2004). "Aurora B regulates MCAK at the mitotic centromere." Dev Cell **6**(2): 253-268.

Asbury, C. L. (2005). "Kinesin: world's tiniest biped." Curr Opin Cell Biol **17**(1): 89-97.

Asbury, C. L., A. N. Fehr, et al. (2003). "Kinesin moves by an asymmetric hand-over-hand mechanism." Science **302**(5653): 2130-2134.

Asbury, C. L., D. R. Gestaut, et al. (2006). "The Dam1 kinetochore complex harnesses microtubule dynamics to produce force and movement." Proc Natl Acad Sci U S A **103**(26): 9873-9878.

Ashkin, A. and J. M. Dziedzic (1987). "Optical trapping and manipulation of viruses and bacteria." Science **235**(4795): 1517-1520.

Ashkin, A., J. M. Dziedzic, et al. (1987). "Optical trapping and manipulation of single cells using infrared laser beams." Nature **330**(6150): 769-771.

Bar-Haim, A. and J. Klafter (1998). "On mean residence and first passage times in finite one-dimensional systems." Journal of Chemical Physics **109**(13): 5187-5193.

Bell, G. I. (1978). "Models for the specific adhesion of cells to cells." Science **200**(4342): 618-627.

Belmont, L. D., A. A. Hyman, et al. (1990). "Real-time visualization of cell cycle-dependent changes in microtubule dynamics in cytoplasmic extracts." Cell **62**(3): 579-589.

Biggins, S., F. F. Severin, et al. (1999). "The conserved protein kinase Ipl1 regulates microtubule binding to kinetochores in budding yeast." Genes Dev **13**(5): 532-544.

Blainey, P. C., A. M. van Oijen, et al. (2006). "A base-excision DNA-repair protein finds intrahelical lesion bases by fast sliding in contact with DNA." Proc Natl Acad Sci U S A **103**(15): 5752-5757.

Block, S. M. (2007). "Kinesin motor mechanics: binding, stepping, tracking, gating, and limping." Biophys J **92**(9): 2986-2995.

Block, S. M., C. L. Asbury, et al. (2003). "Probing the kinesin reaction cycle with a 2D optical force clamp." Proc Natl Acad Sci U S A **100**(5): 2351-2356.

Bormuth, V., J. Howard, et al. (2007). "LED illumination for video-enhanced DIC imaging of single microtubules." J Microsc **226**(Pt 1): 1-5.

Brinkley, B. R. and E. Stubblefield (1966). "The fine structure of the kinetochore of a mammalian cell in vitro." Chromosoma **19**(1): 28-43.

Brower-Toland, B. D., C. L. Smith, et al. (2002). "Mechanical disruption of individual nucleosomes reveals a reversible multistage release of DNA." Proc Natl Acad Sci U S A **99**(4): 1960-1965.

Castoldi, M. and A. V. Popov (2003). "Purification of brain tubulin through two cycles of polymerization-depolymerization in a high-molarity buffer." Protein Expr Purif **32**(1): 83-88.

Cheeseman, I. M., S. Anderson, et al. (2002). "Phospho-regulation of kinetochore-microtubule attachments by the Aurora kinase Ipl1p." Cell **111**(2): 163-172.

Cheeseman, I. M., C. Brew, et al. (2001). "Implication of a novel multiprotein Dam1p complex in outer kinetochore function." J Cell Biol **155**(7): 1137-1145.

Cheeseman, I. M., J. S. Chappie, et al. (2006). "The conserved KMN network constitutes the core microtubule-binding site of the kinetochore." Cell **127**(5): 983-997.

Cheeseman, I. M. and A. Desai (2008). "Molecular architecture of the kinetochore-microtubule interface." Nat Rev Mol Cell Biol **9**(1): 33-46.

Cheeseman, I. M., D. G. Drubin, et al. (2002). "Simple centromere, complex kinetochore: linking spindle microtubules and centromeric DNA in budding yeast." J Cell Biol **157**(2): 199-203.

Cheeseman, I. M., M. Enquist-Newman, et al. (2001). "Mitotic spindle integrity and kinetochore function linked by the Duo1p/Dam1p complex." J Cell Biol **152**(1): 197-212.

Chretien, D., S. D. Fuller, et al. (1995). "Structure of growing microtubule ends: two-dimensional sheets close into tubes at variable rates." J Cell Biol **129**(5): 1311-1328.

Chretien, D. and R. H. Wade (1991). "New data on the microtubule surface lattice." Biol Cell **71**(1-2): 161-174.

Ciferri, C., J. De Luca, et al. (2005). "Architecture of the human ndc80-hec1 complex, a critical constituent of the outer kinetochore." J Biol Chem **280**(32): 29088-29095.

Ciferri, C., S. Pasqualato, et al. (2008). "Implications for kinetochore-microtubule attachment from the structure of an engineered Ndc80 complex." Cell **133**(3): 427-439.

Cimini, D., X. Wan, et al. (2006). "Aurora kinase promotes turnover of kinetochore microtubules to reduce chromosome segregation errors." Curr Biol **16**(17): 1711-1718.

Civelekoglu-Scholey, G., D. J. Sharp, et al. (2006). "Model of chromosome motility in Drosophila embryos: adaptation of a general mechanism for rapid mitosis." Biophys J **90**(11): 3966-3982.

Cottingham, F. R., L. Gheber, et al. (1999). "Novel roles for saccharomyces cerevisiae mitotic spindle motors." J Cell Biol **147**(2): 335-350.

Coue, M., V. A. Lombillo, et al. (1991). "Microtubule depolymerization promotes particle and chromosome movement in vitro." J Cell Biol **112**(6): 1165-1175.

Daga, R. R., A. Yonetani, et al. (2006). "Asymmetric microtubule pushing forces in nuclear centering." Curr Biol **16**(15): 1544-1550.

De Wulf, P., A. D. McAinsh, et al. (2003). "Hierarchical assembly of the budding yeast kinetochore from multiple subcomplexes." Genes Dev **17**(23): 2902-2921.

DeLuca, J. G., Y. Dong, et al. (2005). "Hec1 and nuf2 are core components of the kinetochore outer plate essential for organizing microtubule attachment sites." Mol Biol Cell **16**(2): 519-531.

DeLuca, J. G., W. E. Gall, et al. (2006). "Kinetochore microtubule dynamics and attachment stability are regulated by Hec1." Cell **127**(5): 969-982.

DeLuca, J. G., B. Moree, et al. (2002). "hNuf2 inhibition blocks stable kinetochore-microtubule attachment and induces mitotic cell death in HeLa cells." J Cell Biol **159**(4): 549-555.

Desai, A. and T. J. Mitchison (1997). "Microtubule polymerization dynamics." Annu Rev Cell Dev Biol **13**: 83-117.

Dogterom, M. and B. Yurke (1997). "Measurement of the force-velocity relation for growing microtubules." Science **278**(5339): 856-860.

Drummond, D. R. (2011). "Regulation of microtubule dynamics by kinesins." Semin Cell Dev Biol **22**(9): 927-934.

Efremov, A., E. L. Grishchuk, et al. (2007). "In search of an optimal ring to couple microtubule depolymerization to processive chromosome motions." Proc Natl Acad Sci U S A **104**(48): 19017-19022.

Emanuele, M. J., M. L. McCleland, et al. (2005). "Measuring the stoichiometry and physical interactions between components elucidates the architecture of the vertebrate kinetochore." Mol Biol Cell **16**(10): 4882-4892.

Erdmann, T. and U. S. Schwarz (2004). "Stability of adhesion clusters under constant force." Phys Rev Lett **92**(10).

Erdmann, T. and U. S. Schwarz (2004). "Stochastic dynamics of adhesion clusters under shared constant force and with rebinding." Journal of Chemical Physics **121**(18): 8997-9017.

Franck, A. D., A. F. Powers, et al. (2010). "Direct physical study of kinetochore-microtubule interactions by reconstituion and interrogation with an optical force clamp." Methods. In press.

Franck, A. D., A. F. Powers, et al. (2007). "Tension applied through the Dam1 complex promotes microtubule elongation providing a direct mechanism for length control in mitosis." Nat Cell Biol **9**(7): 832-837.

Gadde, S. and R. Heald (2004). "Mechanisms and molecules of the mitotic spindle." Curr Biol **14**(18): R797-805.

Gaitanos, T. N., A. Santamaria, et al. (2009). "Stable kinetochore-microtubule interactions depend on the Ska complex and its new component Ska3/C13Orf3." EMBO J **28**(10): 1442-1452.

Garcia, M. A., N. Koonrugsa, et al. (2002). "Two kinesin-like Kin I family proteins in fission yeast regulate the establishment of metaphase and the onset of anaphase A." Curr Biol **12**(8): 610-621.

Gardner, M. K., C. G. Pearson, et al. (2005). "Tension-dependent regulation of microtubule dynamics at kinetochores can explain metaphase congression in yeast." Mol Biol Cell **16**(8): 3764-3775.

Gestaut, D. R., J. Cooper, et al. (2010). "Reconstitution and functional analysis of kinetochore subcomplexes." Meth Cell Biol. In press.

Gestaut, D. R., B. Graczyk, et al. (2008). "Phosphoregulation and depolymerization-driven movement of the Dam1 complex do not require ring formation." Nat Cell Biol **10**(4): 407-414.

Gillespie, D. T. (1977). "Exact Stochastic Simulation of Coupled Chemical-Reactions." Journal of Physical Chemistry **81**(25): 2340-2361.

Gordon, D. J., B. Resio, et al. (2012). "Causes and consequences of aneuploidy in cancer." Nat Rev Genet **13**(3): 189-203.

Goshima, G., R. Wollman, et al. (2005). "Length control of the metaphase spindle." Curr Biol **15**(22): 1979-1988.

Grishchuk, E. L., A. K. Efremov, et al. (2008). "The Dam1 ring binds microtubules strongly enough to be a processive as well as energy-efficient coupler for chromosome motion." Proc Natl Acad Sci U S A **105**(40): 15423-15428.

Grishchuk, E. L. and J. R. McIntosh (2006). "Microtubule depolymerization can drive poleward chromosome motion in fission yeast." EMBO J **25**(20): 4888-4896.

Grishchuk, E. L., M. I. Molodtsov, et al. (2005). "Force production by disassembling microtubules." Nature **438**(7066): 384-388.

Grishchuk, E. L., I. S. Spiridonov, et al. (2008). "Different assemblies of the DAM1 complex follow shortening microtubules by distinct mechanisms." Proc Natl Acad Sci U S A **105**(19): 6918-6923.

Guimaraes, G. J., Y. Dong, et al. (2008). "Kinetochore-microtubule attachment relies on the disordered N-terminal tail domain of Hec1." Curr Biol **18**(22): 1778-1784.

Hanisch, A., H. H. Sillje, et al. (2006). "Timely anaphase onset requires a novel spindle and kinetochore complex comprising Ska1 and Ska2." EMBO J **25**(23): 5504-5515.

Hauf, S., R. W. Cole, et al. (2003). "The small molecule Hesperadin reveals a role for Aurora B in correcting kinetochore-microtubule attachment and in maintaining the spindle assembly checkpoint." J Cell Biol **161**(2): 281-294.

He, X., D. R. Rines, et al. (2001). "Molecular analysis of kinetochore-microtubule attachment in budding yeast." Cell **106**(2): 195-206.

Hill, T. L. (1985). "Theoretical problems related to the attachment of microtubules to kinetochores." Proc Natl Acad Sci U S A **82**(13): 4404-4408.

Hofmann, C., I. M. Cheeseman, et al. (1998). "Saccharomyces cerevisiae Duo1p and Dam1p, novel proteins involved in mitotic spindle function." J Cell Biol **143**(4): 1029-1040.

Howard, J. (1996). "The movement of kinesin along microtubules." Annu Rev Physiol **58**: 703-729.

Howard, J. (2001). Mechanics of motor proteins and the cytoskeleton. Sunderland, Mass., Sinauer Associates, Publishers.

Inoue, S. and H. Ritter, Jr. (1975). "Dynamics of mitotic spindle organization and function." Soc Gen Physiol Ser **30**: 3-30.

Inoue, S. and E. D. Salmon (1995). "Force generation by microtubule assembly/disassembly in mitosis and related movements." Mol Biol Cell **6**(12): 1619-1640.

Janke, C., J. Ortiz, et al. (2002). "Four new subunits of the Dam1-Duo1 complex reveal novel functions in sister kinetochore biorientation." EMBO J **21**(1-2): 181-193.

Janson, M. E., M. E. de Dood, et al. (2003). "Dynamic instability of microtubules is regulated by force." J Cell Biol **161**(6): 1029-1034.

Janson, M. E. and M. Dogterom (2004). "Scaling of microtubule force-velocity curves obtained at different tubulin concentrations." Phys Rev Lett **92**(24): 248101.

Joglekar, A. P., K. Bloom, et al. (2009). "In vivo protein architecture of the eukaryotic kinetochore with nanometer scale accuracy." Curr Biol **19**(8): 694-699.

Joglekar, A. P., D. Bouck, et al. (2008). "Molecular architecture of the kinetochore-microtubule attachment site is conserved between point and regional centromeres." J Cell Biol **181**(4): 587-594.

Joglekar, A. P., D. C. Bouck, et al. (2006). "Molecular architecture of a kinetochore-microtubule attachment site." Nat Cell Biol **8**(6): 581-585.

Joglekar, A. P. and A. J. Hunt (2002). "A simple, mechanistic model for directional instability during mitotic chromosome movements." Biophys J **83**(1): 42-58.

Jones, M. H., X. He, et al. (2001). "Yeast Dam1p has a role at the kinetochore in assembly of the mitotic spindle." Proc Natl Acad Sci U S A **98**(24): 13675-13680.

Kampen, N. G. v. (1992). Stochastic processes in physics and chemistry. Amsterdam ; New York, North-Holland.

Kapoor, T. M., M. A. Lampson, et al. (2006). "Chromosomes can congress to the metaphase plate before biorientation." Science **311**(5759): 388-391.

Keating, P., N. Rachidi, et al. (2009). "Ipl1-dependent phosphorylation of Dam1 is reduced by tension applied on kinetochores." J Cell Sci **122**(Pt 23): 4375-4382.

Kelly, A. E. and H. Funabiki (2009). "Correcting aberrant kinetochore microtubule attachments: an Aurora B-centric view." Curr Opin Cell Biol **21**(1): 51-58.

Kelman, Z. (1997). "PCNA: structure, functions and interactions." Oncogene **14**(6): 629-640.

Khodjakov, A. and C. L. Rieder (1996). "Kinetochores moving away from their associated pole do not exert a significant pushing force on the chromosome." J Cell Biol **135**(2): 315-327.

King, S. J. and T. A. Schroer (2000). "Dynactin increases the processivity of the cytoplasmic dynein motor." Nat Cell Biol **2**(1): 20-24.

Kinoshita, K., I. Arnal, et al. (2001). "Reconstitution of physiological microtubule dynamics using purified components." Science **294**(5545): 1340-1343.

Kline-Smith, S. L., S. Sandall, et al. (2005). "Kinetochore-spindle microtubule interactions during mitosis." Curr Opin Cell Biol **17**(1): 35-46.

Koshland, D. E., T. J. Mitchison, et al. (1988). "Polewards chromosome movement driven by microtubule depolymerization in vitro." Nature **331**(6156): 499-504.

Lang, M. J., C. L. Asbury, et al. (2002). "An automated two-dimensional optical force clamp for single molecule studies." Biophys J **83**(1): 491-501.

Lang, M. J. and S. M. Block (2003). "Resource Letter: LBOT-1: Laser-based optical tweezers." Am J Phys **71**(3): 201-215.

Li, Y., J. Bachant, et al. (2002). "The mitotic spindle is required for loading of the DASH complex onto the kinetochore." Genes Dev **16**(2): 183-197.

Lombillo, V. A., M. Coue, et al. (1993). "In vitro motility assays using microtubules tethered to Tetrahymena pellicles." Methods Cell Biol **39**: 149-165.

Lombillo, V. A., R. J. Stewart, et al. (1995). "Minus-end-directed motion of kinesin-coated microspheres driven by microtubule depolymerization." Nature **373**(6510): 161-164.

Maddox, P., A. Straight, et al. (2003). "Direct observation of microtubule dynamics at kinetochores in Xenopus extract spindles: implications for spindle mechanics." J Cell Biol **162**(3): 377-382.

Mandelkow, E. M., E. Mandelkow, et al. (1991). "Microtubule dynamics and microtubule caps: a time-resolved cryo-electron microscopy study." J Cell Biol **114**(5): 977-991.

McAinsh, A. D., J. D. Tytell, et al. (2003). "Structure, function, and regulation of budding yeast kinetochores." Annu Rev Cell Dev Biol **19**: 519-539.

McEwen, B. F., Y. Ding, et al. (1998). "Relevance of kinetochore size and microtubule-binding capacity for stable chromosome attachment during mitosis in PtK1 cells." Chromosome Res **6**(2): 123-132.

McIntosh, J. R. (2005). "Rings around kinetochore microtubules in yeast." Nat Struct Mol Biol **12**(3): 210-212.

McIntosh, J. R. and U. Euteneuer (1984). "Tubulin hooks as probes for microtubule polarity: an analysis of the method and an evaluation of data on microtubule polarity in the mitotic spindle." J Cell Biol **98**(2): 525-533.

McIntosh, J. R., E. L. Grishchuk, et al. (2002). "Chromosome-microtubule interactions during mitosis." Annu Rev Cell Dev Biol **18**: 193-219.

McIntosh, J. R., G. E. L., et al. (2008). "Fibrils connect microtubule tips with kinetochores: a mechanism to couple tubulin dynamics to chromosome motion." Cell **135**: 322-333.

Miller, S. A., M. L. Johnson, et al. (2008). "Kinetochore attachments require an interaction between unstructured tails on microtubules and Ndc80(Hec1)." Curr Biol **18**(22): 1785-1791.

Miranda, J. J., P. De Wulf, et al. (2005). "The yeast DASH complex forms closed rings on microtubules." Nat Struct Mol Biol **12**(2): 138-143.

Miranda, J. J., D. S. King, et al. (2007). "Protein arms in the kinetochore-microtubule interface of the yeast DASH complex." Mol Biol Cell **18**(7): 2503-2510.

Mitchison, T. and M. Kirschner (1984). "Dynamic instability of microtubule growth." Nature **312**(5991): 237-242.

Mitchison, T. J. and M. W. Kirschner (1985). "Properties of the kinetochore in vitro. II. Microtubule capture and ATP-dependent translocation." J Cell Biol **101**(3): 766-777.

Molodtsov, M. I., E. L. Grishchuk, et al. (2005). "Force production by depolymerizing microtubules: a theoretical study." Proc Natl Acad Sci U S A **102**(12): 4353-4358.

Neuman, K. C. and S. M. Block (2004). "Optical trapping." Rev Sci Instrum **75**(9): 2787-2809.

Neuman, K. C., E. H. Chadd, et al. (1999). "Characterization of photodamage to Escherichia coli in optical traps." Biophys J **77**(5): 2856-2863.

Nicklas, R. B. (1983). "Measurements of the force produced by the mitotic spindle in anaphase." J Cell Biol **97**(2): 542-548.

Nicklas, R. B. (1988). "The forces that move chromosomes in mitosis." Annu Rev Biophys Biophys Chem **17**: 431-449.

Nicklas, R. B. (1997). "How cells get the right chromosomes." Science **275**(5300): 632-637.

O'Connell, C. B., A. Khodjakov, et al. (2012). "Kinetochore flexibility: creating a dynamic chromosome-spindle interface." Curr Opin Cell Biol **24**(1): 40-47.

Pearson, C. G., P. S. Maddox, et al. (2001). "Budding yeast chromosome structure and dynamics during mitosis." J Cell Biol **152**(6): 1255-1266.

Pearson, C. G., E. Yeh, et al. (2004). "Stable kinetochore-microtubule attachment constrains centromere positioning in metaphase." Curr Biol **14**(21): 1962-1967.

Perez, F., G. S. Diamantopoulos, et al. (1999). "CLIP-170 highlights growing microtubule ends in vivo." Cell **96**(4): 517-527.

Peskin, C. S. and G. F. Oster (1995). "Force production by depolymerizing microtubules: load-velocity curves and run-pause statistics." Biophys J **69**(6): 2268-2276.

Pinsky, B. A., C. Kung, et al. (2006). "The Ipl1-Aurora protein kinase activates the spindle checkpoint by creating unattached kinetochores." Nat Cell Biol **8**(1): 78-83.

Powers, A. F., A. D. Franck, et al. (2009). "The Ndc80 kinetochore complex forms load-bearing attachments to dynamic microtubule tips via biased diffusion." Cell **136**(5): 865-875.

Raaijmakers, J. A., M. E. Tanenbaum, et al. (2009). "RAMA1 is a novel kinetochore protein involved in kinetochore-microtubule attachment." J Cell Sci **122**(Pt 14): 2436-2445.

Rice, S., A. W. Lin, et al. (1999). "A structural change in the kinesin motor protein that drives motility." Nature **402**(6763): 778-784.

Rieder, C. L., E. A. Davison, et al. (1986). "Oscillatory movements of monooriented chromosomes and their position relative to the spindle pole result from the ejection properties of the aster and half-spindle." J Cell Biol **103**(2): 581-591.

Rieder, C. L. and E. D. Salmon (1994). "Motile kinetochores and polar ejection forces dictate chromosome position on the vertebrate mitotic spindle." J Cell Biol **124**(3): 223-233.

Rieder, C. L. and E. D. Salmon (1998). "The vertebrate cell kinetochore and its roles during mitosis." Trends Cell Biol **8**(8): 310-318.

Sakamoto, T., M. R. Webb, et al. (2008). "Direct observation of the mechanochemical coupling in myosin Va during processive movement." Nature **455**(7209): 128-132.

Sanchez-Perez, I., S. J. Renwick, et al. (2005). "The DASH complex and Klp5/Klp6 kinesin coordinate bipolar chromosome attachment in fission yeast." EMBO J **24**(16): 2931-2943.

Sassoon, I., F. F. Severin, et al. (1999). "Regulation of Saccharomyces cerevisiae kinetochores by the type 1 phosphatase Glc7p." Genes Dev **13**(5): 545-555.

Schrader, F. (1953). Mitosis; the movements of chromosomes in cell division. New York,, Columbia Univ. Press.

Schuyler, S. C. and D. Pellman (2001). "Microtubule "plus-end-tracking proteins": The end is just the beginning." Cell **105**(4): 421-424.

Shang, C., T. R. Hazbun, et al. (2003). "Kinetochore protein interactions and their regulation by the Aurora kinase Ipl1p." Mol Biol Cell **14**(8): 3342-3355.

Sharp, D. J., G. C. Rogers, et al. (2000). "Cytoplasmic dynein is required for poleward chromosome movement during mitosis in Drosophila embryos." Nat Cell Biol **2**(12): 922-930.

Sheetz, M. P. and J. A. Spudich (1983). "Movement of myosin-coated fluorescent beads on actin cables in vitro." Nature **303**(5912): 31-35.

Shimogawa, M. M., B. Graczyk, et al. (2006). "Mps1 phosphorylation of Dam1 couples kinetochores to microtubule plus ends at metaphase." Curr Biol **16**(15): 1489-1501.

Skibbens, R. V., C. L. Rieder, et al. (1995). "Kinetochore motility after severing between sister centromeres using laser microsurgery: evidence that kinetochore directional instability and position is regulated by tension." J Cell Sci **108 (Pt 7)**: 2537-2548.

Skibbens, R. V. and E. D. Salmon (1997). "Micromanipulation of chromosomes in mitotic vertebrate tissue cells: tension controls the state of kinetochore movement." Exp Cell Res **235**(2): 314-324.

Skibbens, R. V., V. P. Skeen, et al. (1993). "Directional instability of kinetochore motility during chromosome congression and segregation in mitotic newt lung cells: a push-pull mechanism." J Cell Biol **122**(4): 859-875.

Sorger, P. K., F. F. Severin, et al. (1994). "Factors required for the binding of reassembled yeast kinetochores to microtubules in vitro." J Cell Biol **127**(4): 995-1008.

Spudich, J. A. (2001). "The myosin swinging cross-bridge model." Nat Rev Mol Cell Biol **2**(5): 387-392.

Stumpff, J., G. von Dassow, et al. (2008). "The kinesin-8 motor Kif18A suppresses kinetochore movements to control mitotic chromosome alignment." Dev Cell **14**(2): 252-262.

Svoboda, K. and S. M. Block (1994). "Biological applications of optical forces." Annu Rev Biophys Biomol Struct **23**: 247-285.

Svoboda, K., C. F. Schmidt, et al. (1993). "Direct observation of kinesin stepping by optical trapping interferometry." Nature **365**(6448): 721-727.

Tan, S. (2001). "A modular polycistronic expression system for overexpressing protein complexes in Escherichia coli." Protein Expr Purif **21**(1): 224-234.

Tanaka, K., E. Kitamura, et al. (2007). "Molecular mechanisms of microtubule-dependent kinetochore transport toward spindle poles." J Cell Biol **178**(2): 269-281.

Tanaka, K., N. Mukae, et al. (2005). "Molecular mechanisms of kinetochore capture by spindle microtubules." Nature **434**(7036): 987-994.

Tanaka, T. U. and A. Desai (2008). "Kinetochore-microtubule interactions: the means to the end." Curr Opin Cell Biol **20**(1): 53-63.

Tanaka, T. U., N. Rachidi, et al. (2002). "Evidence that the Ipl1-Sli15 (Aurora kinase-INCENP) complex promotes chromosome bi-orientation by altering kinetochore-spindle pole connections." Cell **108**(3): 317-329.

Taylor, J. R. (1982). An introduction to error analysis : the study of uncertainties in physical measurements. Mill Valley, CA, University Science Books.

Tirnauer, J. S., S. Grego, et al. (2002). "EB1-microtubule interactions in Xenopus egg extracts: role of EB1 in microtubule stabilization and mechanisms of targeting to microtubules." Mol Biol Cell **13**(10): 3614-3626.

Tran, P. T., P. Joshi, et al. (1997). "How tubulin subunits are lost from the shortening ends of microtubules." J Struct Biol **118**(2): 107-118.

Ullah, M., H. Schmidt, et al. (2006). "Deterministic modelling and stochastic simulation of biochemical pathways using MATLAB." Syst Biol (Stevenage) **153**(2): 53-60.

Vale, R. D. (2003). "The molecular motor toolbox for intracellular transport." Cell **112**(4): 467-480.

Vale, R. D. (2003). "Myosin V motor proteins: marching stepwise towards a mechanism." J Cell Biol **163**(3): 445-450.

Vale, R. D., T. S. Reese, et al. (1985). "Identification of a novel force-generating protein, kinesin, involved in microtubule-based motility." Cell **42**(1): 39-50.

Verde, F., M. Dogterom, et al. (1992). "Control of microtubule dynamics and length by cyclin A- and cyclin B-dependent kinases in Xenopus egg extracts." J Cell Biol **118**(5): 1097-1108.

Visscher, K. and S. M. Block (1998). "Versatile optical traps with feedback control." Methods Enzymol **298**: 460-489.

Walker, R. A., E. T. O'Brien, et al. (1988). "Dynamic instability of individual microtubules analyzed by video light microscopy: rate constants and transition frequencies." J Cell Biol **107**(4): 1437-1448.

Wan, X., R. P. O'Quinn, et al. (2009). "Protein architecture of the human kinetochore microtubule attachment site." Cell **137**(4): 672-684.

Wang, H. W. and E. Nogales (2005). "Nucleotide-dependent bending flexibility of tubulin regulates microtubule assembly." Nature **435**(7044): 911-915.

Wang, H. W., V. H. Ramey, et al. (2007). "Architecture of the Dam1 kinetochore ring complex and implications for microtubule-driven assembly and force-coupling mechanisms." Nat Struct Mol Biol **14**(8): 721-726.

Waters, J. C., R. V. Skibbens, et al. (1996). "Oscillating mitotic newt lung cell kinetochores are, on average, under tension and rarely push." J Cell Sci **109 (Pt 12)**: 2823-2831.

Weaver, B. A., Z. Q. Bonday, et al. (2003). "Centromere-associated protein-E is essential for the mammalian mitotic checkpoint to prevent aneuploidy due to single chromosome loss." J Cell Biol **162**(4): 551-563.

Wei, R. R., J. Al-Bassam, et al. (2007). "The Ndc80/HEC1 complex is a contact point for kinetochore-microtubule attachment." Nat Struct Mol Biol **14**(1): 54-59.

Wei, R. R., J. R. Schnell, et al. (2006). "Structure of a central component of the yeast kinetochore: the Spc24p/Spc25p globular domain." Structure **14**(6): 1003-1009.

Wei, R. R., P. K. Sorger, et al. (2005). "Molecular organization of the Ndc80 complex, an essential kinetochore component." Proc Natl Acad Sci U S A **102**(15): 5363-5367.

Welburn, J. P., E. L. Grishchuk, et al. (2009). "The human kinetochore Ska1 complex facilitates microtubule depolymerization-coupled motility." Dev Cell **16**(3): 374-385.

West, R. R., T. Malmstrom, et al. (2001). "Two related kinesins, klp5+ and klp6+, foster microtubule disassembly and are required for meiosis in fission yeast." Mol Biol Cell **12**(12): 3919-3932.

Westermann, S., A. Avila-Sakar, et al. (2005). "Formation of a dynamic kinetochore-microtubule interface through assembly of the Dam1 ring complex." Mol Cell **17**(2): 277-290.

Westermann, S., I. M. Cheeseman, et al. (2003). "Architecture of the budding yeast kinetochore reveals a conserved molecular core." J Cell Biol **163**(2): 215-222.

Westermann, S., D. G. Drubin, et al. (2007). "Structures and functions of yeast kinetochore complexes." Annu Rev Biochem **76**: 563-591.

Westermann, S., H. W. Wang, et al. (2006). "The Dam1 kinetochore ring complex moves processively on depolymerizing microtubule ends." Nature **440**: 565-569.

Westermann, S., H. W. Wang, et al. (2006). "The Dam1 kinetochore ring complex moves processively on depolymerizing microtubule ends." Nature **440**(7083): 565-569.

Winey, M., C. L. Mamay, et al. (1995). "Three-dimensional ultrastructural analysis of the Saccharomyces cerevisiae mitotic spindle." J Cell Biol **129**(6): 1601-1615.

Yang, Z., U. S. Tulu, et al. (2007). "Kinetochore dynein is required for chromosome motion and congression independent of the spindle checkpoint." Curr Biol **17**(11): 973-980.

VITA

Andrew Franck's interest in science and nature was instilled in him at a young age by his father and grandfathers. He graduated in 2001 with an Arts Baccalaureate in Physics from the University of California at Berkeley. In 2012 he earned a Doctor of Philosophy at the University of Washington in Physiology and Biophysics.